DEVELOPMENT OF MODAL ANALYSIS TOOLS FOR SYSTEMS WITH TRANSPORT DELAYS

José Guilherme de Souza Machado

Dissertação de Mestrado apresentada ao Programa de Pós-graduação em Engenharia Elétrica, COPPE, da Universidade Federal do Rio de Janeiro, como parte dos requisitos necessários à obtenção do título de Mestre em Engenharia Elétrica.

Orientadores: Tatiana Mariano Lessa de Assis
Sergio Gomes Junior

Rio de Janeiro
Dezembro de 2019

DEVELOPMENT OF MODAL ANALYSIS TOOLS FOR SYSTEMS WITH TRANSPORT DELAYS

José Guilherme de Souza Machado

DISSERTAÇÃO SUBMETIDA AO CORPO DOCENTE DO INSTITUTO ALBERTO LUIZ COIMBRA DE PÓS-GRADUAÇÃO E PESQUISA DE ENGENHARIA (COPPE) DA UNIVERSIDADE FEDERAL DO RIO DE JANEIRO COMO PARTE DOS REQUISITOS NECESSÁRIOS PARA A OBTENÇÃO DO GRAU DE MESTRE EM CIÊNCIAS EM ENGENHARIA ELÉTRICA.

Examinada por:

Prof. Tatiana Mariano Lessa de Assis, D.Sc.

Prof. Sergio Gomes Junior, D.Sc.

Prof. Glauco Nery Taranto, Ph.D.

Prof. Rodrigo Andrade Ramos, D.Sc.

RIO DE JANEIRO, RJ – BRASIL
DEZEMBRO DE 2019

Machado, José Guilherme de Souza

Development of Modal Analysis Tools for Systems With Transport Delays /José Guilherme de Souza Machado. – Rio de Janeiro: UFRJ/COPPE, 2019.

XV, 93 p.: il.; 29, 7cm.

Orientadores: Tatiana Mariano Lessa de Assis
Sergio Gomes Junior

Dissertação (mestrado) – UFRJ/COPPE/Programa de Engenharia Elétrica, 2019.

Bibliography: p. 90 – 93.

1. Sistemas de Potência. 2. Análise linear. 3. Estabilidade a pequenos sinais. 4. Análise modal. 5. Controle do amortecimento de oscilações. 6. Atraso de Transporte. I. Assis, Tatiana Mariano Lessa de *et al.* II. Universidade Federal do Rio de Janeiro, COPPE, Programa de Engenharia Elétrica. III. Título.

Dedico este trabalho à minha família.

"Sempre faça tudo com muito amor e com muita fé em Deus, que um dia você chega lá. De alguma maneira você chega lá."

Ayrton Senna

Agradecimentos

Primeiramente, agradeço a Deus, pela minha existência e pelas oportunidades que Ele me permitiu agarrar ao longo dos meus anos de vida. Gostaria, ainda, de agradecer a Ele a vida de todas as pessoas que cruzaram o meu caminho até hoje.

Agradeço aos meus pais, Júlio e Rosângela, por toda minha criação, instrução e, mais importante, por toda paciência demonstrada comigo durante meus anos de estudo.

Agradeço a minha irmã, Rafaela, por fazer parte de toda minha jornada que, mesmo sem entender muito bem sobre o que se tratava, muitas vezes, estava ao meu lado dando suporte e por me dar o maior presente que eu já recebi em toda a minha vida, meus sobrinhos lindos.

Agradeço aos grandes amigos que fiz durante minha vida, e não são poucos, graças a Deus, todos vocês foram muito importantes para a pessoa que eu sou hoje.

Agradeço aos amigos da UFF, e aos amigos do CEPEL e aos amigos do apê 503 que me proporcionaram muito crescimento pessoal, profissional e muitas boas risadas durante esse árduo período de mestrado.

Agradeço aos meus orientadores, Tatiana Mariano Lessa de Assis e Sergio Gomes Junior, por ter me acompanhado durante todo o desenvolvimento do trabalho.

Gostaria de fazer um agradecimento especial ao pesquisador do CEPEL, Thiago Masseran, que sem o qual, com toda certeza, esse trabalho não seria possível.

Por último, agradeço aos professores do Programa de Engenharia Elétrica (PEE) do Instituto Alberto Luiz Coimbra de Pós-Graduação e Pesquisa de Engenharia (COPPE) pela participação na minha formação.

Resumo da Dissertação apresentada à COPPE/UFRJ como parte dos requisitos necessários para a obtenção do grau de Mestre em Ciências (M.Sc.)

DESENVOLVIMENTO DE FERRAMENTAS DE ANÁLISE MODAL PARA SISTEMAS COM ATRASOS DE TRANSPORTE

José Guilherme de Souza Machado

Dezembro/2019

Orientadores: Tatiana Mariano Lessa de Assis
Sergio Gomes Junior

Programa: Engenharia Elétrica

Este trabalho propõe avanços matemáticos e metodologias computacionais para permitir uma análise modal abrangente usando uma representação precisa dos atrasos no transporte. Contemplando o desenvolvimento de ferramentas de análise modal para sistemas com atrasos de transporte, o trabalho aqui apresentado representa um avanço no estado da arte da estabilidade e controle de sistemas de energia.

Tendo em vista o recente uso generalizado de sistemas de comunicação em redes elétricas, a representação usual dos atrasos de transporte transformam o modelo do sistema em um sistema com um número infinito de polos. Como resultado, as representações tradicionais, como espaço de estados e sistemas de descritores, se tornam inviáveis.

As metodologias propostas nessa dissertação são analisadas através de simulações em um sistema tutorial e no Sistema Interligado Brasileiro. Os resultados obtidos com a formulação proposta são comparados com a representação historicamente utilizada e demonstram a importância da modelagem mais precisa dos atrasos de transporte na avaliação de problemas de estabilidade eletromecânica.

Abstract of Dissertation presented to COPPE/UFRJ as a partial fulfillment of the requirements for the degree of Master of Science (M.Sc.)

DEVELOPMENT OF MODAL ANALYSIS TOOLS FOR SYSTEMS WITH TRANSPORT DELAYS

José Guilherme de Souza Machado

December/2019

Advisors: Tatiana Mariano Lessa de Assis
Sergio Gomes Junior

Department: Electrical Engineering

This thesis proposes mathematical advances and computational methodologies to enable a comprehensive modal analysis using an accurate representation of transport delays. Contemplating the development of modal analysis tools for transport delay systems, the work presented here represents a breakthrough in the state of the art of stability and control of power systems.

Given the recent widespread use of communication systems in power grids, the usual representation of transport delays turns the system model into a system with an infinite number of poles. As a result, traditional representations, such as state space and descriptor systems, become unfeasible.

The proposed methodologies are analyzed through simulations in a tutorial system and in the Brazilian Interconnected System. The results obtained using the proposed formulation are compared with the historical representation and demonstrate the importance of more accurate modeling of transport delays in the evaluation of electromechanical stability problems.

Contents

List of Figures

List of Tables

Chapter 1

Introduction

This chapter describes the main subjects discussed in this work. It contains the motivation, objectives and contributions of the presented research. The thesis focuses on power system stability and control, small signal stability, linear analysis, modal analysis and transport delay.

1.1 Context

Traditionally, power system stability control strategies mostly use local information. The measuring delays associated to local information are usually very small (less than 10 ms), so these delays are commonly ignored in power system stability analysis and controllers design.

The general configuration of a modern power system, with huge dimensions, presents power sources and loads widely dispersed. Generators and loads may be hundreds of miles apart. As a result, the number of bulk power exchanges over long distances has increased. Usually, a distributed control scheme is adopted, which includes power system stabilizers (PSSs) and automatic voltage regulators (AVRs). The independent local design may result in an inappropriate coordination between the local controllers, causing serious problems, such as inter-area oscillations.[1]

The rapid development of phase measurement units (PMUs) and wide area measurement systems (WAMSs) has brought more attention to coordinated stability control that uses remote sensing given by WAMS/PMU. The time delay in wide area measurement can be significant and cannot be ignored. So it is very important to evaluate the impact of those time delays on power system stability analysis and controls.

In order to obtain accurate results in computational simulations, the time delay related to remote sensing must be modelled. In the Laplace domain, the transport

delay can be expressed as $e^{-s.\tau}$[1]. However, historically, it is represented by a rational transfer functions as Bessel functions, Padé approximations, Laguerre polynomials, hyperbolic functions, etc [2–4].

The Brazilian Interconnected Power System (BIPS), as other power systems worldwide, is constantly subjected to a wide range of disturbances. Whether large or small disturbances, the BIPS may be able to react to adverse conditions and operate satisfactorily.

The optimal use of power resources presented in different areas all over the country is relevant for an economic and reliable operation of the BIPS. In this context, the interconnection of electrical subsystems plays an important role.

For an adequate, continuous and secure supply of electrical energy, it becomes necessary improving power system analysis tools. The results provided by such tools drive the planning and operation decisions and their accuracy helps to minimize the risks of failure. The higher penetration of PMUs and the increasingly widespread WAMS bring benefits to the system observability and improve the possibilities of using remote signals in the control schemes. However, stability studies should consider remote signals in order to allow a precise evaluation of system performance.

Modal analysis has a special contribution on small-signal studies because it carries structural information about the electrical system, such as badly damped modes, or the best location for installing a specific control.

1.2 Research Motivations

The main motivation of this research is the increasing development of communication structure in electrical systems all over the world. This development may change the system operation and control paradigms, as it brings a range of new possibilities. Furthermore, there is a lack of methodologies and computational tools for systems that use remote signals, especially focused on small-signal stability. In this way, it is difficult to analyze alternative solutions based on remote sensing, including the use of remote signals for damp local and inter-area oscillations.

1.3 Objectives and Contributions

The use of remote signals for stability control is not a practice currently adopted by power system planners. However, with the growing development of communication structure, this is a promising future alternative. In order to obtain accurate results, stability analysis and controller design methods must take into account

[1]Where: s is the complex frequency and τ is the time delay.

time delays and practical tools should be developed to study the dynamic behavior of time-delayed power systems.

This work presents the main concepts of small signal stability and proposes new tools for modal analysis, considering the presence of transport delays in remote control schemes. In addition, methods and corrective measures that can be used to increase the damping factor of power system oscillations are evaluated, taking into account the setting of controllers that use remote signals.

The mathematical development of modal analysis tools for systems with remote signals is the main contribution of this thesis. The employed theory is based on frequency modelling methods that allows a more precise representation of transport delays and considers higher frequencies modes, historically ignored in electromechanical stability studies [5].

The development of modal analysis tools for systems with transport delays represent an advance in the state of art of power system stability and control. With the proposed approach, it is possible to determine better settings to controllers based on remote signals, improving the dynamic behavior of power systems.

1.4 Thesis Outline

This thesis is divided in chapters as follow:

- Chapter 1 – Introduction: The main topics of this research are described, including the motivations and contributions of this thesis;
- Chapter 2 – Modal Analysis Concepts: The basic concepts of power system stability are reviewed, focusing on small-signal stability;
- Chapter 3 – Frequency Domain Modelling: The current state of art related to the power system modelling is presented, including the full transport delay modelling and modal analysis methodology for systems with remote signals;
- Chapter 4 – Tests and Results: Results obtained using the methods and computational tools developed in this thesis are presented. Initially, a two-area system is exploited in a tutorial and detailed analysis. After that, results for the Brazilian Interconnected Power System are presented;
- Chapter 5 – Conclusion: Conclusions and proposals of future work are addressed.

Chapter 2

Modal Analysis Concepts

The main goal of this chapter is to review the basic concepts related to power system stability analyses, focusing on the rotor angle stability. Transient and small-signal stability analyses are described.

2.1 Introduction

A system is a set of physical elements acting together and realizing a common goal. Usually, mathematical models adopted to represent the behaviour of a system do not contain a universal character, but rather reflect some characteristic phenomena which are of interest [6].

A dynamic systems modelled by ordinary differential has equations of the form:

$$\dot{\boldsymbol{x}} = \boldsymbol{F}(\boldsymbol{x}) \tag{2.1}$$

$$\dot{\boldsymbol{x}} = \boldsymbol{A}\boldsymbol{x} \tag{2.2}$$

Equation (2.1) describes a nonlinear system, while (2.2) describes a linear system. $\boldsymbol{F}(\boldsymbol{x})$ is a vector of nonlinear functions and $\boldsymbol{A}$ is a square matrix and $\boldsymbol{x}$ is the state vector and $\dot{\boldsymbol{x}}$ is the time derivative of $\boldsymbol{x}$.

A curve $x(t)$ in the state space containing system states values in consecutive time instants is referred to as the system trajectory. A trivial one-point trajectory is referred to as the equilibrium point if all partial derivatives are zero, i.e., $\dot{x} = 0$. According to (2.1) and (2.2), the equilibrium point, denoted by $\hat{x}$, satisfies the following equations [6]:

$$\boldsymbol{F}(\hat{\boldsymbol{x}}) = \boldsymbol{0} \tag{2.3}$$

$$\boldsymbol{A}\hat{\boldsymbol{x}} = \boldsymbol{0} \tag{2.4}$$

A nonlinear system may have more than one equilibrium point because nonlinear

equations may have generally more than one solution. In the case of linear systems, according to the Cramer theorem concerning linear equations, there exists only one uniquely specified equilibrium point $\dot{\boldsymbol{x}} = 0$ if and only if the matrix A is non-singular ($det\boldsymbol{A} \neq 0$) [6].

Power system stability has three major areas: voltage, frequency and angular stability, as illustrated in Figure 2.1. This work focuses on angular stability, more specifically on small signal stability.

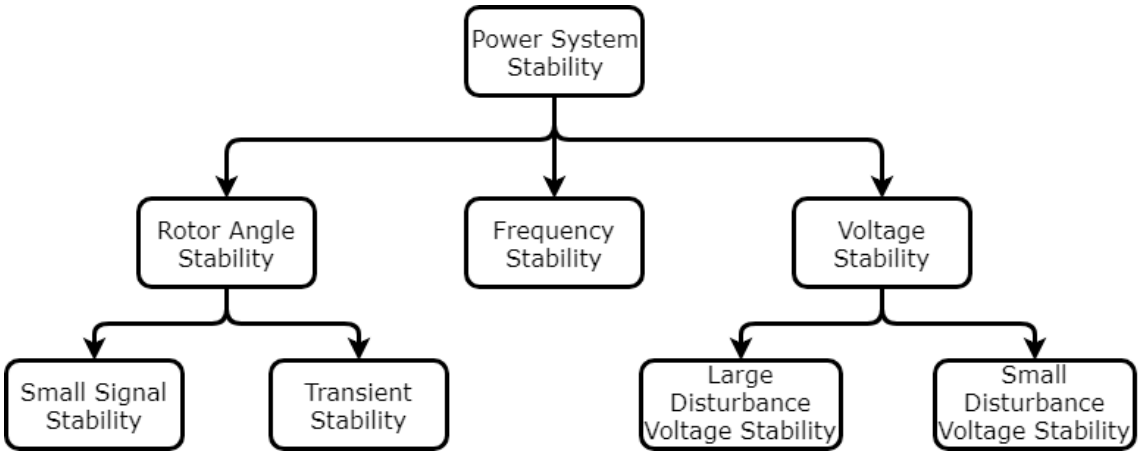

Figure 2.1: Stability Areas

2.2 Transient Stability

According to [7], transient stability is the ability of the power system to maintain synchronism when subjected to a severe transient disturbance such as a fault on transmission lines, loss of generation, or loss of a large load. In order to analyze the system stability, the dynamic behavior of the rotor angles and rotor speed of power plants are observed [7, 8].

In general, the stability of nonlinear systems depends on the size of the disturbance which the system is subjected to. A nonlinear system may be stable for a small disturbance, but unstable for a large one. Critical disturbance is the name given for the disturbance in which a nonlinear system is still stable [6].

Several factors may influence the transient stability of power systems, including the generators loading, the fault-clearing time, the post fault system topology and the system inertia [7].

2.2.1 Non-linear System Modelling

A nonlinear dynamic system can be generally described by the following set of algebraic and differential equations:

$$\dot{\boldsymbol{x}} = \boldsymbol{F}(\boldsymbol{x}, \boldsymbol{u}) \tag{2.5}$$

$$\boldsymbol{y} = \boldsymbol{G}(\boldsymbol{x}, \boldsymbol{u}) \tag{2.6}$$

While a linear dynamic system model can be described by:

$$\dot{\boldsymbol{x}} = \boldsymbol{A}\boldsymbol{x} + \boldsymbol{B}\boldsymbol{u} \tag{2.7}$$

$$\boldsymbol{y} = \boldsymbol{C}\boldsymbol{x} + \boldsymbol{D}\boldsymbol{u} \tag{2.8}$$

The most practical available method for transient stability analysis is the time-domain simulation in which the nonlinear differential equations are solved using numerical techniques [7, 9].

The differential equations to be solved in power system stability analysis are nonlinear ordinary differential equations (2.9), where the initial values of state variables are known [7].

$$\dot{\boldsymbol{x}} = \boldsymbol{f}(\boldsymbol{x}, \boldsymbol{t}) \tag{2.9}$$

As previosly said, $\boldsymbol{x}$ is the state vector of n dependent variables, and t is the independent variable (time). The main goal of solving numeric equations for dynamics purposes is to solve $\boldsymbol{x}$ as a function of t, with the initial values of $\boldsymbol{x}$ and t equal to $\boldsymbol{x_0}$ and t_0, respectively [7, 10].

There are many numerical methods which solve the differential equations as (2.9). As examples, it is possible to quote the Euler, Runge-Kutta and Trapezoidal methods [7, 10].

2.3 Small-Signal Stability

The stability of linear systems is entirely independent of the input. The state of a stable system with zero input will always return to the origin of the state space [7, 10].

In contrast, for nonlinear systems, the stability depends on the type, the magnitude of the input and the initial state [7, 10].

Usually, the stability of a nonlinear system is classified into three major categories, depending on the region of state space in which the state vector ranges [7]:

- Local stability;
- Finite stability;
- Global stability.

The system is said to be a *local stable* system if, when subjected to a small perturbation, it remains into a small region surrounding the equilibrium point. If the system returns to the original equilibrium point as t increases, the system is called a *asymptotically stable* system. If the state of a system remains within a finite region R, the system is said to be a *Finite Stable*. And, finally, the system is called *Global Stable* if R includes the entire finite space [7].

2.3.1 System Model Linearization

In order to investigate the small-signal stability of an general system, (2.3) and (2.4) can be linearized around an equilibrium point ($\boldsymbol{x_0}$, $\boldsymbol{u_0}$) as given by (2.10) [7, 9, 10].

$$\dot{\boldsymbol{x_0}} = \boldsymbol{F(x_0, u_0)} = 0 \tag{2.10}$$

Considering a small perturbation on the initial state of the system:

$$\boldsymbol{x} = \boldsymbol{x_0} + \Delta\boldsymbol{x} \tag{2.11}$$

$$\boldsymbol{u} = \boldsymbol{u_0} + \Delta\boldsymbol{u} \tag{2.12}$$

Therefore, according to Equation (2.3):

$$\dot{\boldsymbol{x}} = \dot{\boldsymbol{x}}_{\boldsymbol{0}} + \boldsymbol{\Delta\dot{x}} = \boldsymbol{f}[(\boldsymbol{x_0} + \boldsymbol{\Delta x}), (\boldsymbol{u_0} + \boldsymbol{\Delta u})] \tag{2.13}$$

Once the perturbation is assumed to be small, the nonlinear functions can be expressed in terms of Taylor's series expansion with terms involving second and higher orders of Δx and Δu neglected. Then, for example, one arbitrary line of (2.13) turns into:

$$\begin{aligned} \dot{x_i} = \dot{x}_{i0} + \Delta\dot{x_i} = f_i[(\boldsymbol{x_0} + \boldsymbol{\Delta x}), (\boldsymbol{u_0} + \boldsymbol{\Delta u})] = \\ f_i(\boldsymbol{x_0}, \boldsymbol{u_0}) + \frac{\partial f_i}{\partial x_1}\Delta x_1 + ... + \frac{\partial f_i}{\partial x_n}\Delta x_n \\ + \frac{\partial f_i}{\partial u_1}\Delta u_1 + ... + \frac{\partial f_i}{\partial u_r}\Delta u_r \end{aligned} \tag{2.14}$$

Since $\dot{x}_{i0} = f_i(\boldsymbol{x_0}, \boldsymbol{u_0})$, then:

$$\Delta\dot{x}_i = \frac{\partial f_i}{\partial x_1}\Delta x_1 + ... + \frac{\partial f_i}{\partial x_n}\Delta x_n + \frac{\partial f_i}{\partial u_1}\Delta u_1 + ... + \frac{\partial f_i}{\partial u_r}\Delta u_r \tag{2.15}$$

With i = 1,2, ..., n. In the same way:

$$\Delta\dot{y}_i = \frac{\partial g_i}{\partial x_1}\Delta x_1 + ... + \frac{\partial g_i}{\partial x_n}\Delta x_n + \frac{\partial g_i}{\partial u_1}\Delta u_1 + ... + \frac{\partial g_i}{\partial u_r}\Delta u_r \tag{2.16}$$

With i = 1,2, ..., m.
Therefore, the linearized equations derived from (2.3) are:

$$\boldsymbol{\Delta\dot{x}} = \boldsymbol{A\Delta x} + \boldsymbol{B\Delta u} \tag{2.17}$$

$$\boldsymbol{\Delta y} = \boldsymbol{C\Delta x} + \boldsymbol{D\Delta u} \tag{2.18}$$

Where:

$$\boldsymbol{A} = \begin{bmatrix} \frac{\partial f_1}{\partial x_1} & ... & \frac{\partial f_1}{\partial x_n} \\ ... & ... & ... \\ \frac{\partial f_i}{\partial x_1} & ... & \frac{\partial f_i}{\partial x_n} \\ ... & ... & ... \\ \frac{\partial f_n}{\partial x_1} & ... & \frac{\partial f_n}{\partial x_n} \end{bmatrix} \tag{2.19}$$

$$\boldsymbol{B} = \begin{bmatrix} \frac{\partial f_1}{\partial u_1} & ... & \frac{\partial f_1}{\partial u_r} \\ ... & ... & ... \\ \frac{\partial f_i}{\partial u_1} & ... & \frac{\partial f_i}{\partial u_r} \\ ... & ... & ... \\ \frac{\partial f_n}{\partial u_1} & ... & \frac{\partial f_n}{\partial u_r} \end{bmatrix} \tag{2.20}$$

$$\boldsymbol{C} = \begin{bmatrix} \frac{\partial g_1}{\partial x_1} & ... & \frac{\partial g_1}{\partial x_n} \\ ... & ... & ... \\ \frac{\partial g_i}{\partial x_1} & ... & \frac{\partial g_i}{\partial x_n} \\ ... & ... & ... \\ \frac{\partial g_m}{\partial x_1} & ... & \frac{\partial g_m}{\partial x_n} \end{bmatrix} \tag{2.21}$$

$$\boldsymbol{D} = \begin{bmatrix} \frac{\partial g_1}{\partial u_1} & \cdots & \frac{\partial g_1}{\partial u_r} \\ \cdots & \cdots & \cdots \\ \frac{\partial g_i}{\partial u_1} & \cdots & \frac{\partial g_i}{\partial u_r} \\ \cdots & \cdots & \cdots \\ \frac{\partial g_m}{\partial u_1} & \cdots & \frac{\partial g_m}{\partial u_r} \end{bmatrix} \tag{2.22}$$

Once small-signal stability is being analyzed, the partial derivatives are related to the equilibrium point. For (2.17) and (2.18):

- $\boldsymbol{\Delta x}$ is the state vector of dimension n;
- $\boldsymbol{\Delta y}$ is the output vector of dimension m;
- $\boldsymbol{\Delta u}$ is the input vector of dimension r;
- $\boldsymbol{A}$ is the state matrix of size $n \times n$;
- $\boldsymbol{B}$ is the control or input matrix of size $n \times r$;
- $\boldsymbol{C}$ is the output matrix of size $m \times n$;
- $\boldsymbol{D}$ is the feedforward matrix. This Matrix defines the proportion of input which appears directly in the output, size $m \times r$;

2.3.2 Eigenvalues and Eigenvectors

Taking the Laplace transform of (2.17) and (2.18), it is possible to obtain the state equations in the frequency domain:

$$\boldsymbol{s\Delta x(s)} - \boldsymbol{\Delta x(0)} = \boldsymbol{A\Delta x(s)} + \boldsymbol{B\Delta u(s)} \tag{2.23}$$

$$\boldsymbol{\Delta y(s)} = \boldsymbol{C\Delta x(s)} + \boldsymbol{D\Delta u(s)} \tag{2.24}$$

Which can be represented by the block diagram shown in Figure 2.2.

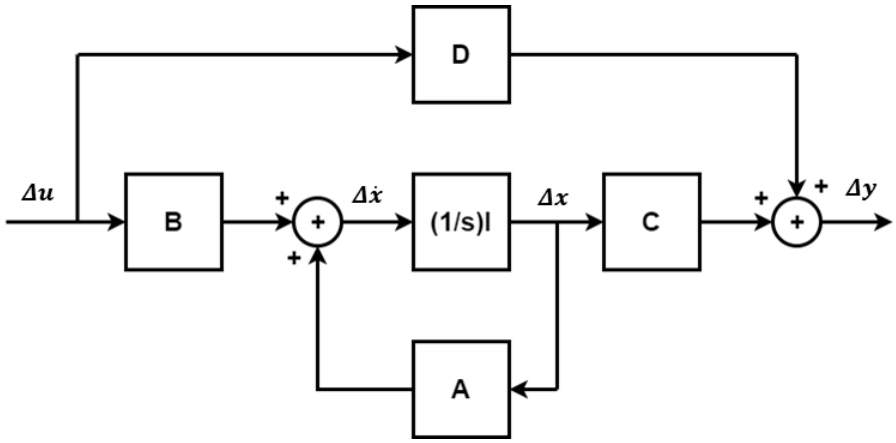

Figure 2.2: Block Diagram - state equations.

Since the representation is on the transfer function of the system, the initial conditions $\Delta x(0)$ are assumed to be zero.

In order to obtain the system eigenvalues, (2.23) can be rearranged, resulting in:

$$s\boldsymbol{\Delta x}(s) - \boldsymbol{A}\boldsymbol{\Delta x}(s) = \boldsymbol{B}\boldsymbol{\Delta u}(s) \tag{2.25}$$

$$(s\boldsymbol{I} - \boldsymbol{A})\boldsymbol{\Delta x}(s) = \boldsymbol{B}\boldsymbol{\Delta u}(s) \tag{2.26}$$

$$\boldsymbol{\Delta x}(s) = (s\boldsymbol{I} - \boldsymbol{A})^{-1}\boldsymbol{B}\boldsymbol{\Delta u}(s) \tag{2.27}$$

Using (2.27) in Equation (2.24) one can obtained (2.28) and (2.29):

$$\boldsymbol{\Delta y}(s) = \boldsymbol{C}(s\boldsymbol{I} - \boldsymbol{A})^{-1}\boldsymbol{B}\boldsymbol{\Delta u}(s) + \boldsymbol{D}\boldsymbol{\Delta u}(s) \tag{2.28}$$

$$\Delta\boldsymbol{y}(s) = (\boldsymbol{C}(s\boldsymbol{I} - \boldsymbol{A})^{-1}\boldsymbol{B} + \boldsymbol{D})\Delta\boldsymbol{u}(s) \tag{2.29}$$

The system poles are given by the roots of (2.30):

$$\det(s\boldsymbol{I} - \boldsymbol{A}) = 0 \tag{2.30}$$

Equation (2.30) is known as the *characteristic equation* of matrix $\boldsymbol{A}$. The values of s that satisfy (2.30) are known as the *eigenvalues* of matrix $\boldsymbol{A}$.

The eigenvalues are the values of scalar parameter λ for which there exist non-trivial solution to the (2.31):

$$\boldsymbol{A}\boldsymbol{\phi} = \boldsymbol{\lambda}\boldsymbol{\phi} \tag{2.31}$$

Where:

- $\boldsymbol{\phi}$ is an vector of size *nx1*;

The n solutions of Equation (2.30) gives the *eigenvalues* of $\boldsymbol{A}$ ($\boldsymbol{\lambda} = \lambda_1, \lambda_2, ..., \lambda_n$).

Any vector $\boldsymbol{\phi_i}$ that satisfies (2.31) is called to be an *right eigenvector* of $\boldsymbol{A}$ associated with the eigenvalue λ_i. Therefore, for an ordinary eigenvalue:

$$\boldsymbol{A\phi_i} = \boldsymbol{\lambda_i\phi_i} \qquad i = 1, 2, ..., n \tag{2.32}$$

The eigenvector ϕ_i has the form:

$$\boldsymbol{\phi_i} = \begin{bmatrix} \boldsymbol{\phi_{1i}} \\ \boldsymbol{\phi_{2i}} \\ ... \\ \boldsymbol{\phi_{ni}} \end{bmatrix} \tag{2.33}$$

One should note that $k.\boldsymbol{\phi_i}$ is also a solution.

Similarly, the n-row vector $\boldsymbol{\psi_i}$ which satisfies the (2.34) is known as the *left eigenvector* associated to the eigenvalue λ_i.

$$\boldsymbol{\psi_i A} = \boldsymbol{\psi_i \lambda_i} \qquad i = 1, 2, ..., n \tag{2.34}$$

The left and right eigenvectors corresponding to different eigenvalues are orthogonal, therefore:

$$\boldsymbol{\psi_j \phi_i} = 0 \tag{2.35}$$

However, if the eigenvectors correspond to the same eigenvalue:

$$\boldsymbol{\psi_i \phi_i} = \boldsymbol{K} \tag{2.36}$$

Where, $\boldsymbol{K}$ is a non-zero constant.

It is usual to *normalize* the eigenvectors. Therefore, (2.36) takes the form shown in Equation (2.37):

$$\boldsymbol{\psi_i \phi_i} = 1 \tag{2.37}$$

The system modes obtained through the eigenvalues of matrix $\boldsymbol{A}$, shown in (2.30), provides the system dynamic behavior in face of small disturbances.

These modes may represent characteristics of power system natural oscillations. The oscillation modes related to electromechanical dynamics can be divided into 4 main categories:

- intra-plant modes: represent oscillations between generation units into the same power plant;
- local modes: represent oscillations of a power plant against all other system machines;
- inter-area modes: represent oscillations between power plants that belong to different areas;
- multi-machine modes: represent oscillations between several machines of several areas.

2.3.3 Stability from Small-Signal Point of View

Equation (2.17) with zero input can be expressed as Equation (2.38), which is referred as free motion equation:

$$\boldsymbol{\Delta \dot{x}} = \boldsymbol{A \Delta x} \tag{2.38}$$

Equation (2.38) can be expressed in a decoupled form by using linear techniques. First, consider a new state vector $\boldsymbol{z}$ related to the original state vector $\Delta \boldsymbol{x}$ by (2.39):

$$\Delta \boldsymbol{x} = \boldsymbol{\phi z} \tag{2.39}$$

Therefore:

$$\boldsymbol{\phi \dot{z}} = \boldsymbol{A \phi z} \tag{2.40}$$

Then:

$$\boldsymbol{\dot{z}} = \boldsymbol{\phi^{-1} A \phi z} \tag{2.41}$$

Using the new state vector (2.38) become:

$$\boldsymbol{\dot{z}} = \boldsymbol{\Lambda z} \tag{2.42}$$

Where $\boldsymbol{\Lambda}$ is a diagonal matrix. The main diagonal of matrix $\boldsymbol{\Lambda}$ contains the n eigenvalues of system. Therefore:

$$\dot{z}_i = \lambda_i z_i \qquad i = 1, 2, ..., n \tag{2.43}$$

Using the transformation given by (2.39), it's possible to obtain the *uncoupled* state equations given by (2.43).

Equation (2.43) is a simple first-order differential equation with the following solution:

$$z_i = z_i(0)e^{\lambda_i t} \tag{2.44}$$

The time dependent characteristic of a mode corresponding to an eigenvalue λ_i is given by $e^{\lambda_i t}$. Therefore, the system stability is determined by the eigenvalues as follows:

- *Real eigenvalues* correspond to non-oscillatory modes. A negative real eigenvalue represents a stable decaying mode, while a positive real eigenvalue means an aperiodic instability. The bigger its magnitude, the faster its decay (stable) or increase (unstable);
- *Complex eigenvalues* correspond to an oscillatory mode, with the real component giving the damping and the imaginary component giving the frequency of the oscillation. A negative real part corresponds to a damped oscillation. On the other hand, a positive real part corresponds to an undamped oscillation;

  Since a complex eigenvalue, λ, composed by a real part σ and a imaginary part ω, is given by:

$$\lambda = \sigma + j\omega \tag{2.45}$$

  The damping ratio, ζ, is given by:

$$\zeta = \frac{-\sigma}{\sqrt{\sigma^2 + \omega^2}} \tag{2.46}$$

The step responses for real and complex eigenvalues are illustrated in Figures 2.3 to 2.7.

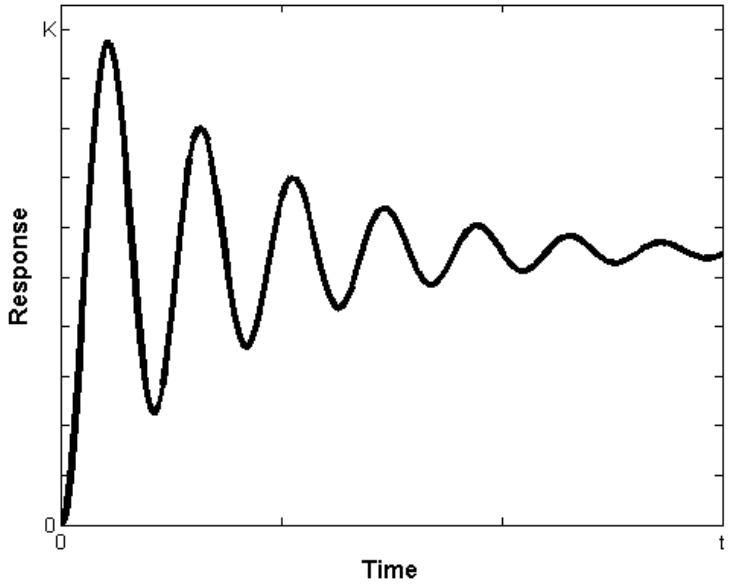

Figure 2.3: Complex eigenvalues with a positive damping ratio step response

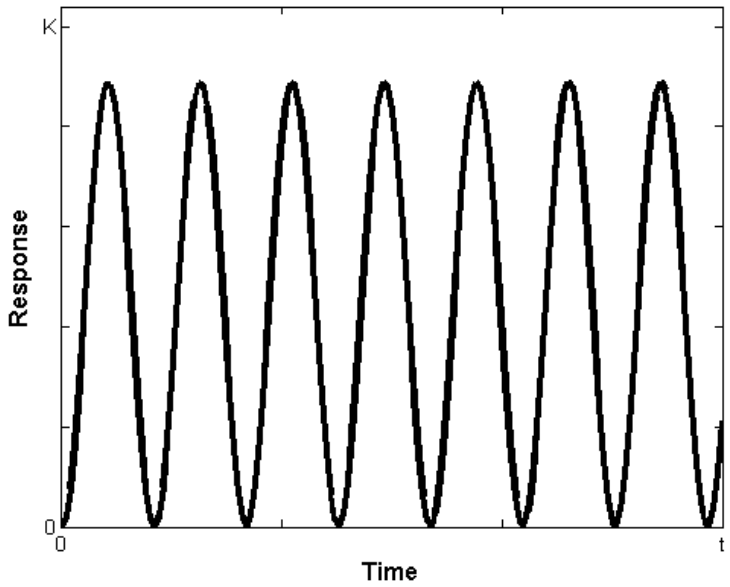

Figure 2.4: Complex eigenvalues with a zero damping ratio step response

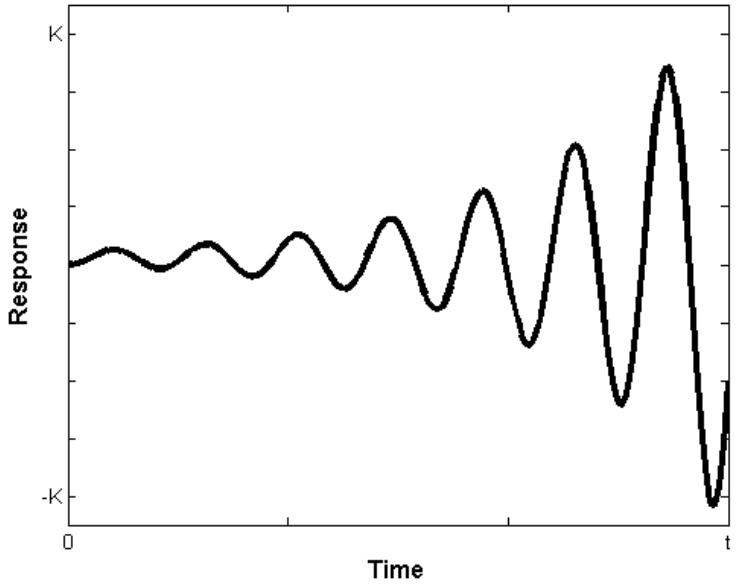

Figure 2.5: Complex eigenvalues with a negative damping ratio step response

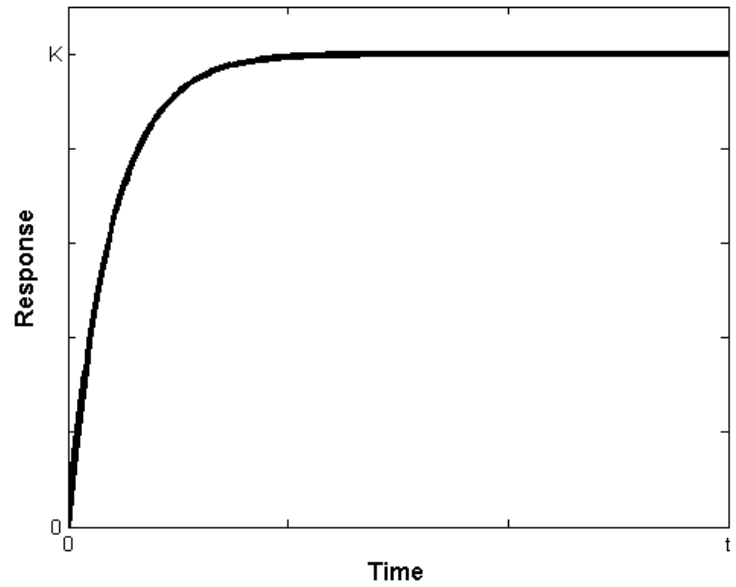

Figure 2.6: Real eigenvalue with a positive damping ratio step response

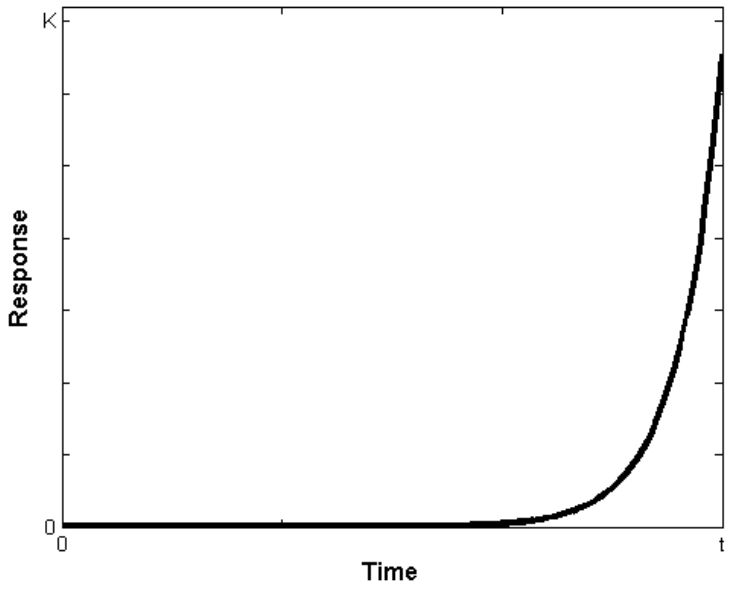

Figure 2.7: Real eigenvalue with negative damping ratio step response

2.3.4 Participation Factors and Mode Shapes

Defining the Modal Matrices as:

$$\boldsymbol{\phi} = \begin{bmatrix} \boldsymbol{\phi_1} & \boldsymbol{\phi_2} & ... & \boldsymbol{\phi_n} \end{bmatrix} \tag{2.47}$$

$$\boldsymbol{\psi} = \begin{bmatrix} \boldsymbol{\psi_1} & \boldsymbol{\psi_2} & ... & \boldsymbol{\psi_n} \end{bmatrix} \tag{2.48}$$

$$\Lambda = \begin{bmatrix} \lambda_1 & 0 & ... & 0 \\ 0 & \lambda_2 & ... & 0 \\ ... & ... & ... & ... \\ 0 & 0 & ... & \lambda_n \end{bmatrix} \tag{2.49}$$

Where each matrix in (2.47), (2.48), (2.49) has dimension $n \times n$. Equations (2.31) and (2.43) can be expanded as:

$$\boldsymbol{A\phi} = \boldsymbol{\phi\Lambda} \tag{2.50}$$

$$\boldsymbol{\psi\phi} = \boldsymbol{I} \qquad \boldsymbol{\psi} = \boldsymbol{\phi^{-1}} \tag{2.51}$$

The Equation (2.39) shows the relationship between the state vectors $\boldsymbol{\Delta x}$ and $\boldsymbol{z}$. Then:

$$\boldsymbol{\Delta x}(t) = \boldsymbol{\phi z}(t) = \begin{bmatrix} \boldsymbol{\phi_1} & \boldsymbol{\phi_2} & ... & \boldsymbol{\phi_n} \end{bmatrix} \boldsymbol{z}(t) \tag{2.52}$$

And:

$$\boldsymbol{z}(t) = \boldsymbol{\psi \Delta x}(t) = \begin{bmatrix} \boldsymbol{\psi_1^T} & \boldsymbol{\psi_2^T} & ... & \boldsymbol{\psi_n^T} \end{bmatrix}^T \boldsymbol{\Delta x}(t) \tag{2.53}$$

The transformed state variables $\boldsymbol{z}$ are directly related to the system modes. On the other hand, the original state variables $\Delta \boldsymbol{x}$ gives the dynamic performance of system [7].

Equation (2.52) shows that the *right eigenvector* gives the relative activity of the *"original state variables"* when a particular mode is excited. Therefore, the magnitudes of the elements $\boldsymbol{\phi_i}$ gives the magnitudes of the eigenvalue i in the n *"original state variables"*. These relative activity is called *mode shape*.

In other hand, the Equation (2.53) shows the "participation" of each *"original state variable"* in a eigenvalue i. The left eigenvector measures the relative participation of each *"original state variable"* in the ith mode.

In order to determine the sensitivity of eigenvalues to the elements of state matrix $\boldsymbol{A}$, one should examine (2.32) with respect to an ordinary eigenvalue λ_i as shown in (2.54):

$$\boldsymbol{A}\boldsymbol{\phi_i} = \lambda_i \boldsymbol{\phi_i} \tag{2.54}$$

Computing the derivative of (2.54) with respect to a_{kj} (kth row, jth column):

$$\frac{\partial \mathbf{A}}{\partial a_{kj}}\boldsymbol{\phi_i} + \mathbf{A}\frac{\partial \boldsymbol{\phi_i}}{\partial a_{kj}} = \frac{\partial \lambda_i}{\partial a_{kj}}\boldsymbol{\phi_i} + \lambda_i \frac{\partial \boldsymbol{\phi_i}}{\partial a_{kj}} \tag{2.55}$$

Multiplying (2.55) by $\boldsymbol{\psi_i}$...

$$\boldsymbol{\psi_i}\frac{\partial \mathbf{A}}{\partial a_{kj}}\boldsymbol{\phi_i} = \frac{\partial \lambda_i}{\partial a_{kj}} \tag{2.56}$$

One should note that all elements of $\frac{\partial \mathbf{A}}{\partial a_{kj}}$ are zero, except the element *"k,j"*. Therefore:

$$\psi_i \phi_i = \frac{\partial \lambda_i}{\partial a_{kj}} \tag{2.57}$$

The matrix *participation matrix* ($\boldsymbol{P}$), which combines the right and left eigenvectors,can be used to measure the association between the state variables and modes:

$$\boldsymbol{P} = \begin{bmatrix} \boldsymbol{p_1} \\ \boldsymbol{p_2} \\ ... \\ \boldsymbol{p_n} \end{bmatrix} \tag{2.58}$$

Then:

$$\boldsymbol{p_i} = \begin{bmatrix} p_{1i} \\ p_{2i} \\ ... \\ p_{ni} \end{bmatrix} = \begin{bmatrix} \phi_{1i}\psi_{i1} \\ \phi_{2i}\psi_{i2} \\ ... \\ \phi_{ni}\psi_{in} \end{bmatrix} \tag{2.59}$$

Where:

- ϕ_{ki} = the element *"k,i"* of modal matrix $\boldsymbol{\phi}$
- ψ_{ik} = the element *"i,k"* of modal matrix $\boldsymbol{\psi}$

The element $p_{ki} = \phi_{ki}\psi_{ik}$ is called *participation factor* and measures the participation of kth state variable in the ith eigenvalue.

The sum of all participation factors of all state variables related to ith eigenvalue equals 1.

2.3.5 Controllability, Observability and Residue

The concepts of controllability and observability play an important role in the design of control systems in state space. The conditions of controllability and observability govern the existence of a complete solution to the control system design problem [9].

It is possible the physical system being controllable and observable and the correspondent mathematical model may not possess the property of controllability and observability. Then, it's necessary to know the conditions under which a mathematical model is controllable and observable [9].

Consider the system given by (2.60):

$$\dot{\boldsymbol{x}} = \boldsymbol{A}\boldsymbol{x} + \boldsymbol{B}\boldsymbol{u} \tag{2.60}$$

The system is completely state controllable if and only if the vectors $\boldsymbol{B}, \boldsymbol{AB}, ..., \boldsymbol{A^{n-1}B}$ are linearly independent, or the n x nr matrix, given by (2.61), is of rank n [9].

$$\left[\boldsymbol{B} \;\; | \;\; \boldsymbol{AB} \;\; | \;\; \boldsymbol{...} \;\; | \;\; \boldsymbol{A^{n-1}B}\right] \tag{2.61}$$

The matrix given by (2.61) is known as *controllability matrix*.

The system is said to be completely observable if every state $\boldsymbol{x}(t_0)$ can be determined from the observation of $\boldsymbol{y}(t)$ over a finite time interval, $t_0 \leq t \leq t_f$. The system is, therefore, completely observable if every transition of the state eventually affects every element of the output vector [9].

The concept of observability is very important because, in practice, some of the state variables are not accessible for direct measurement. In those cases, it is necessary to estimate these state variables in order to design controllers [9].

Consider the unforced system given by (2.62) and (2.63):

$$\dot{\boldsymbol{x}} = \boldsymbol{A}\boldsymbol{x} \tag{2.62}$$

$$\boldsymbol{y} = \boldsymbol{C}\boldsymbol{x} \tag{2.63}$$

The system is completely observable if the matrix n x nm given by (2.64) is of rank n (n linearly independent column vectors). In this case, matrix (2.64) is called *observability matrix*.

$$\left[\boldsymbol{C^*} \quad | \quad \boldsymbol{A^*C^*} \quad | \quad \boldsymbol{...} \quad | \quad \boldsymbol{(A^*)^{n-1}C^*}\right] \tag{2.64}$$

The decoupled (normal form) system modeling is given by (2.65) and (2.66), which can be obtained using the modal matrices.

$$\boldsymbol{\dot{z} = \Lambda z + B'\Delta u} \tag{2.65}$$

$$\boldsymbol{\Delta y = C'z + D\Delta u} \tag{2.66}$$

Where:

- $\boldsymbol{B' = \phi^{-1}B}$
- $\boldsymbol{C' = C\phi}$

Equations (2.65) and (2.66) show that if one row of matrix $\boldsymbol{B'}$ is zero, then the inputs have no effect on the mode related to these line. Then, in such case, this mode is called *uncontrollable* [7]. On other hand, if a column of matrix $\boldsymbol{C'}$ is zero, the corresponding mode is *unobservable*, which means that the variable z_i does not contribute to the formation of the outputs. [7]

The nxr matrix $\boldsymbol{B' = \phi^{-1}B}$ is called *mode controllability matrix*, and the mxn matrix $\boldsymbol{C' = C\phi}$ is called *mode observability matrix*.

By inspecting $\boldsymbol{B'}$ and $\boldsymbol{C'}$ it is possible to classify the modes into observable, controllable, unobservable and uncontrollable.

Consider the system given by (2.67) and (2.68):

$$\boldsymbol{\Delta\dot{x} = A\Delta x + b}\Delta u \tag{2.67}$$

$$\Delta y = \boldsymbol{c\Delta x} \tag{2.68}$$

The transfer function is:

$$G(s) = \frac{\Delta y(s)}{\Delta u(s)} = \boldsymbol{c}(s\boldsymbol{I} - \boldsymbol{A})^{-1}\boldsymbol{b} \tag{2.69}$$

Equation (2.69) can be expressed as:

$$G(s) = \frac{R_1}{s - p_1} + \frac{R_2}{s - p_2} + ... + \frac{R_n}{s - p_n} \tag{2.70}$$

Where R_i is known as the *residue* of G(s) at pole p_i. [11, 12]

It is possible to express the transfer function in terms of eigenvalues and eigenvectors by expressing the state variables $\boldsymbol{\Delta x}$ in terms of transformed transformed variables $\boldsymbol{z}$:

$$G(s) = \frac{\Delta y(s)}{\Delta u(s)} = \boldsymbol{c\phi}(s\boldsymbol{I} - \boldsymbol{\Lambda})^{-1}\boldsymbol{\psi b} \tag{2.71}$$

Since $\boldsymbol{\Lambda}$ is a diagonal matrix:

$$G(s) = \sum_{i=1}^{n} \frac{R_i}{s - p_i} \tag{2.72}$$

Where

$$R_i = \boldsymbol{c\phi_i\psi_i b} \tag{2.73}$$

2.4 Final Considerations

The basic concepts of angular stability of power systems have been described in this chapter, including transient and small-signal stability analyses review. These concepts are used in the next chapters of this thesis.

Modal analysis principles have been presented, including the concepts of eigenvalues, eigenvectors, participation factors, mode shapes, controllability, observability and transfer functions residues.

Chapter 3

Transport Delay Modeling

The main objective of this chapter is review basic concepts related to power system modelling and discuss the representation of transport delays. Based on the presented concepts, advances in techniques for small-signal stability analysis are developed and the theoretical and mathematical aspects behind these advances are described.

3.1 Basic Concepts

Chapter 2 has described the conventional small-signal state space modelling, presenting the traditional and the decoupled equations form. Moreover, elementary theory about the well-known modal sensibility analysis has been introduced.

However, for large scale power systems, the linear techniques for small-signal stability analysis are usually based on the descriptor system representation (*"Differential and Algebraic Equations – DAE"*), as follows:

$$\boldsymbol{T}\dot{\boldsymbol{x}} = \boldsymbol{A}\boldsymbol{x} + \boldsymbol{B}\boldsymbol{u} \tag{3.1}$$

$$\boldsymbol{y} = \boldsymbol{C}\boldsymbol{x} + \boldsymbol{D}\boldsymbol{u} \tag{3.2}$$

Where:

- For the general case, $\boldsymbol{T}$ has constant elements and is not necessarily reversible.

One can see that the main difference between the state space representation shown in (2.7) and (2.8) and the descriptor system representation shown in (3.1) and (3.2) is the matrix $\boldsymbol{T}$.

In the particular case where $\boldsymbol{T}$ has only unitary elements, it becomes the identity matrix and the formulation results on the state space modelling.

Another particular case consists in a matrix $\boldsymbol{T}$ with only unitary and zero elements. In this case, the differential equations and algebraic equations may be separated and (3.1) and (3.2) can be written as:

$$\begin{bmatrix} \dot{\boldsymbol{x}} \\ 0 \end{bmatrix} = \begin{bmatrix} \boldsymbol{A_1} & \boldsymbol{A_2} \\ \boldsymbol{A_3} & \boldsymbol{A_4} \end{bmatrix} . \begin{bmatrix} \boldsymbol{x} \\ \boldsymbol{r} \end{bmatrix} + \begin{bmatrix} \boldsymbol{B_x} \\ \boldsymbol{B_r} \end{bmatrix} \boldsymbol{u} \tag{3.3}$$

$$\boldsymbol{y} = \boldsymbol{C_x x} + \boldsymbol{C_r r} + \boldsymbol{D u} \tag{3.4}$$

Where the vector $\boldsymbol{r}$ is the algebraic variable vector and the matrix $\boldsymbol{T}$ is given by (3.5).

$$\boldsymbol{T} = \begin{bmatrix} \boldsymbol{I} & \boldsymbol{0} \\ \boldsymbol{0} & \boldsymbol{0} \end{bmatrix} \tag{3.5}$$

Where $\boldsymbol{I}$ is the identity matrix with the dimension equal to the number of system state variables.

Equations (3.3) and (3.4) can be transformed into a space state modelling by the algebraic variables elimination as follows:

$$\boldsymbol{A_3 x} + \boldsymbol{A_4 r} + \boldsymbol{B_r u} = \boldsymbol{0} \rightarrow \boldsymbol{r} = -\boldsymbol{A_4}^{-1}\boldsymbol{A_3 x} - \boldsymbol{A_4}^{-1}\boldsymbol{B_r u} \tag{3.6}$$

Using (3.6) in (3.3) and (3.4):

$$\dot{\boldsymbol{x}} = (\boldsymbol{A_1} - \boldsymbol{A_2}\boldsymbol{A_4}^{-1}\boldsymbol{A_3})\boldsymbol{x} + (\boldsymbol{B_x} - \boldsymbol{A_2}\boldsymbol{A_4}^{-1}\boldsymbol{B_r})\boldsymbol{u} \tag{3.7}$$

$$\boldsymbol{y} = (\boldsymbol{C_x} - \boldsymbol{C_r}\boldsymbol{A_4}^{-1}\boldsymbol{A_3})\boldsymbol{x} + (\boldsymbol{D} - \boldsymbol{C_r}\boldsymbol{A_4}^{-1}\boldsymbol{B_r})\boldsymbol{u} \tag{3.8}$$

Equations (3.7) and (3.8) show the system modelled into a differential and algebraic equations and transformed into a space state modeling.

In order to include the transport delay representation, frequency modelling, here called as *Y(s)*-formulation, is used. In fact, the formulation presented in (3.7) and (3.8) has some constrains associated to delays modelling as will be shown in the next section. The mathematical expressions of *Y(s)*-formulation are shown in (3.9) and (3.10) and have been derived from [13]:

$$\boldsymbol{Y(s)\Delta x(s)} = \boldsymbol{B\Delta u(s)} \tag{3.9}$$

$$\boldsymbol{\Delta y(s)} = \boldsymbol{C\Delta x(s)} + \boldsymbol{D\Delta u(s)} \tag{3.10}$$

Where:

- $\boldsymbol{Y}(s)$ is the system matrix;
- $\boldsymbol{B}$ is the input matrix;
- $\boldsymbol{C}$ is the output matrix;
- $\boldsymbol{D}$ is the matrix which direct links the input with the output;
- $\boldsymbol{\Delta x}(s)$ is the state vector in frequency domain;
- $\boldsymbol{\Delta u}$ is the input vector in frequency domain;
- $\boldsymbol{\Delta y}$ is the output vector in frequency domain;

The system matrix $\boldsymbol{Y(s)}$ in the s-domain is in general a non-linear function of s. The descriptor system shown in (3.1) and (3.2) is a particular case where $\boldsymbol{Y(s)} = (s.\boldsymbol{T} - \boldsymbol{A})$, as shown below.

Applying the Laplace transformation in (3.1) and (3.2) and considering null initial conditions, it is possible to obtain:

$$s\boldsymbol{T}\boldsymbol{x}(s) = \boldsymbol{A}\boldsymbol{x}(s) + \boldsymbol{B}\boldsymbol{u}(s) \tag{3.11}$$

$$\boldsymbol{y}(s) = \boldsymbol{C}\boldsymbol{x}(s) + \boldsymbol{D}\boldsymbol{u}(s) \tag{3.12}$$

Rewritten (3.11):

$$(s\boldsymbol{T} - \boldsymbol{A})\boldsymbol{x}(s) = \boldsymbol{B}\boldsymbol{u}(s) \tag{3.13}$$

$$\boldsymbol{y}(s) = \boldsymbol{C}\boldsymbol{x}(s) + \boldsymbol{D}\boldsymbol{u}(s) \tag{3.14}$$

The $\boldsymbol{Y(s)}$-formulation was used previously for electromagnetic and harmonic analysis where the transmission system dynamics was fully represented by a nodal admittance non-linear function of s. [14–16]

3.2 The Transport Delay

The transport delay can be understood as the time between one action and the sensitivity of its effects. [9]

The mathematical definition of a transport delay in time domain is:

$$x_d(t) = x(t - \tau) \tag{3.15}$$

Where x_d is a system variable delayed in relation to x by a time period τ.

In the complex frequency domain, the transfer function between variables x_d and x can be obtained by using the Laplace transform in both terms of (3.15). Therefore:

$$X_d(s) = \int_0^\infty e^{-st}.x(t - \tau).dt = X(s).e^{-s\tau} \tag{3.16}$$

Here, the variable x_d is called as a delayed variable in time domain and X_d is called as a delayed variable in frequency domain.

The representation of transport delays as shown in (3.15) and (3.16) turns the system model (3.1) and (3.2) into an infinite system, with an infinite number of poles. Therefore, the traditional modelling cannot be used for an accurate representation of the transport delay in linear analysis.

In order to include the transport delay more accurately in the traditional modelling, a high order series in the Laplace domain, such as Padé approximations (3.17) or Taylor expansions (3.18), using a rational transfer function, may be used. However, these representations are still approximated. Moreover, the system dimension increases significantly and eventually spurious high frequency poles may appear in the frequency range where the infinite series is truncated. In order to avoid such problems, the transport delay has not been fully represented in power system studies. In fact, just a first order approximation has been considered.

$$e^{-s\tau} = \frac{1 - \frac{s\tau}{2.1!} + \frac{s^2\tau^2}{2^2.2!} - \frac{s^3\tau^3}{2^3.3!} + ...}{1 + \frac{s\tau}{2.1!} + \frac{s^2\tau^2}{2^2.2!} + \frac{s^3\tau^3}{2^3.3!} + ...} \tag{3.17}$$

$$e^{-s\tau} = \frac{1}{1 + s\tau + \frac{s^2\tau^2}{2!} + \frac{s^3\tau^3}{3!} + ...} \tag{3.18}$$

This thesis proposes the use of non-conventional s-domain modelling (3.9) and (3.10) for small-signal analysis of large power systems with multiple transport delays.

A particular approach is here proposed for dealing with power system dynamics, considering the inclusion of multiple transport delays, yielding the following formulation:

$$(\boldsymbol{M}(s) + s\boldsymbol{T} - \boldsymbol{A})\Delta\boldsymbol{x}(s) = \boldsymbol{B}\Delta\boldsymbol{u}(s) \tag{3.19}$$

$$\Delta\boldsymbol{y}(s) = \boldsymbol{C}\Delta\boldsymbol{x}(s) + \boldsymbol{D}\Delta\boldsymbol{u}(s) \tag{3.20}$$

The differences between (3.13) and (3.14) and (3.19) and (3.20) are the terms Δ and $\boldsymbol{M}(s)$. While the former means that for each variable vector, there are deviations in relation to the operation point, the latter is a diagonal matrix with $e^{-s\tau_i}$ at the positions with equations with transport delays and zeros at the other positions.

Supposing a generic transport delay equation i, associated to the variable Δx_i, which is delayed by τ_i in relation to variable Δx_j, the following relationship is obtained, based on (3.16):

$$e^{s\tau_i}.\Delta v_i - \Delta x_j = 0 \tag{3.21}$$

Therefore, at line i, $a_{i,j} = 1$, $a_{i,k\neq j} = 0$, $m_{i,i} = e^{s\tau_i}$ and $m_{i,k\neq i} = 0$, where $a_{i,j}$ and $m_{i,j}$ are elements of A and M, respectively.

Computationally, the information of M and T are condensed in an column vector with the same dimension of $\boldsymbol{x}$ where the numbers 0, 1 and 2, are flags that represent algebraic, differential and transport delay equations, as shown in (3.22) [17].

$$Vector \rightarrow \begin{bmatrix} 1 \\ \dots \\ 2 \\ \dots \\ \dots \\ 0 \\ 0 \end{bmatrix} \begin{matrix} \Rightarrow Differential \\ \\ \Rightarrow \quad Delay \\ \\ \\ \Rightarrow \quad Algebraic \\ \Rightarrow \quad Algebraic \end{matrix} \tag{3.22}$$

3.3 Modal Analysis Tools for Systems with Transport Delays

This section presents mathematical advances and computational methodologies to allow a comprehensive modal analysis using accurate representation of transport de- lays. The proposed modelling and methodologies are implemented in the production-grade software PacDyn [18], developed by the Electrical Energy Research Centre (CEPEL).

3.3.1 Time and Frequency Response

The time response of a descriptor system is efficiently obtained using trapezoidal rule. When considering transport delay equations, each delayed variable $\Delta x_i(t)$ is equal to the previous value $\Delta x_j(t - \tau_i)$ as shown by (3.15).

The transport delay function, although conceptually simple, presents some complications for its implementation, such as:

- Memory allocation;
- Interpolation for points not matching memory;
- Copy and transfer values for each response step.

From the computational point of view, the transport delay equation is replaced by an algebraic equation with the diagonal element of A equal to 1 ($a_{(i,i)} = 1$) and the right-hand side term is equal to $\Delta x_j(t - \tau_i)$ that is already known at time t. At the end of each iteration, the values of all variables $\Delta x_j(t)$ is saved to be used after the period τ_i. If τ_i is not multiple of the time step, a linear interpolation may be used. In the efficient implementation of the method, a circular list is used to save the values of $\Delta x_j(t)$ during the period τ_i.

In a simulation with step Δt, it is necessary that N points represent the delay τ of the block output relative to the input. Assuming initially that the delay time τ is divisible by the value of the integration step, then one has to:

$$N = \frac{\tau}{\Delta t} \tag{3.23}$$

In cases where the delay time is not divisible by the integration step, it is necessary to allocate more memory space for the value vector, therefore (3.23) turns:

$$N = \frac{\tau}{\Delta t} + 1 \tag{3.24}$$

Logically, one can infer that there is not only a transport delay block in the system. There may be K delay units in the system, therefore, the memory allocation becomes more complicated.

Assuming that for K transport delay blocks, the numbers of points required for their representation have already been defined, namely:

$$\begin{bmatrix} \tau_1 \\ \tau_2 \\ \vdots \\ \tau_j \\ \vdots \\ \tau_K \end{bmatrix} \begin{matrix} \Rightarrow N_1 \\ \Rightarrow N_2 \\ \vdots \\ \Rightarrow N_j \\ \vdots \\ \Rightarrow N_K \end{matrix} \tag{3.25}$$

The amount of memory space to be allocated by each transport delay block will not necessarily be equal, thus, it was necessary to develop two vectors:

- a vector of size $N = \sum_{i=1}^{K} N_i$ to store the input values of the blocks;
- pointer vector of size K, which indicates where is the position representing the current time for each block.

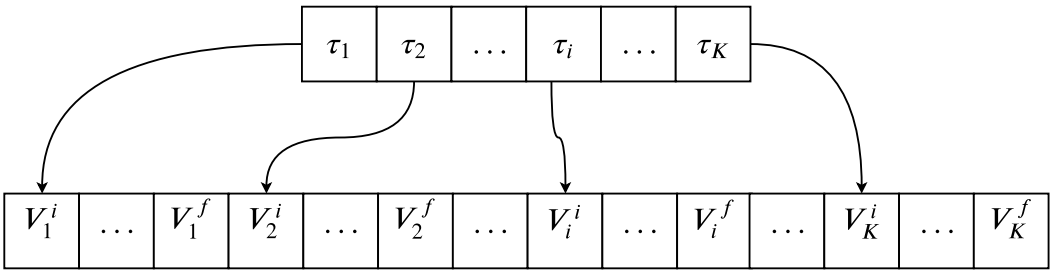

Figure 3.1: Pointing vector and value vector.

In cases where the delay time is not divisible by the integration step. it is necessary to use a linear interpolation method, so that the value of the delayed function is effectively passed to the value vector.

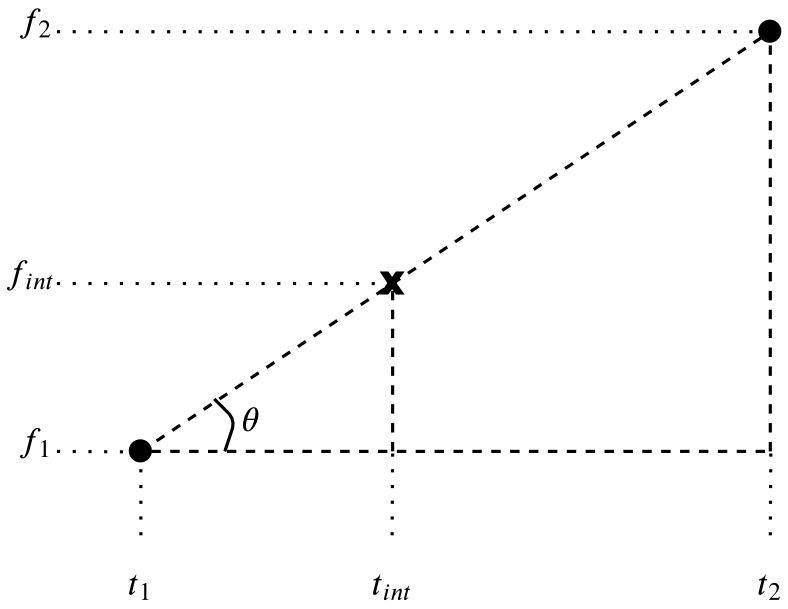

Figure 3.2: Interpolation of unmatched points in memory.

Thus:

$$tan\theta = \frac{f_2 - f_{int}}{t_2 - t_{int}} = \frac{f_{int} - f_1}{t_{int} - t_1} \tag{3.26}$$

Where:

$$\Delta t_2 = t_2 - t_{int} \quad and \quad \Delta t_1 = t_{int} - t_1 \tag{3.27}$$

Then:

$$f_{int} = \frac{f_2 \Delta t_1 + f_1 \Delta t_2}{\Delta t_1 + \Delta t_2} \tag{3.28}$$

After the value of the current time v_j^i being plotted, the values vector must be updated to make room to a v_j^f value, i.e., the last position values vector must be completed with the current time value delay block input variable.

The values vector must be updated with the forward travel of all values, i.e., the simulation time update. The process is illustrated by the figure below.

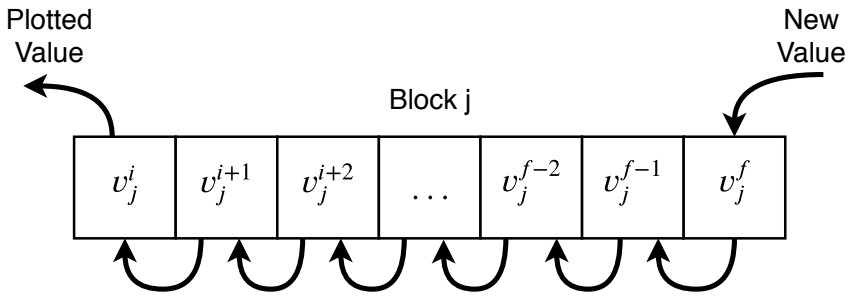

Figure 3.3: Delay vector update.

The frequency scan method corresponds to the graphs of the magnitude and phase of the transfer function $G_{i,j}(s)$ as a function of the frequency ω, where s is substituted for $j\omega$ and ω varies from a small value (ideally zero) to a large value (ideally infinite). The frequency scan of the magnitude provides an overview of the whole set of dominant poles and zeros, since its maxima frequencies are near the imaginary parts of the poles and the minima frequencies are near the imaginary parts of the zeros. Therefore, the frequency scan method can be used for yielding automatic estimates for dominant pole algorithm, as presented in [14]. Other interesting information is related to the band width of the maxima, where a small band width means a low damping ratio pole. The maxima magnitude is also related to the pole influence, a larger magnitude means more pole dominance.

The control system design here proposed to be used in systems with transport delays is the Damped Nyquist Plot (DNP) method [19]. It is based on the frequency response along the complex frequencies of a constant damping ratio line.

The frequency response computation will be presented later in this Chapter.

3.3.2 Eigenvalues, Eigenvectors and Participation Factors

The main feature of modal analysis is the pole calculation that defines the natural oscillation modes of the system. For large scale power systems, partial pole solutions are used. There are methods based on proximity to the estimates, or, based on the dominance of a transfer function. The last ones, called dominant pole methods, are of more practical use, since it allows the analyst to define a transfer function at the region of interest and the algorithm will converge to some dominant pole of that region.

An algorithm for partial pole solution is proposed in [14] to calculate sequentially the whole set of dominant poles of a certain transfer function for the general s-domain

formulation, shown in (3.29) and (3.30). The term D is supposed to be zero, but there is no lack of generality.

$$\boldsymbol{Y}(\boldsymbol{s})\boldsymbol{x}(\boldsymbol{s}) = \boldsymbol{B}\boldsymbol{u}(\boldsymbol{s}) \tag{3.29}$$

$$\boldsymbol{y}(\boldsymbol{s}) = \boldsymbol{C}^t\boldsymbol{x}(\boldsymbol{s}) \tag{3.30}$$

The mathematical basis developed in [14] is reproduced bellow. Equation (3.31) describes a transfer function and (3.32) gives a system pole λ:

$$G(s) = \frac{y(s)}{u(s)} = \boldsymbol{c^t}\boldsymbol{Y}(s)^{-1}\boldsymbol{b} \tag{3.31}$$

$$\begin{gathered}\boldsymbol{Y}(\lambda)\boldsymbol{v} = \boldsymbol{0} \\ \boldsymbol{v} \neq \boldsymbol{0}\end{gathered} \tag{3.32}$$

One should note that if λ is a system pole, there is a non-null vector $\boldsymbol{v}$ which multiplied by $\boldsymbol{Y}(\lambda)$ gives the null vector. Therefore:

$$\begin{gathered}\boldsymbol{w}^t\boldsymbol{Y}(\lambda) = \boldsymbol{0}^t \\ \boldsymbol{W}^t \neq \boldsymbol{0}^t\end{gathered} \tag{3.33}$$

$$F(\lambda) = \frac{1}{G(\lambda)} = 0 \tag{3.34}$$

Using Newton method in (3.34):

$$\frac{1}{G(\lambda^{(k)})} - \frac{1}{G(\lambda^{(k)})^2}\frac{dG(\lambda^{(k)})}{ds}\Delta\lambda^{(k)} = 0 \tag{3.35}$$

And:

$$\frac{dG(\lambda^{(k)})}{ds}\Delta\lambda^{(k)} = G(\lambda^{(k)}) \tag{3.36}$$

Using (3.31) in (3.36):

$$\boldsymbol{c^t}\frac{d\boldsymbol{Y}(\lambda^{(k)})^{-1}}{ds}\boldsymbol{b}\Delta\lambda^{(k)} = \boldsymbol{c^t}\boldsymbol{Y}(\lambda^{(k)})^{-1}\boldsymbol{b} \tag{3.37}$$

And:

$$\Delta\lambda^{(k)} = \frac{\boldsymbol{c^t}\boldsymbol{Y}(\lambda^{(k)})^{-1}\boldsymbol{b}}{\boldsymbol{c^t}\frac{d\boldsymbol{Y}(\lambda^{(k)})^{-1}}{ds}\boldsymbol{b}} \tag{3.38}$$

The inverse matrix of $\frac{d\boldsymbol{Y}(\lambda^{(k)})^{-1}}{ds}$ can be obtained using the following property:

$$\boldsymbol{Y}\boldsymbol{Y}^{-1} = \boldsymbol{I} \;\; \rightarrow \;\; \frac{d(\boldsymbol{Y}\boldsymbol{Y}^{-1})}{ds} = \frac{d(\boldsymbol{I})}{ds} = \boldsymbol{0} \tag{3.39}$$

Therefore:

$$\frac{d(\boldsymbol{Y}\boldsymbol{Y}^{-1})}{ds} = \boldsymbol{Y}\frac{d\boldsymbol{Y}^{-1}}{ds} + \frac{d\boldsymbol{Y}}{ds}\boldsymbol{Y}^{-1} = \boldsymbol{0} \tag{3.40}$$

And:

$$\frac{d\boldsymbol{Y}^{-1}}{ds} = -\boldsymbol{Y}^{-1}\frac{d\boldsymbol{Y}}{ds}\boldsymbol{Y}^{-1} \tag{3.41}$$

Finally:

$$\Delta\lambda^{(k)} = -\frac{\boldsymbol{c^t}\boldsymbol{Y}(\lambda^{(k)})^{-1}\boldsymbol{b}}{\boldsymbol{c^t}\boldsymbol{Y}(\lambda^{(k)})^{-1}\frac{d\boldsymbol{Y}(\lambda^{(k)})}{ds}\boldsymbol{Y}(\lambda^{(k)})^{-1}\boldsymbol{b}} \tag{3.42}$$

With the pole corrected by:

$$\lambda^{(k+1)} = \lambda^{(k)} + \Delta\lambda^{(k)} \tag{3.43}$$

And, for the case with transport delays, assuming the particular case for the $Y(s)$:

$$\boldsymbol{Y}(s) = (\boldsymbol{M}(s) + s.\boldsymbol{T} - \boldsymbol{A}) \tag{3.44}$$

$Y(s)$ derivative in relation to s:

$$\frac{d\boldsymbol{Y}(s)}{ds} = \boldsymbol{T} + \frac{d\boldsymbol{M}(s)}{ds} \tag{3.45}$$

Where the diagonal elements of $\frac{d\boldsymbol{M}(s)}{ds}$ for the lines with transport delays are given in (3.46). The other elements are zero.

$$\frac{dm_{i,i}(s)}{ds} = \tau_i e^{s\tau_i} \tag{3.46}$$

In the proposed $\boldsymbol{Y}(s)$-formulation, the elements in vectors Δx may be state, algebraic or delayed variables. When considering delayed vectors, it is not possible to compute the eigenvectors, since the system with transport delays are infinite systems. As a result, the eigenvectors, whose dynamics are embedded in the corresponding delayed variables of Δx, would have infinite dimensions.

As explained in Chapter 2, the participation factor $p_{i,k}$ is the sensitivity of the eigenvalue λ_k to the diagonal element $a_{i,i}$ of the state matrix A. The participation factor can also be interpreted as the contribution of state variables of the system on a certain pole.

The participation factors cannot be calculated as a function of eigenvectors, since the system with transport delays is an infinite system.

As shown in [20], the participation factor of a certain state variable Δx_i is equal

to the residue of a transfer function whose input variable Δu_j is a signal applied to the differential equation corresponding to Δx_i, and the output variable is the same state variable Δx_i before the input application.

Therefore, to calculate participation factors as a function of the residues of a certain transfer function $G_{i,i}(s)$ for the $\boldsymbol{Y}(s)$-formulation, for each state variable, $G_{i,i}(s)$ is defined by the column vector $\boldsymbol{c}_i$ and line vector $\boldsymbol{c}_i^t$ that are built with 1 at the position of the state variable Δx_i and 0 at the other positions.

$$p_{i,k} = R_k^{i,i} \tag{3.47}$$

One should note that the participation factors are not calculated for algebraic equations nor for the delayed equations. Theoretically, there would be an infinite number of participation factors embedded into each delayed variable. However, considering that the key purpose of participation factors calculation is to identify the main state variable responsible for a certain pole, when a delayed variable has a large participation for a certain pole, the other state variables in that control loop also will present large participation. Consequently, the same information is obtained.

3.3.3 Residue, Controlability and Observability

The transfer function residues can be calculated during the iterative procedure using the dominant pole algorithm, described in previous subsection, but more robust methods can be used, as shown in [21]. The mathematical procedure for residue calculation using the dominant pole algorithm will be described below.

The residue of a transfer function can be described as follows:

$$R_i = \lim_{s \to \lambda_i} G(s)(s - \lambda_i) \tag{3.48}$$

Where, numerically, $s = \lambda_i - \Delta\lambda_i$. (with $\Delta\lambda_i$ being a very small value, 10^{-8}, for example.)

Therefore:

$$R_i = -G(\lambda_i - \Delta\lambda_i)\Delta\lambda_i \tag{3.49}$$

The value λ_i is the pole λ^{k+1} and the value $\Delta\lambda_i$ is the last pole correction before the convergence $\Delta\lambda^k$. Therefore, the value $\lambda_i - \Delta\lambda_i$ is the shift immediately before convergence λ^k. Thus:

$$R_i = -G(\lambda^{k+1} - \Delta\lambda^k)\Delta\lambda_k \tag{3.50}$$

Finally:

$$R_i = -G(\lambda_k)\Delta\lambda_k \tag{3.51}$$

The algorithm for computation of residues will be shown in the next subsection.

After dominant poles calculation, the transfer function is analytically written as the following summation:

$$G_{i,j}(s) = \sum_k \frac{R^k_{i,j}}{s - \lambda_k} \tag{3.52}$$

Where λ_k are the dominant poles of the transfer function $G_{i,j}(s)$ and $R^k_{i,j}$ are the associated residues. Transfer function residues can be interpreted as a measure of the system pole influence in the selected output variable Δy_i when this pole is excited by the selected input variable Δu_j [20].

In [20], it is shown that the residue also corresponds to the sensitivity of the pole shift for an incremental gain feedback. Therefore, the residue can be used to identify the most adequate transfer function to be used for feedback stabilization.

Equations (2.65) and (2.66), repeated below, show the decoupled form of a dynamic system:

$$\dot{\boldsymbol{z}} = \boldsymbol{\Lambda z} + \boldsymbol{B'}\Delta\boldsymbol{u} \tag{2.65 Revisited}$$

$$\Delta\boldsymbol{y} = \boldsymbol{C'z} + \boldsymbol{D}\Delta\boldsymbol{u} \tag{2.66 Revisited}$$

Since Λ is diagonal, the system can be solved for each mode variable z_k associated to eigenvalue λ_k. For simplicity, a SISO transfer function $G_{i,j}(s)$ (input Δu_i, output Δy_i) is considered. Therefore:

$$\Delta\dot{z}_k(t) = \lambda_k.\Delta z_k(t) + b'_k\Delta u_j(t) \tag{3.53}$$

Where the lower-case coefficients correspond to their respective matrix elements. The s-domain solution for $z_k(s)$ is then obtained from (3.53):

$$\Delta z_k(s) = \frac{b'_{i,j}}{s - \lambda_k}\Delta u_j(s) \tag{3.54}$$

The output variable Δy_i can be obtained from line i of (2.66):

$$\Delta y_i(s) = \boldsymbol{c'_i}\Delta\boldsymbol{z_k}(s) + d_{i,j}\Delta u_j(s) \tag{3.55}$$

Expanding the vector multiplication $\boldsymbol{c'_i}\Delta\boldsymbol{z_k}(s)$ into a summation and substituting Equation (3.53) into Equation (3.55):

$$G_{i,j}(s) = \frac{\Delta y_i(s)}{\Delta u_j(s)} = \sum_k \frac{c'_{i,k}b'_{k,j}}{s - \lambda_k} + d_{i,j} \tag{3.56}$$

Therefore, comparing (3.52) and (3.56), the residue of a pole λ_k can be given as the product of the observability factor of that pole, associated to the output variable Δy_i, by the controllability factor of the same pole associated to the input variable Δu_j:

$$R^k_{i,j} = c'_{i,k}b'_{k,j} \tag{3.57}$$

The residue is a measure of the influence of a pole into a transfer function. Consequently, the controllability factor measures the separated influence into the input variables and the observability factor measures the pole influence into the output variables. In other words, the controllability factor measures the capability of the input variable to excite a modal component of a pole, in frequency or time domain. Analogously, the observability factor measures how much of the pole appears at the output variable.

The traditional method for stabilization uses the residues for the loop selection

for stabilization, once the control scheme is local. Indirectly, controllability and observability are used to identify the best input and output variables for the control. However, controllability and observability factors can be used to select separately the most adequate input and output variables to be used for feedback stabilization. In control systems with remote signals, those variables are not necessarily in the same geographic location. In the $\boldsymbol{Y}(s)$-formulation proposed here, the elements in vectors Δx may be state, algebraic or delayed variables. The residues can be obtained using the dominant pole algorithm or other method as shown in [21], but not the eigenvectors. When considering delayed vectors, it is not possible to compute eigenvectors, since the system with transport delays are infinite systems. As a result, the eigenvectors, whose dynamics are embedded in the corresponding delayed variables of Δx, would have infinite dimensions.

In order to overcome this issue, it is proposed to use the residues for obtaining the observability and controllability factors. From Equation (3.57), one can see that the residue is the product of them. So, maintaining constant an input variable Δu_j, the residue $R_k^{i,j}$ may be calculated for several output variables Δy_i and the observability factor would be given by the division of this residue by the controllability factor. This controllability factor could not be calculated for infinite systems. However, assuming an infinite norm for the observability factor, the observability factor associated to output variable Δy_m with the largest residue may be considered as unitary ($c'_{m,k} = 1$). Consequently, the other variables will have relative values of it, equal to the residue of them divided by the largest residue:

$$c'_{i,k} = \frac{R_k^{i,j}}{R_k^{m,j}} \tag{3.58}$$

Similarly, the controllability factor, normalized for the input variable Δu_n of largest residue, is given by:

$$b'_{k,j} = \frac{R_k^{i,j}}{R_k^{i,n}} \tag{3.59}$$

Then, the controllability and observability factors still can be used in the proposed $\boldsymbol{Y}(s)$-formulation for measuring pole influence into the input and output variables or for selection of stabilization control loops, including the use of remote signals.

3.3.4 Computational Developments

The computational developments implemented for systems with transport delays will be described as follows. The methods were implemented first in MATLAB and later in software PacDyn [18].

3.3.4.1 Frequency Response

The frequency response development is illustrated in the diagram of Figure 3.4.

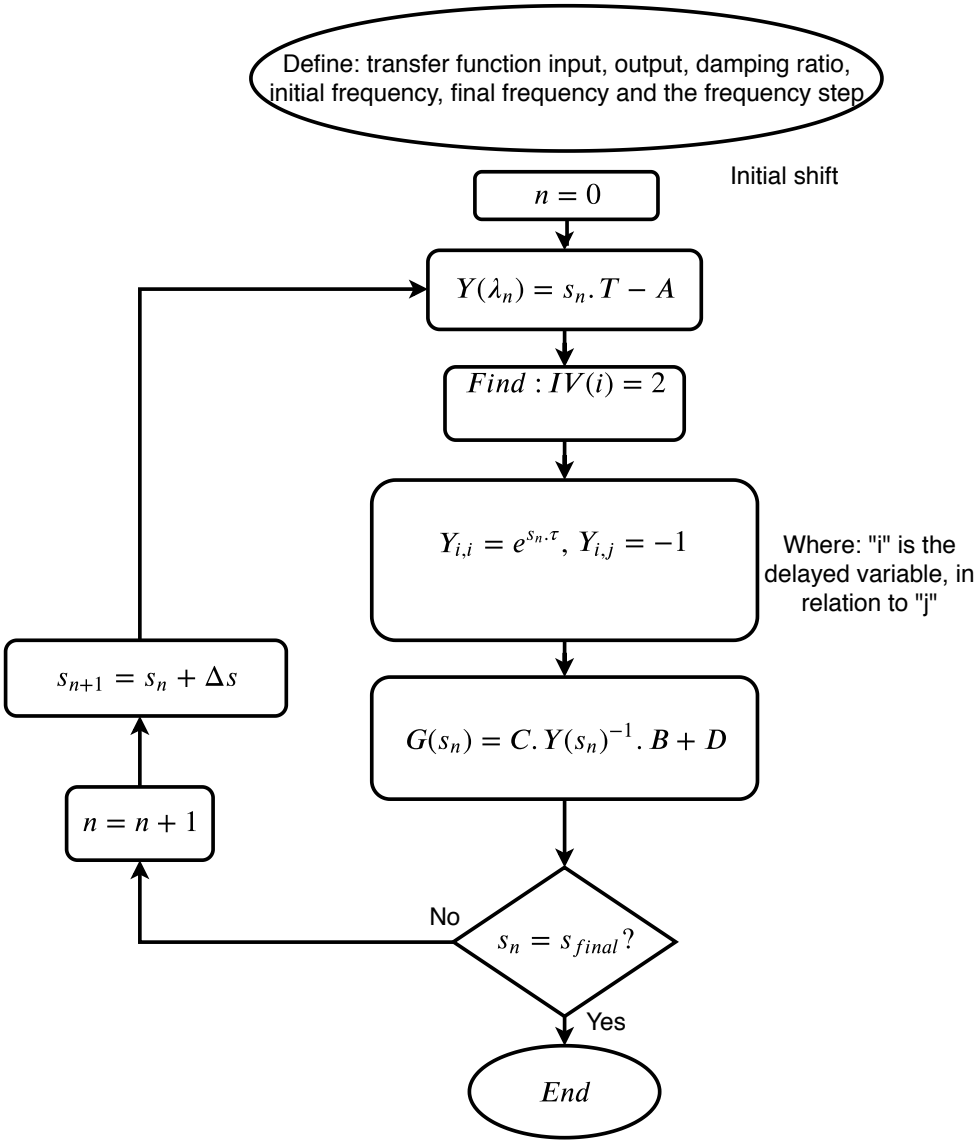

Figure 3.4: Frequency response calculation algorithm.

3.3.4.2 Single Dominant Pole Algorithm

The method implementation is based on the dominant pole calculation as described in [14] and is illustrated in the diagram presented in Figure 3.5.

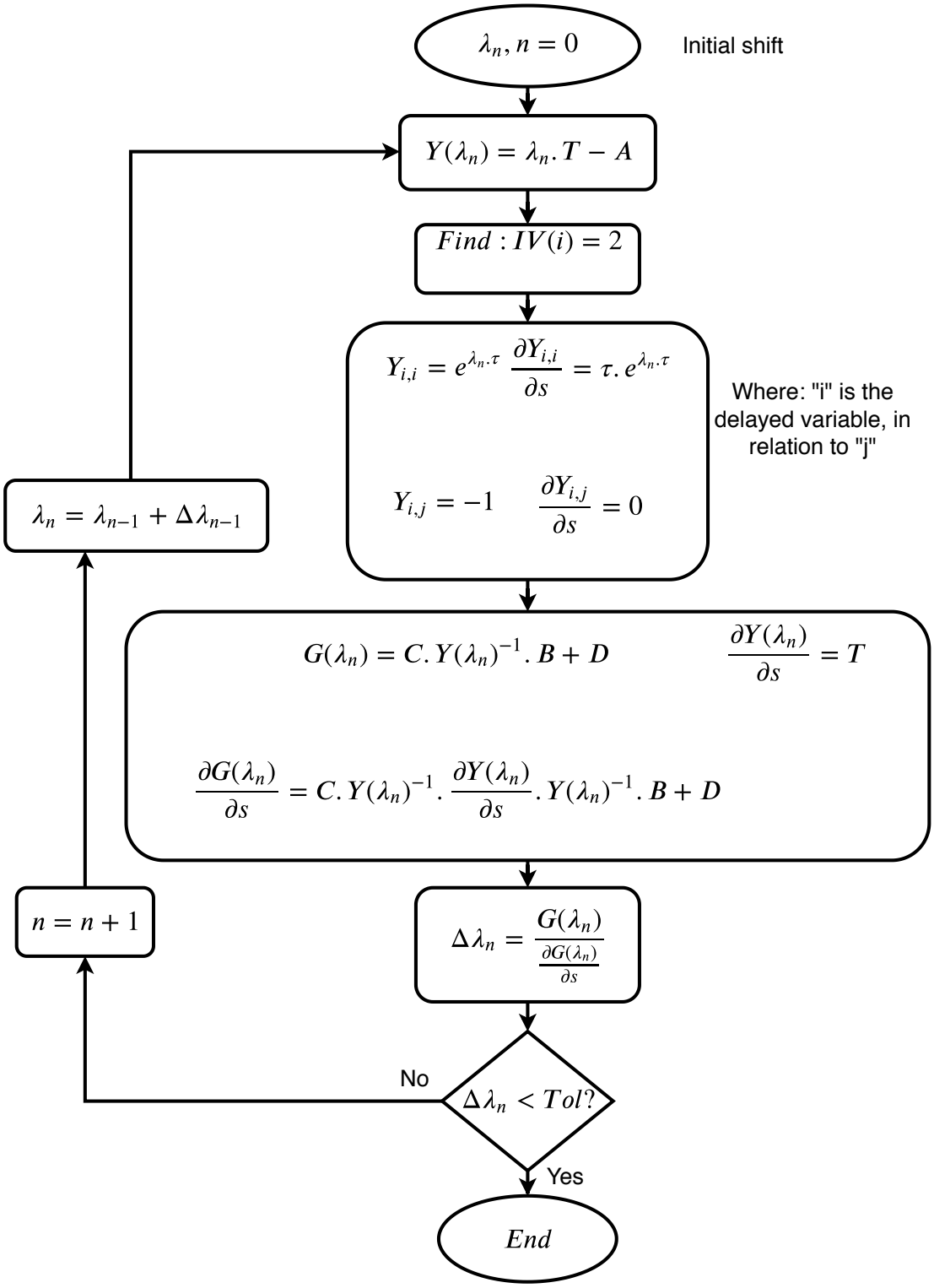

Figure 3.5: Dominant Pole Algorithm.

3.3.4.3 Residue

The algorithm for residue computation is depicted in Figure 3.6 and is based on (3.48) to (3.51).

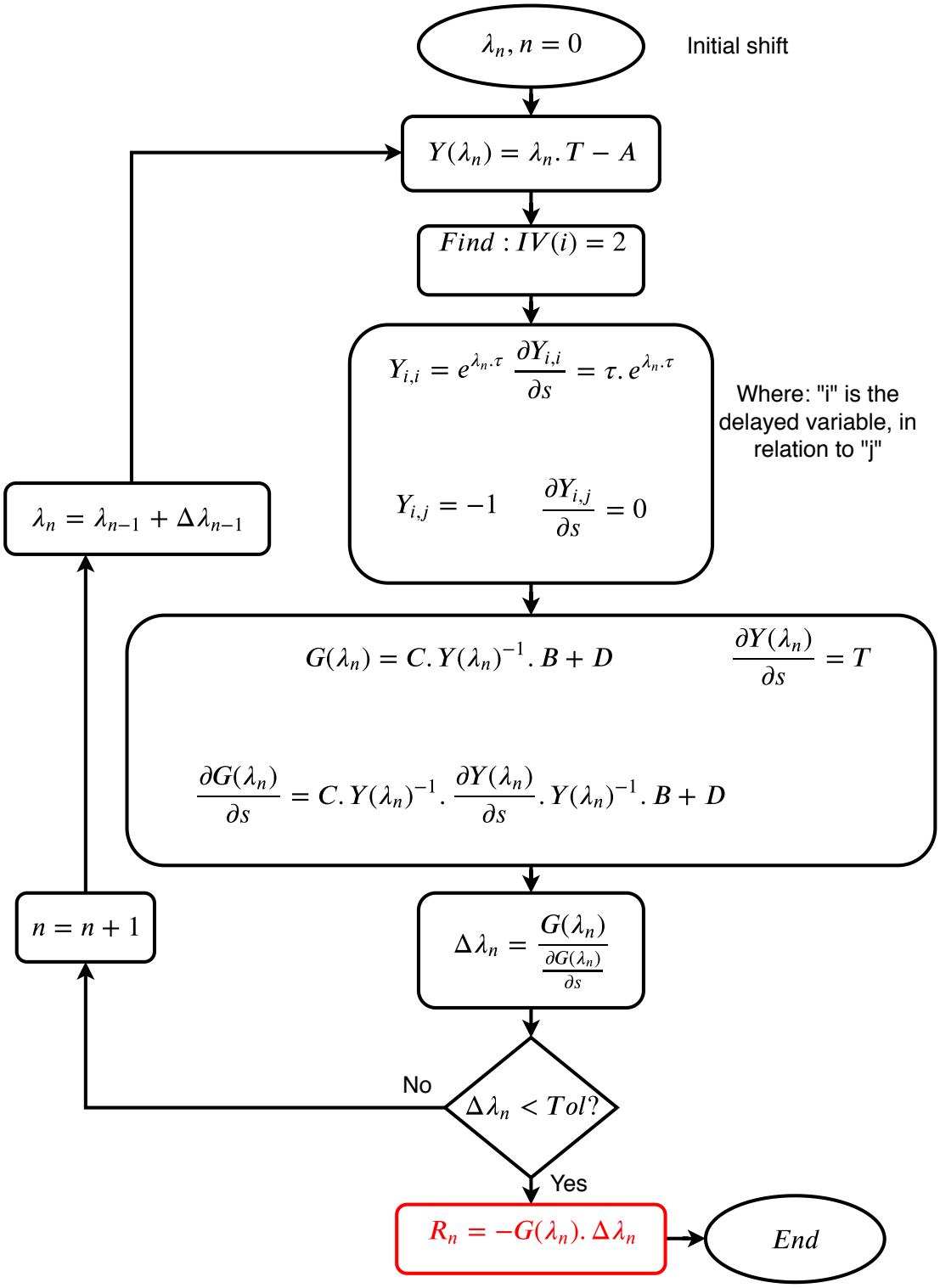

Figure 3.6: Residue using Dominant Pole Algorithm Diagram.

3.3.4.4 Sequential Dominant Pole Algorithm

After the development of residue computation algorithm, it is possible to remove the contributions of converged poles into a transfer function allowing to converge other poles with lower dominance, as illustrated in the diagram of Figure 3.7.

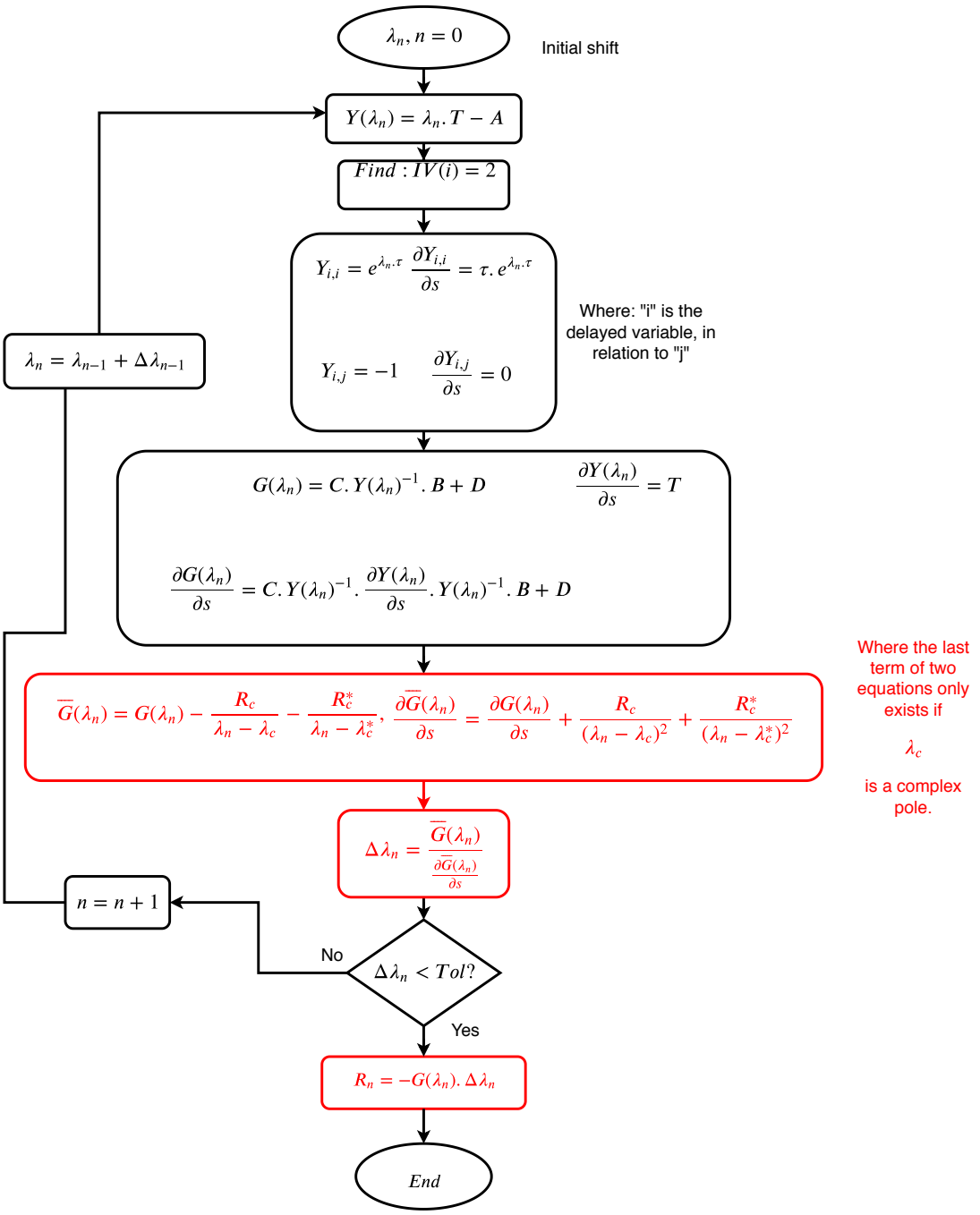

Figure 3.7: Sequential Dominant Pole Algorithm.

3.3.4.5 Observability Factor for Systems with Transport Delays Algorithm

The observability factor for systems with transport delays algorithm is presented in Figure 3.8.

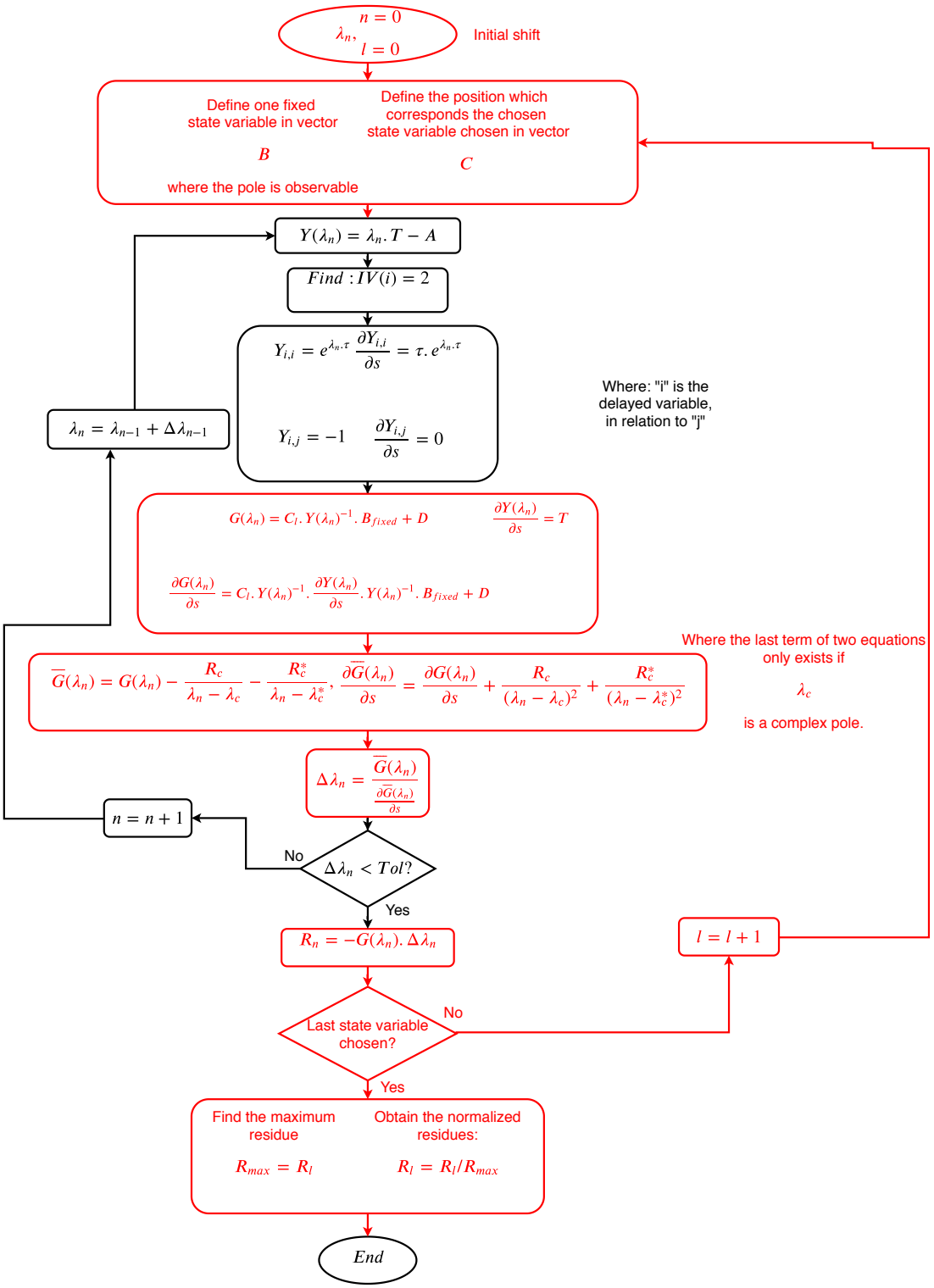

Figure 3.8: Observability Factor for Systems with Transport Delay Algorithm.

3.3.4.6 Controllability Factor for Systems with Transport Delays Algorithm

The controllability factor for systems with transport delays algorithm is presented in Figure 3.9.

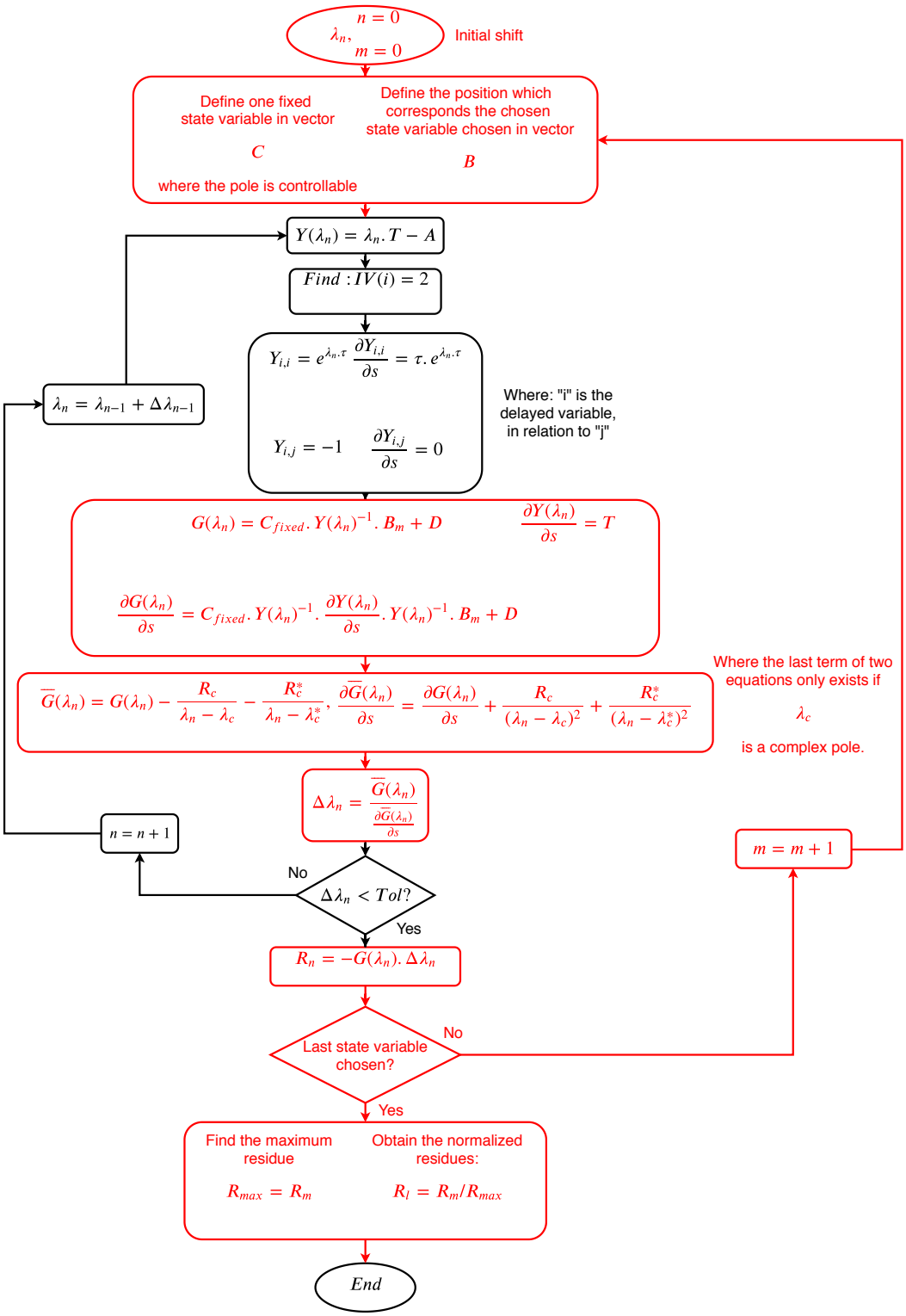

Figure 3.9: Controllability Factor for Systems with Transport Delay Algorithm.

3.4 Final Considerations

The concepts of frequency modelling, transport delay modelling and the limitations associated to the traditional modal analysis have been described in this chapter.

In addition, the advances in sensibilities calculation for systems with transport delays have been proposed in this chapter.

All theoretical formulations described in this chapter have been implemented in PacDyn software [18].

Chapter 4

Tests and Results

This chapter presents tests and simulation results using the methods developed in this thesis. The results are evaluated in order to highlight the benefits obtained through applying these methods in power system analysis. Initially, a two-area system is exploited in a tutorial and detailed analysis. After that, results for the Brazilian Interconnected Power System are presented.

4.1 Two-Areas System

The modal analysis tools for systems with transport delays are tested in a two-area system. This tutorial system has 11 buses and 4 machines [22].

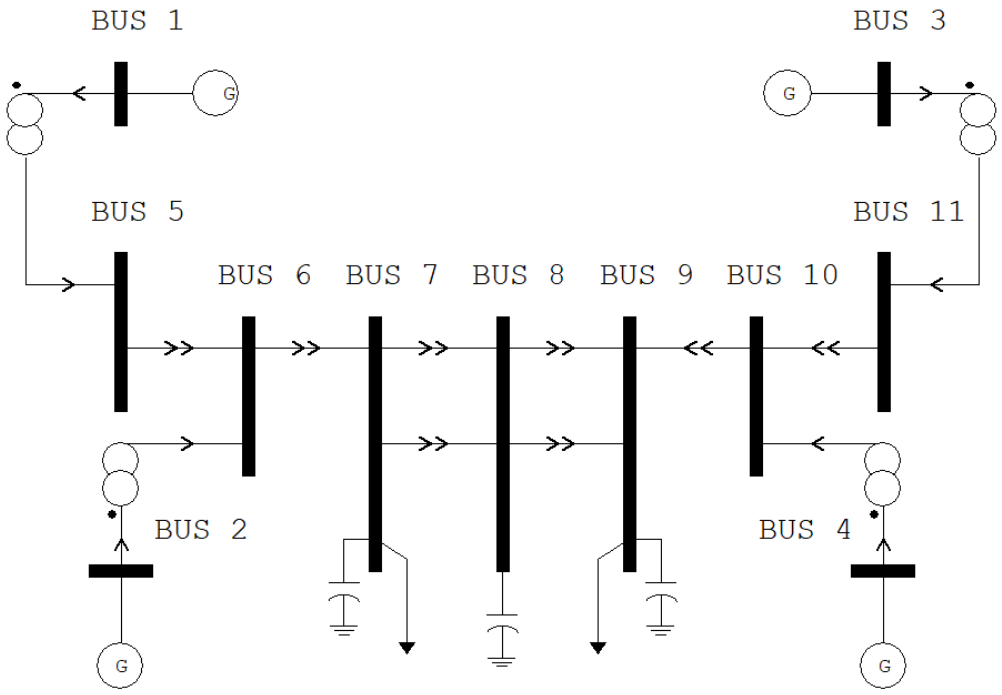

Figure 4.1: Single-line diagram of the two-area system.

Figure 4.1 presents the single-line diagram of the two-area system, showing interconnections between Areas #1 and #2. Area #1 has power plants at Buses #1 and #2, while, Area 2 has power plants at Buses #3 and #4.

The system was presenting a base case with the following characteristics:

- Power plant dispatch and terminal voltage at bus 1 = 1100 MW and 1.05 pu;
- Power plant dispatch and terminal voltage at bus 2 = 700 MW and 1.02 pu;
- Power plant dispatch and terminal voltage at bus 3 = 755 MW and 1.03 pu;
- Power plant dispatch and terminal voltage at bus 4 = 300 MW and 1.01 pu;
- Load at bus 7 = 1167 MW;
- Load at bus 9 = 1567 MW.

Using the QR method [23, 24], electromechanical poles can be identified by the largest participation factors being speed or loading angle of generators [7, 9, 25]. These poles are shown in Table 4.1, together with the frequency in hertz and damping ratio. The first pole has a negative damping ratio (-1.25%), responsible for the system instability, the second pole has a moderate damping ratio of (7.41%) and the third one is poorly damped (3.59%).

Table 4.1: Electromechanical System Poles, Without PSS.

Poles	**Frequency (Hz)**	**Damping Ratio (%)**
0.04912 + j 3.9397	0.6270	-1.2468
-0.5473 + j 7.3670	1.1725	7.4082
-0.2557 + j 7.1248	1.1339	3.5861

4.1.1 Solution Based on Local Signals

This system was primary used in [22] whose electromechanical modes were analyzed. The results obtained in [22] has been reproduced here for comparison purposes. Two local power system stabilizers are used in order to improve damping ratio of the three poles shown in Table 4.1. The parameter settings have been obtained using the Damped Nyquist Plot (DNP) [19] aiming at a pole placement design of local power system stabilizers, shown in Figure 4.2.

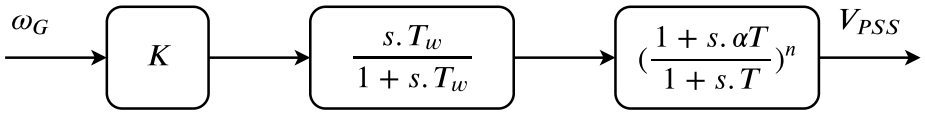

Figure 4.2: Structure of simple PSS stabilizing loop.

In [22], the generator G3 proved to be adequate to improve damping ratio of the first two poles, while G1 was adequate to improve the third pole. Table 4.2 shows the parameters of power system stabilizers connected to Machines 3 and 1, respectively.

Table 4.2: Local Power System Stabilizers, connected to G3 and G1.

Generator	**n**	**K**	T_w	**T**	α	w_c	w_{max}
G3	2	8.1561	10	0.12480	3.9548	7.37	4.00
G1	1	10.255	3	0.30000	1.8903	7.12	2.397

The electromechanical system poles, with PSS connected at generator G3, are shown in Table 4.3.

Table 4.3: Electromechanical System Poles, with PSS at G3.

Poles	**Frequency (Hz)**	**Damping Ratio (%)**
-0.8907 + j 3.9227	0.6243	22.144
-0.8908 + j 7.3700	1.1730	12.000
-0.2486 + j 7.1091	1.1315	3.4948

The electromechanical system poles, with PSSs connected at generators G3 and G1, are shown in Table 4.4.

Table 4.4: Electromechanical System Poles, with PSS at G3 and G1.

Poles	**Frequency (Hz)**	**Damping Ratio (%)**
-0.7667 + j 3.9817	0.6337	18.908
-0.9006 + j 7.3675	1.1726	12.133
-1.0802 + j 7.1200	1.1332	15.000

4.1.2 Solution Based on Remote Signals

Contrasting a local solution used in [22] and reproduced in Section 4.1.1, remote signal solution is proposed in order to improve the damping ratio of electromechanical oscillation modes. In order to illustrate the proposed methodology, the damping ratio improvement is performed by designing a single centralized PSS, using frequency measurements from dedicated channels, which is unusual, the two channels contain remote signals as shown in Figure 4.3.

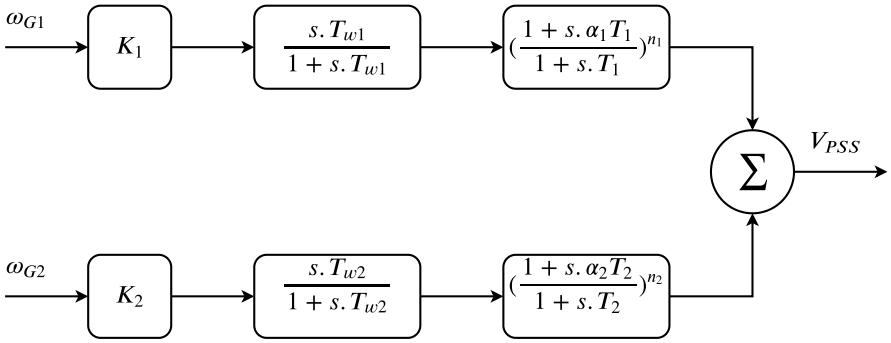

Figure 4.3: Figure 3. Structure of a two-channel centralized PSS.

It is noteworthy that the designer should include a limitation block after the summation block, usually of the order of +/- 0.1 pu, to avoid large PSS impact on the voltage regulation during the first period of large disturbances and to prevent inappropriate voltage offsets during significant speed machine variations. Non-windup limits can also be included at each channel to improve performance. For the linear analysis here presented, these limits were not included since they do not influence in the small-signal dynamics.

Table 4.5 shows the normalized observability factors of generators rotor speed for all three poles shown in Table 4.1, aiming at to evaluate the best input variables for a centralized power system stabilizer.

Table 4.5: Normalized Observability Factors, Electromechanical Poles.

Poles	**Machine 1**	**Machine 2**	**Machine 3**	**Machine 4**
0.04912 + j 3.9397	0.1035∠ 167	0.08706∠ -70	1.0∠ 178	0.8596∠ -180
-0.5473 + j 7.3670	0.07409∠ 75	0.1190∠ -89	0.2573∠ -178	1.0∠ -0.018
-0.2557 + j 7.1248	0.6230∠ -6.06	1.0∠ 173	0.1064∠ 20.73	0.1854∠ 165

Table 4.6 shows the normalized controllability factors of automatic voltage regulators for all three poles shown in Table 4.1, aiming at to evaluate the best output variables for a centralized power system stabilizer.

Table 4.6: Normalized Controllability Factors, Electromechanical Poles.

Poles	Machine 1	Machine 2	Machine 3	Machine 4
0.04912 + j 3.9397	1.0000	0.1090	0.5936	0.1119
-0.5473 + j 7.3670	0.4408	0.1010	1.0000	0.4594
-0.2557 + j 7.1248	1.0000	0.09724	0.05908	0.01176

Using the results shown in Table 4.6 the centralized PSS is selected to be installed at G1, since its controllability factors are the largest for the two most critical poles.

In same way, the generator speeds of G3 and G4 were chosen as remote signals, since they have the largest observability factors for two most critical poles. These signals are weighted approximately by the observability factors to yield a good observer for the stabilizing loop input.

A PSS design using weighted signals from generators G4 and G3 rotor speed as input and acting at voltage regulator of generator G1 is evaluated (PSS G43). The transfer function using signals coming from rotor speed generators G4 and G3 and acting at voltage regulator of generator G1 are shown in the following equation:

$$\frac{w_4 - 0.25 * w_3}{V_1^{REF}} \tag{4.1}$$

The inverse DNP of (4.1) for damp $\xi = 20\%$ is shown in Figure 4.4.

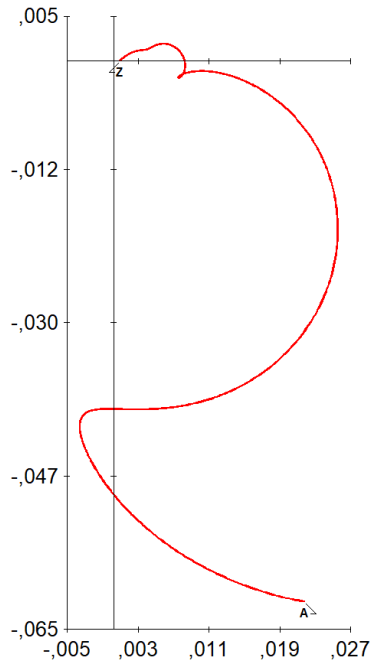

Figure 4.4: Uncompensated Nyquist Diagram for The First PSS Design.

Figure 4.4 shows the DNP for frequencies ranging from 1 rad/s to 20 rad/s. The point with frequency 6.86 rad/s is used for the pole placement, following the steps

presented in [22]. The compensated Nyquist diagram (blue) is shown in Figure 4.5.

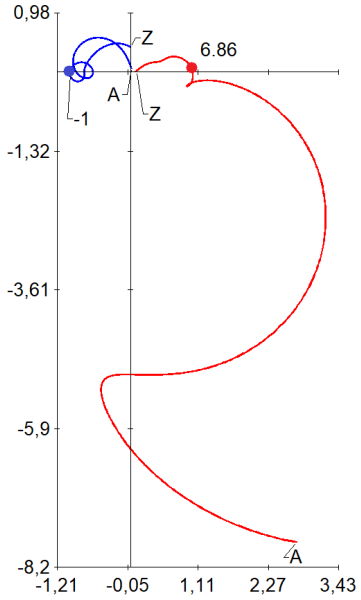

Figure 4.5: Compensated and Uncompensated Nyquist Diagram for The First PSS Design.

The PSS parameters are presented in the second row of Table 4.6.

Table 4.7: First Power System Stabilizer, Signals From G4 and G3, Acting at G1.

Generator	**n**	**K**	T_w	**T**	α	w_c	w_{max}
G43	3	0.38545	10	0.09	11.888	6.86	3.1575

The poles with PSS G43 at G1 are presented in Table 4.8. The pole placement is not performed exactly in the frequency of 6.86 rad/s and damping ratio of 20% because of the lack of significant digits in the PSS design.

Table 4.8: Electromechanical System Poles, with PSS G43 at G1.

Poles	**Frequency (Hz)**	**Damping Ratio (%)**
-0.2060 + j 8.1885	1.3032	2.5152
-0.7499 + j 4.2581	0.6777	17.345
-1.4004 + j 6.8599	1.0918	20.002

Even though with a PSS installed, the system still has a poorly damped electromechanical pole. Therefore, it is necessary another PSS design.

Table 4.9 shows the normalized observability factor calculation of generators rotor speed for poorly damped pole shown in Table 4.8, also aiming at to evaluate the best input variables for a centralized power system stabilizer.

Table 4.9: Normalized Observability Factors, Poorly Damped Pole.

Poles	Machine 1	Machine 2	Machine 3	Machine 4
-0.2060 + j 8.1885	0.8609∠ 7.22	1.0∠ -172	0.04433∠ 109	0.1362∠ 158

A PSS design using weighted signals from generators G2 and G1 rotor speed as input and acting at voltage regulator of generator G1 at the same time is the first PSS is proposed (PSS G21). The transfer function using signals coming from rotor speed generators G2 and G1 and acting at voltage regulator of generator G1 are shown in the following equation:

$$\frac{w_2 - 0.86 * w_1}{V_1^{REF}} \tag{4.2}$$

The inverse uncompensated DNP, for frequencies ranging from 1 rad/s to 20 rad/s, of transfer function shown 4.2 for $\xi = 13\%$ is shown in Figure 4.6.

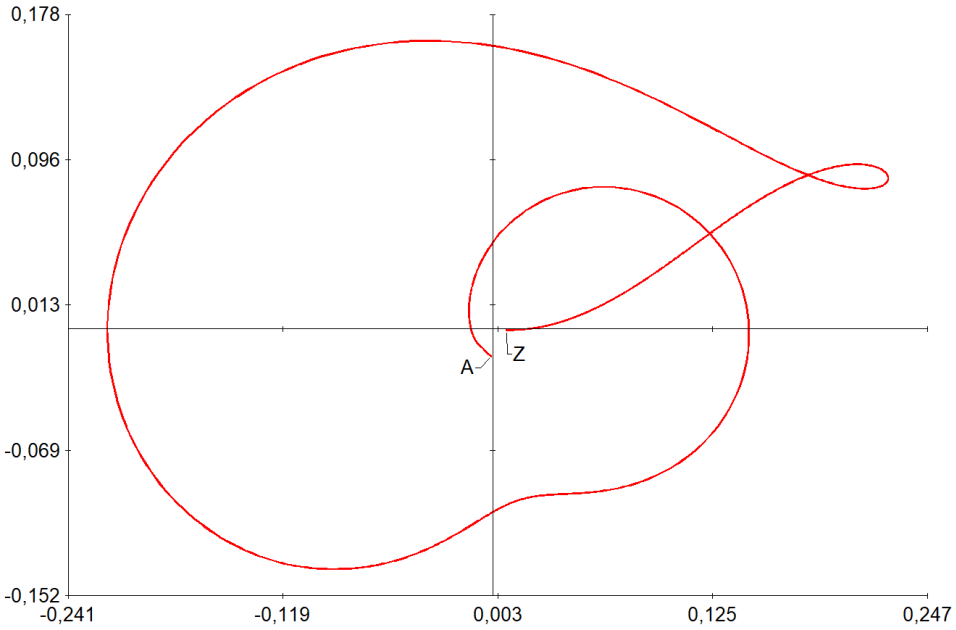

Figure 4.6: Uncompensated Nyquist Diagram for The Second PSS Design.

The point with frequency 8.43 rad/s is used for the pole placement. The compensated Nyquist diagram (blue) is shown in Figure 4.7.

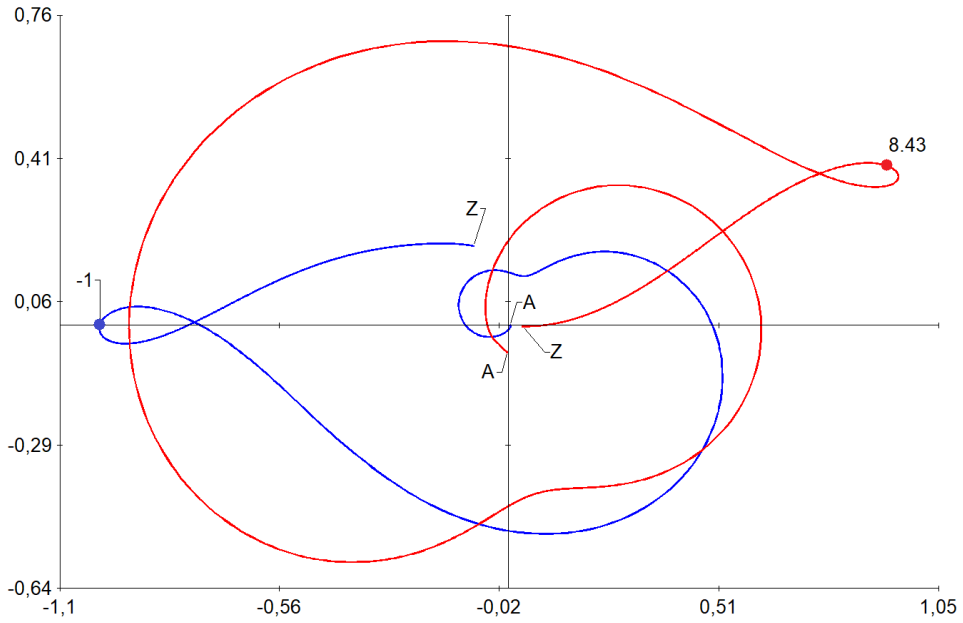

Figure 4.7: Compensated and Uncompensated Nyquist Diagram for The Second PSS Design.

The PSS parameters are presented in Table 4.10.

Table 4.10: Second Power System Stabilizer, Signals From G2 and G1, Acting at G1.

Generator	**n**	**K**	T_w	**T**	α	w_c	w_{max}
G21	3	0.27805	3	0.047509	6.1289	8.43	8.43

The poles with PSSs G43 and G21 at G1 are presented in Table 4.11. The pole placement is exactly performed in the frequency of 8.43 rad/s and damping ratio of 13%, even though the lack of significant digits in the PSS design.

Table 4.11: Electromechanical System Poles, with PSS G43 and G21 at G1.

Poles	**Frequency (Hz)**	**Damping Ratio (%)**
-1.1052 + j 8.4300	1.3417	13.000
-0.7222 + j 4.2588	0.6778	16.720
-1.5708 + j 8.4984	1.3526	18.175

4.1.3 Solution Based on Remote Signals With The Inclusion of Delays

The solution presented in Section 4.1.2 has been developed without accounting any latency effects. Including a small delay (20 ms), which will primarily represented as a first order polynomial approximation, those effects in electromechanical oscillation modes can be evaluated.

The effects at system electromechanical eigenvalues including approximated delay on signals coming from generators G4, G3, and G2 are shown in Table 4.12.

Table 4.12: Electromechanical System Poles with first order approximation - small delay.

Poles	**Frequency (Hz)**	**Damping Ratio (%)**
-0.2401 + j 8.8299	1.4053	2.7182
-0.6829 + j 4.3487	0.6921	15.513
-1.2062 + j 7.6498	1.2175	15.576

Representing the small delay with the complete model, it is not feasible to perform a QR decomposition. Therefore, the sequential dominant pole algorithm [11, 14] is used, once it is a partial pole computation algorithm.

The effects at system electromechanical eigenvalues including the complete delay model on signals coming from generators G4, G3, and G2 are shown in 4.13.

Table 4.13: Electromechanical System Poles with complete - small delay.

Poles	**Frequency (Hz)**	**Damping Ratio (%)**
-0.2282 + j 8.8797	1.41	2.57
-0.6869 + j 4.3503	0.69	15.60
-1.1961 + j 7.6648	1.22	15.42

As expected, a small delay represented by the complete model has not impacted the results significantly when compared to a first order approximation.

In order to evaluate the impact of a bigger delay, a relevant time delay (100 ms) is considered. Initially, a first order polynomial approximation is used. After that, the complete model is adopted to analyze the effects in the electromechanical oscillation modes computation.

The approximated delay representation is included in the signals coming from generators G4,G 3, and G2. The electromechanical poles are shown in Table 4.14.

Table 4.14: Electromechanical System Poles with first order approximation - relevant delay.

Poles	**Frequency (Hz)**	**Damping Ratio (%)**
0.3941 + j 8.0513	1.2814	-4.8894
-0.3967 + j 4.5110	0.7180	8.7604
-0.9357 + j 7.4584	1.1870	12.448

Using the sequential dominant pole algorithm [11, 14] in order to evaluate transport delay with complete model, Table 4.15 shows the results.

Table 4.15: Electromechanical System Poles with complete model - relevant delay.

Poles	**Frequency (Hz)**	**Damping Ratio (%)**
0.7270 + j 8.0520	1.28	-8.99
-0.4179 + j 4.5924	0.73	9.06
-0.9137 + j 7.5193	1.20	12.06

As expected, bigger is the time delay, bigger is its impact on the issues related to the communication of remote control signals and the impact of delays on electromechanical stability of power grid. A precise model of transport delays is important to avoid totally incorrect results in the analysis, mainly for the cases with large values of time constants and widespread remote measurements in control systems. [2–4]

4.1.3.1 Remote Signal Solution Small Delay First Order Approximation

The result presented in Section 4.1.3 shows why it is important to account time delays on small-signal analysis of powers systems. In this section, the controllers are designed taking account a first order approximation time delay.

The results obtained in Section 4.1.2 are used to evaluate the best input variables for a centralized power system stabilizer. The normalized observability factors of machine electrical frequency, shown in Table 4.1, are repeated in 4.16.

Table 4.16: Normalized Observability Factors, Electromechanical Poles.

Poles	**Machine 1**	**Machine 2**	**Machine 3**	**Machine 4**
0.04912 + j 3.9397	0.1035∠ 167	0.08706∠ -70	1.0∠ 178	0.8596∠ -180
-0.5473 + j 7.3670	0.07409∠ 75	0.1190∠ -89	0.2573∠ -178	1.0∠ -0.018
-0.2557 + j 7.1248	0.6230∠ -6.06	1.0∠ 173	0.1064∠ 20.73	0.1854∠ 165

Again, the generator speeds of G3 and G4 were chosen as remote signals, since they have the largest observability factors for two most critical poles. These signals are weighted approximately by the observability factors to yield a good observer for the stabilizing loop input.

A PSS design using weighted signals from generators G4 and G3 rotor speed as input and acting at voltage regulator of generator G1 is evaluated (PSS G43). The transfer function using signals coming from rotor speed generators G4 and G3 and acting at voltage regulator of generator G1 are shown in the following equation:

$$\frac{w_4 - 0.25 * w_3}{V_1^{REF}} \tag{4.3}$$

The inverse DNP of (4.3) for damp $\xi = 20\%$ is shown in Figure 4.8.

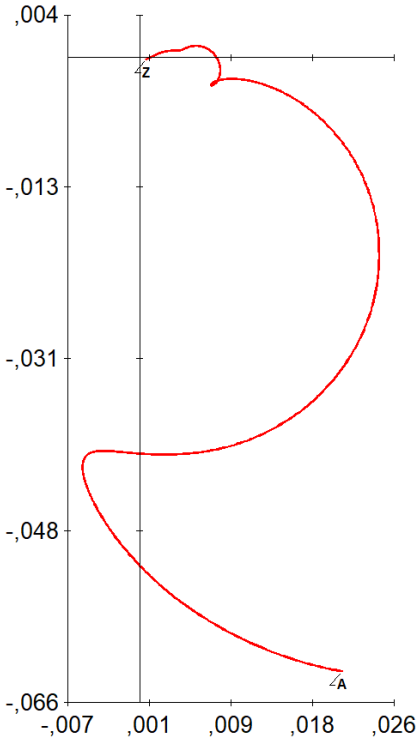

Figure 4.8: Uncompensated Nyquist Diagram for The First PSS Design.

The point with frequency 6.87 rad/s is used for the pole placement. The compensated Nyquist diagram (blue) is shown in Figure 4.9.

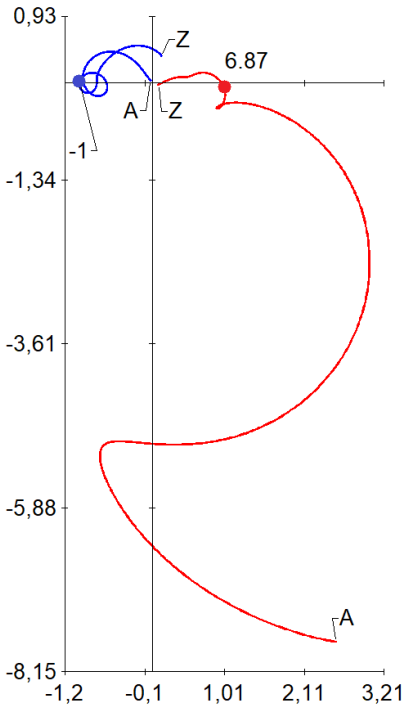

Figure 4.9: Compensated and Uncompensated Nyquist Diagram for The First PSS Design.

The PSS parameters are presented in the second row of Table 4.17.

Table 4.17: First Power System Stabilizer, Signals From G4 and G3, Acting at G1.

Generator	**n**	**K**	T_w	**T**	α	w_c	w_{max}
G43	3	0.11458	8	0.09	17.624	6.87	2.5932

The poles with PSS G43 at G1 are presented in Table 4.18. The pole placement is not performed exactly in the frequency of 6.87 rad/s and damping ratio of 20% because of the lack of significant digits in the PSS design.

Table 4.18: Electromechanical System Poles, with PSS G43 at G1.

Poles	**Frequency (Hz)**	**Damping Ratio (%)**
-0.1358 + j 8.1480	1.2968	1.6662
-0.7634 + j 4.0905	0.6510	18.347
-1.4025 + j 6.8699	1.0934	20.002

As in Section 4.1.2, even with a PSS installed, the system still has a poorly damped electromechanical pole. Therefore, it is necessary another PSS design.

Table 4.19 shows the normalized observability factor calculation of generators rotor speed for poorly damped pole shown in Table 4.18, also aiming at to evaluate the best input variables for a centralized power system stabilizer.

Table 4.19: Normalized Observability Factors, Poorly Damped Pole.

Poles	**Machine 1**	**Machine 2**	**Machine 3**	**Machine 4**
-0.1358 + j 8.1480	0.8522∠-156.5	1.0∠25	0.04682∠-57	0.1411∠-6.4

A PSS design using weighted signals from generators G2 and G1 rotor speed as input and acting at voltage regulator of generator G1 at the same time is the first PSS is proposed (PSS G21). However, differently from Section 4.1.2, the time delay is taken into account using a first order approximation.

The transfer function using signals coming from rotor speed generators G2 and G1 and acting at voltage regulator of generator G1 are shown in the following equation:

$$\frac{w_4 - 0.85 * w_3}{V_1^{REF}} \tag{4.4}$$

The inverse DNP of (4.4) for damp $\xi = 12.5\%$ is shown in Figure 4.10.

Figure 4.10: Uncompensated Nyquist Diagram for The Second PSS Design.

The point with frequency 8.44 rad/s was used for the pole placement. The compensated Nyquist diagram (blue) is shown in Figure 4.11.

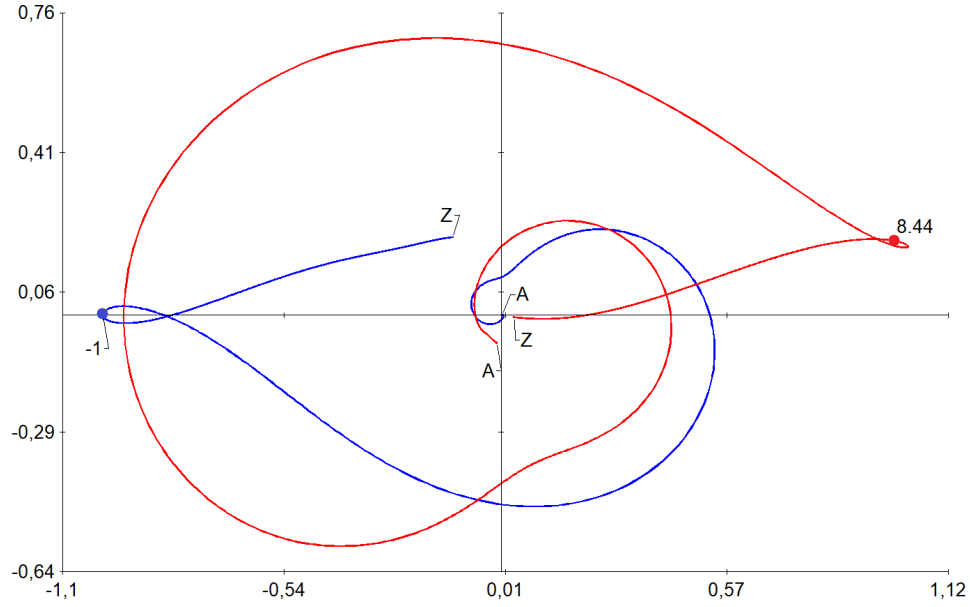

Figure 4.11: Compensated and Uncompensated Nyquist Diagram for The Second PSS Design.

The PSS parameters are presented in the second row of Table 4.20.

Table 4.20: Second Power System Stabilizer, Signals From G2 and G1, Acting at G1.

Generator	**n**	**K**	T_w	**T**	α	w_c	w_{max}
G21	3	0.21792	3	0.042812	7.5397	8.44	8.44

The poles with PSS G43 and G21 at G1 are presented in Table 4.21.

Table 4.21: Electromechanical System Poles, with PSS G43 and G21 at G1.

Poles	**Frequency (Hz)**	**Damping Ratio (%)**
-1.0636 + j 8.4399	1.3433	12.503
-1.2687 + j 8.4084	1.3382	14.920
-0.7430 + j 4.0991	0.6524	17.836

4.1.3.2 Remote Signal Solution Small Delay Complete Model

In this section, the controllers are designed taking account the complete model of transport delay. The results obtained in Section 4.1.2 are used to evaluate the best input variables for a centralized power system stabilizer. The normalized observability factors of machine electrical frequency, shown in Table 4.1, are repeated in 4.22.

Table 4.22: Normalized Observability Factors, Electromechanical Poles.

Poles	Machine 1	Machine 2	Machine 3	Machine 4
0.04912 + j 3.9397	0.1035∠ 167	0.08706∠ -70	1.0∠ 178	0.8596∠ -180
-0.5473 + j 7.3670	0.07409∠ 75	0.1190∠ -89	0.2573∠ -178	1.0∠ -0.018
-0.2557 + j 7.1248	0.6230∠ -6.06	1.0∠ 173	0.1064∠ 20.73	0.1854∠ 165

A PSS design using the complete model of time delay is performed. Initially, remote signals from generators G4 and G3 rotor speed are used as input, acting at voltage regulator of generator G1 (PSS G43). The transfer function using signals coming from rotor speed generators G4 and G3 and acting at voltage regulator of generator G1 are shown in the following equation:

$$\frac{w_4 - 0.25 * w_3}{V_1^{REF}} \tag{4.5}$$

The inverse DNP of (4.5) for damp $\xi = 20\%$ is shown in Figure 4.12.

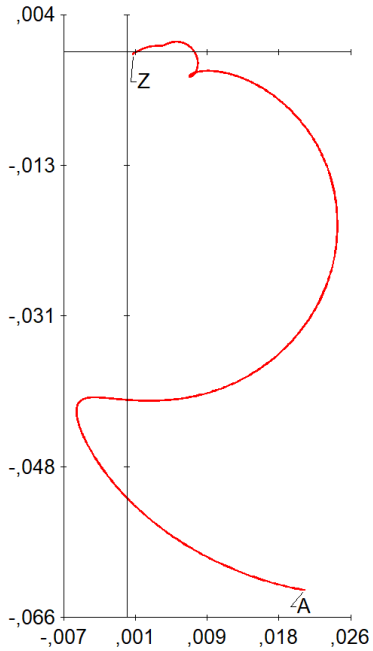

Figure 4.12: Uncompensated Nyquist Diagram for The First PSS Design.

The point with frequency 6.83 rad/s is used for the pole placement. The Compensated Nyquist diagram (blue) is shown in Figure 4.13.

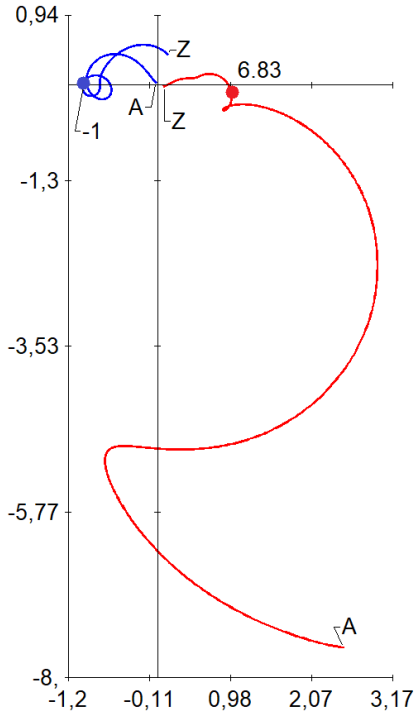

Figure 4.13: Compensated and Uncompensated Nyquist Diagram for The First PSS Design.

The PSS parameters are presented in Table 4.23.

Table 4.23: First Power System Stabilizer, Signals From G4 and G3, Acting at G1.

Generator	**n**	**K**	T_w	**T**	α	w_c	w_{max}
G43	3	0.094987	8	0.09	18.715	6.83	2.5165

The poles with PSS G43 at G1 are presented in Table 4.24.

Table 4.24: Electromechanical System Poles, with PSS G43 at G1.

Poles	**Frequency (Hz)**	**Damping Ratio (%)**
-0.1507 + j 8.1507	1.30	1.85
-0.7613 + j 4.0572	0.65	18.44
-1.3941 + j 6.8301	1.09	20.00

Similarly to the results shown in Section 4.1.3, even with a PSS installed in the system, a poorly damped electromechanical pole still exists. Therefore, it will be necessary other PSS design.

Table 4.25 shows the normalized observability factor of generators rotor speed for the poorly damped pole, aiming at to evaluate the best input variables for a centralized power system stabilizer.

Table 4.25: Normalized Observability Factors, Poorly Damped Pole.

Poles	**Machine 1**	**Machine 2**	**Machine 3**	**Machine 4**
-0.1507 + j 8.1507	0.8528∠1.26	1.0∠-177	0.04614∠100.6	0.1400∠151

A PSS design using weighted signals from generators G2 and G1 rotor speed as input and acting at voltage regulator of generator G1 at the same time as the first PSS is proposed. The transfer function using signals coming from rotor speed generators G2 and G1 and acting at voltage regulator of generator G1 are shown in the following equation:

$$\frac{w_2 - 0.85 * w_1}{V_1^{REF}} \tag{4.6}$$

The inverse uncompensated DNP, for frequencies ranging from 1 rad/s to 20 rad/s, of transfer function shown 4.6 for $\xi = 12.5\%$ is shown in Figure 4.14.

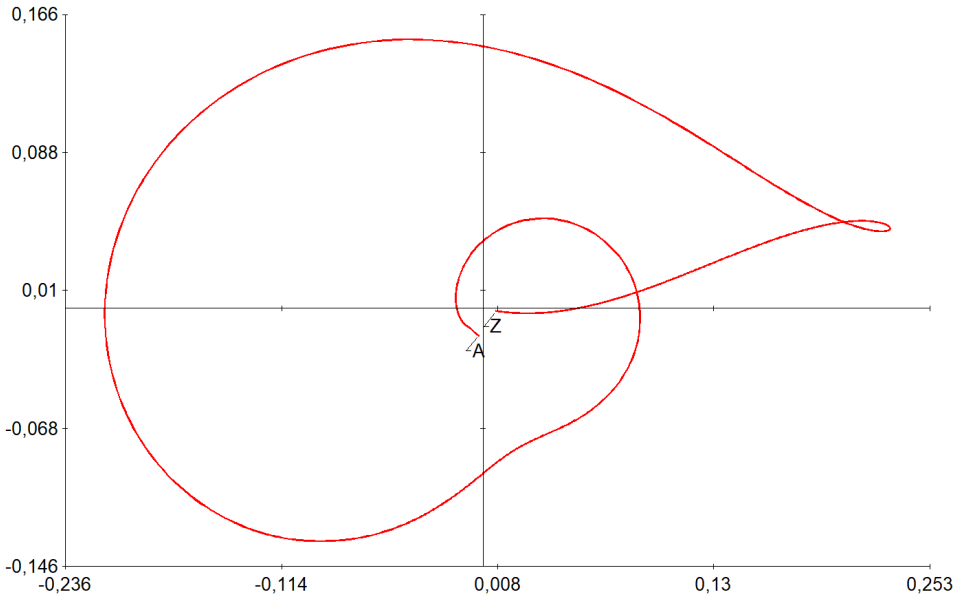

Figure 4.14: Uncompensated Nyquist Diagram for The Second PSS Design.

The point with frequency 8.38 rad/s is used for the pole placement. The Compensated Nyquist diagram (blue) is shown in Figure 4.15.

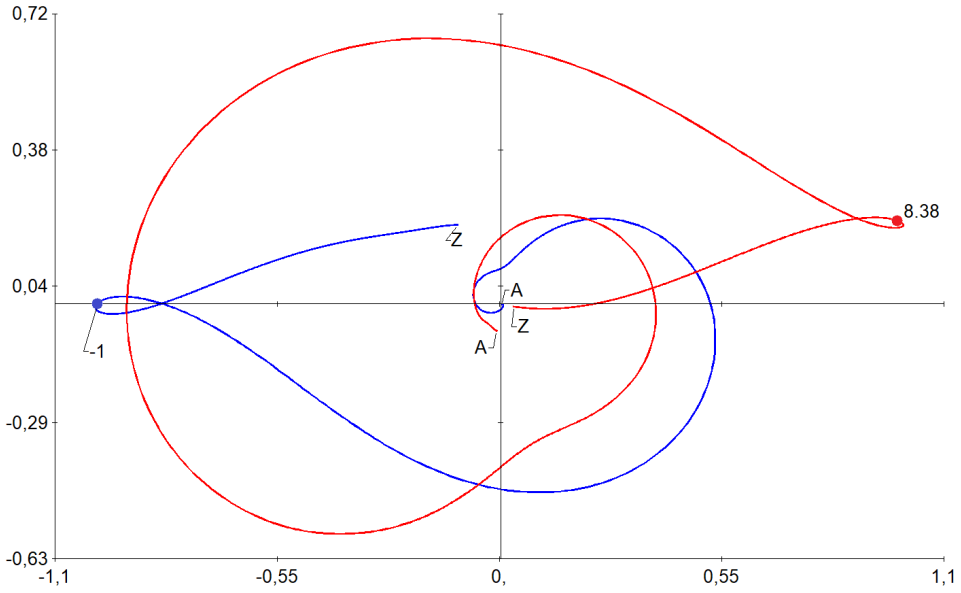

Figure 4.15: Compensated and Uncompensated Nyquist Diagram for The Second PSS Design.

The PSS parameters are presented Table 4.26.

Table 4.26: Second Power System Stabilizer, Signals From G2 and G1, Acting at G1.

Generator	**n**	**K**	T_w	**T**	α	w_c	w_{max}
G21	3	0.21415	3	0.04357	7.3841	8.38	8.38

The poles with PSS G43 and G21 at G1 are presented in Table 4.27.

Table 4.27: Electromechanical System Poles, with PSS G43 and G21 at G1.

Poles	**Frequency (Hz)**	**Damping Ratio (%)**
-1.0558 + j 8.3798	1.33	12.50
-1.2903 + j 8.5393	1.36	14.94
-0.7427 + j 4.0658	0.65	17.97

4.1.3.3 Remote Signal Solution Relevant Delay First Order Approximation

The results presented in Sections 4.1.3.1 and 4.1.3.2 have shown the impact of modelling small time delays using a first order approximation and the developed complete model. This section repeats the analysis for a relevant time delay.

The normalized observability factor of generators rotor speed, shown in Table 4.1 and repeated in Table 4.28, is used to evaluate the best input variables for a centralized power system stabilizer.

Table 4.28: Normalized Observability Factors, Electromechanical Poles.

Poles	**Machine 1**	**Machine 2**	**Machine 3**	**Machine 4**
0.04912 + j 3.9397	0.1035∠ 167	0.08706∠ -70	1.0∠ 178	0.8596∠ -180
-0.5473 + j 7.3670	0.07409∠ 75	0.1190∠ -89	0.2573∠ -178	1.0∠ -0.018
-0.2557 + j 7.1248	0.6230∠ -6.06	1.0∠ 173	0.1064∠ 20.73	0.1854∠ 165

A PSS design using weighted delayed signals from generators G4 and G3 rotor speed as input and acting at voltage regulator of generator G1 is first proposed (PSS G43). Initially, the time delay is represented by a first order approximation.

The transfer function using signals coming from rotor speed generators G4 and G3 and acting at voltage regulator of generator G1 are shown in the following equation:

$$\frac{w_4 - 0.25 * w_3}{V_1^{REF}} \tag{4.7}$$

The inverse DNP of (4.7) for damp $\xi = 18\%$ is shown in Figure 4.16.

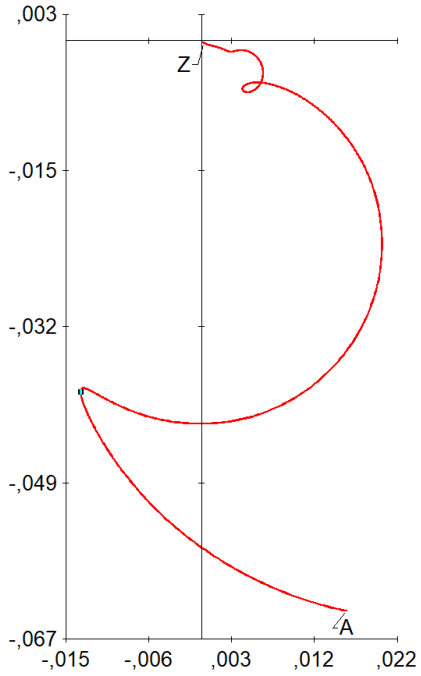

Figure 4.16: Uncompensated Nyquist Diagram for The First PSS Design.

The point with frequency 6.99 rad/s was used for the pole placement. The Compensated Nyquist (blue) diagram is shown in Figure 4.17.

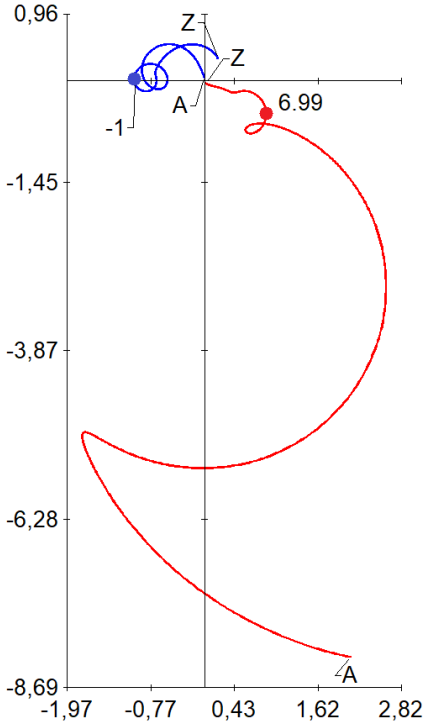

Figure 4.17: Compensated and Uncompensated Nyquist Diagram for The First PSS Design.

The PSS parameters are presented in Table 4.29.

Table 4.29: First Power System Stabilizer, Signals From G4 and G3, Acting at G1.

Generator	**n**	**K**	T_w	**T**	α	w_c	w_{max}
G43	3	0.31146	3	0.06	17.984	6.99	3.8659

The poles with PSS G43 at G1 are presented in Table 4.29. The pole placement is not exactly performed with the frequency of 6.99 rad/s and damping ratio of 18% because of the lack of significant digits in the PSS design.

Table 4.30: Electromechanical System Poles, with PSS G43 at G1.

Poles	**Frequency (Hz)**	**Damping Ratio (%)**
-0.05550 + j 8.0860	1.2869	0.6864
-0.6148 + j 4.1926	0.6673	14.508
-1.2790 + j 6.9900	1.1125	17.998

Even with a PSS installed in the system, a poorly damped electromechanical pole still exists. Therefore, it will be necessary other PSS design.

Table 4.31 shows the normalized observability factor calculation of WW for poorly damped pole shown in Table 4.30 also looking forward evaluate the best input variables for a centralized power system stabilizer.

Table 4.31: Normalized Observability Factors, Poorly Damped Pole.

Poles	**Machine 1**	**Machine 2**	**Machine 3**	**Machine 4**
-0.05550 + j 8.0860	0.8395∠-89.7	1.0∠93	0.05023∠5.34	0.1469∠60

A PSS design using weighted delayed signals modelled through first order aproximation is performed. Rotor speed from generators G2 and G1 are used as input, acting at voltage regulator of generator G1 at the same time as the first PSS is proposed.

The transfer function using signals coming from rotor speed generators G2 and G1 and acting at voltage regulator of generator G1 are shown in the following equation:

$$\frac{w_2 - 0.84 * w_1}{V_1^{REF}} \tag{4.8}$$

The inverse uncompensated DNP, for frequencies ranging from 1 rad/s to 20 rad/s, of transfer function shown 4.8 for $\xi = 11\%$ is shown in Figure 4.18.

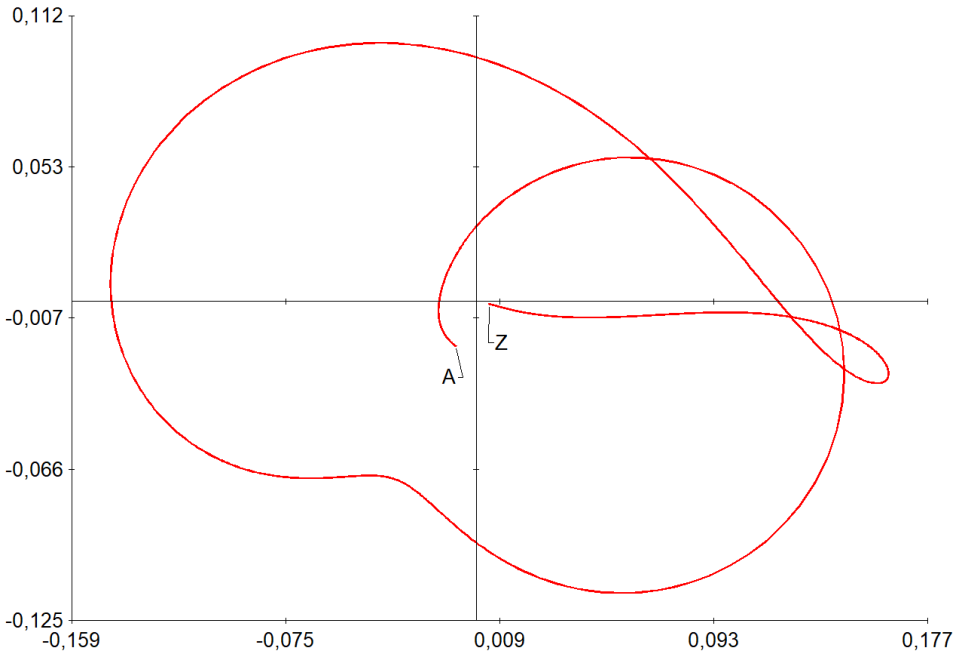

Figure 4.18: Uncompensated Nyquist Diagram for The Second PSS Design.

The point with frequency 8.48 rad/s is used for the pole placement. The Compensated Nyquist (blue) diagram is shown in Figure 4.19.

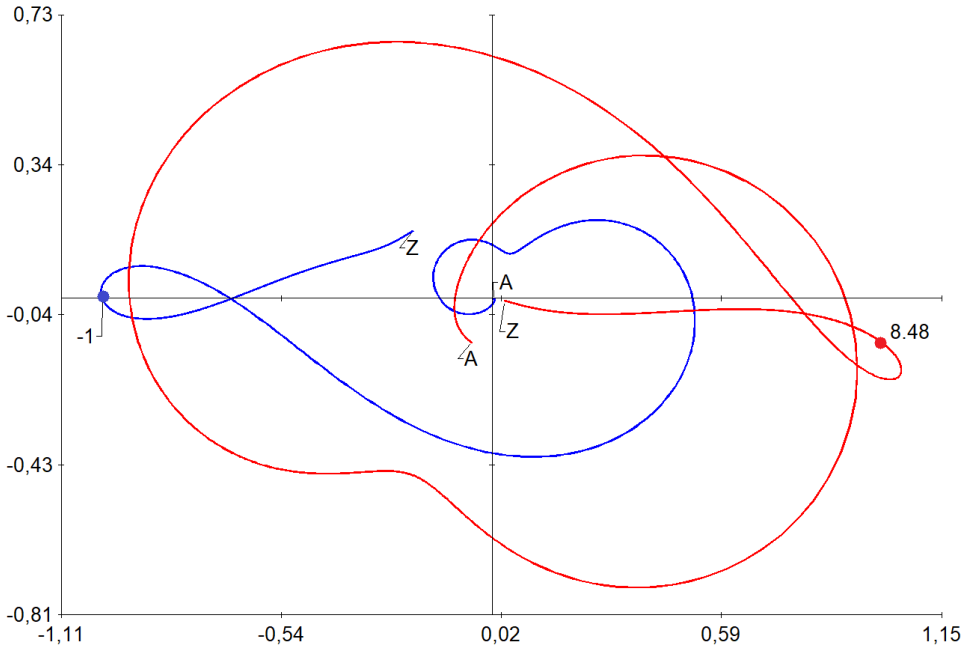

Figure 4.19: Compensated and Uncompensated Nyquist Diagram for The Second PSS Design.

The PSS parameters are presented in of Table 4.32.

Table 4.32: Second Power System Stabilizer, Signals From G2 and G1, Acting at G1.

Generator	**n**	**K**	T_w	**T**	α	w_c	w_{max}
G21	3	0.18445	3	0.035844	10.693	8.48	8.48

The poles with PSS G43 and G21 at G1 are presented in Table 4.33.

Table 4.33: Electromechanical System Poles, with PSS G43 and G21 at G1.

Poles	**Frequency (Hz)**	**Damping Ratio (%)**
-0.9386 + j 8.4800	1.3496	11.001
-0.5884 + j 4.1910	0.6670	13.903
-1.3866 + j 8.1511	1.2973	16.770

4.1.3.4 Remote Signal Solution Relevant Delay Complete Model

In this section, the control is designed considering the complete model of transport delay in the presence of a relevant time delay (100 ms).

The normalized observability factor of generators rotor speedfor the poorly damped pole, shown in Table 4.1 and repeated in Table 4.34, is used in order to evaluate the best input variables for a centralized power system stabilizer.

Table 4.34: Normalized Observability Factors, Electromechanical Poles.

Poles	Machine 1	Machine 2	Machine 3	Machine 4
0.04912 + j 3.9397	0.1035∠ 167	0.08706∠ -70	1.0∠ 178	0.8596∠ -180
-0.5473 + j 7.3670	0.07409∠ 75	0.1190∠ -89	0.2573∠ -178	1.0∠ -0.018
-0.2557 + j 7.1248	0.6230∠ -6.06	1.0∠ 173	0.1064∠ 20.73	0.1854∠ 165

A PSS design using the complete delay model delayed is performed. Initially, rotor speed signals from generators G4 and G3 are used as input, acting at voltage regulator of generator G1 (PSS G43).

The transfer function using signals coming from rotor speed generators G4 and G3 and acting at voltage regulator of generator G1 are shown in the following equation:

$$\frac{w_4 - 0.25 * w_3}{V_1^{REF}} \tag{4.9}$$

The inverse DNP of (4.9) for damp $\xi = 18\%$ is shown in Figure 4.20.

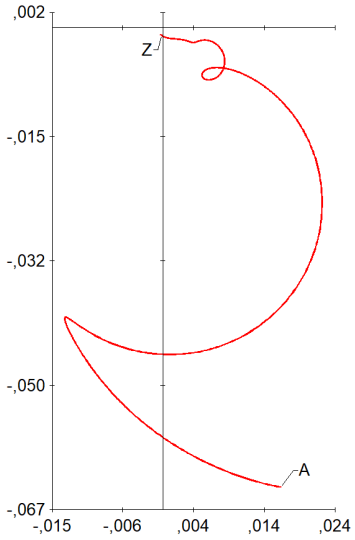

Figure 4.20: Uncompensated Nyquist Diagram for The First PSS Design.

The point with frequency 6.98 rad/s is used for the pole placement. The Compensated Nyquist (blue) diagram is shown in Figure 4.21.

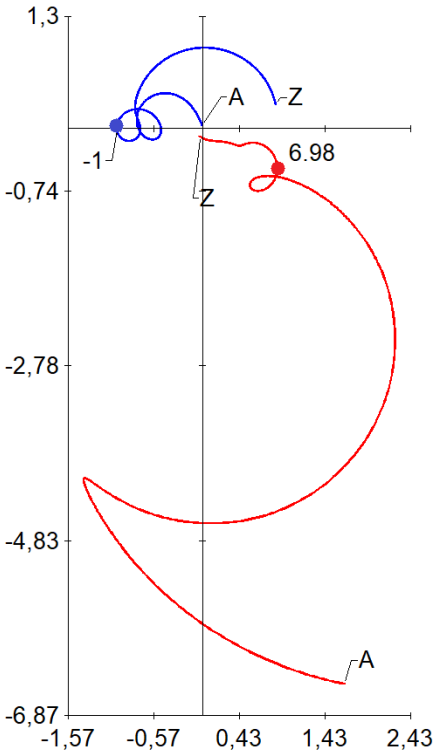

Figure 4.21: Compensated and Uncompensated Nyquist Diagram for The First PSS Design.

The PSS parameters are presented in Table 4.35.

Table 4.35: First Power System Stabilizer, Signals From G4 and G3, Acting at G1.

Generator	**n**	**K**	T_w	**T**	α	w_c	w_{max}
G43	3	0.19275	3	0.06	19.475	6.98	3.715

The poles with PSS G43 at G1 are presented in Table 4.36.

Table 4.36: Electromechanical System Poles, with PSS G43 at G1.

Poles	**Frequency (Hz)**	**Damping Ratio (%)**
-0.05402 + j 8.0790	1.29	-0.67
-0.5034 + j 4.1162	0.66	12.14
-1.2773 + j 6.9800	1.11	18.00

Even with a PSS installed in the system, a poorly damped electromechanical pole still exists. Therefore, will be necessary other PSS design.

As happened before, even a PSS was installed in the system still exist a poorly damped electromechanical pole. Therefore, will be necessary other PSS design.

Table 4.37 shows the normalized observability factors of generators rotor speed for the poorly damped pole shown in Table 4.36, aiming at to evaluate the best input variables for a centralized power system stabilizer.

Table 4.37: Normalized Observability Factors, Poorly Damped Pole.

Poles	**Machine 1**	**Machine 2**	**Machine 3**	**Machine 4**
-0.05402 + j 8.0790	0.8389∠-13.6	1.0∠170.6	0.05642∠81.9	0.1531∠138

A PSS design using weighted delayed signals from generators G2 and G1 rotor speed as input, acting at voltage regulator of generator G1 at the same time as the first PSS is proposed (PSS G21).

The transfer function using signals coming from rotor speed generators G2 and G1 and acting at voltage regulator of generator G1 are shown in the following equation:

$$\frac{w_2 - 0.84 * w_1}{V_1^{REF}} \tag{4.10}$$

The inverse uncompensated DNP, for frequencies ranging from 1 rad/s to 20 rad/s, of transfer function shown 4.8 for $\xi = 10\%$ is shown in Figure 4.22.

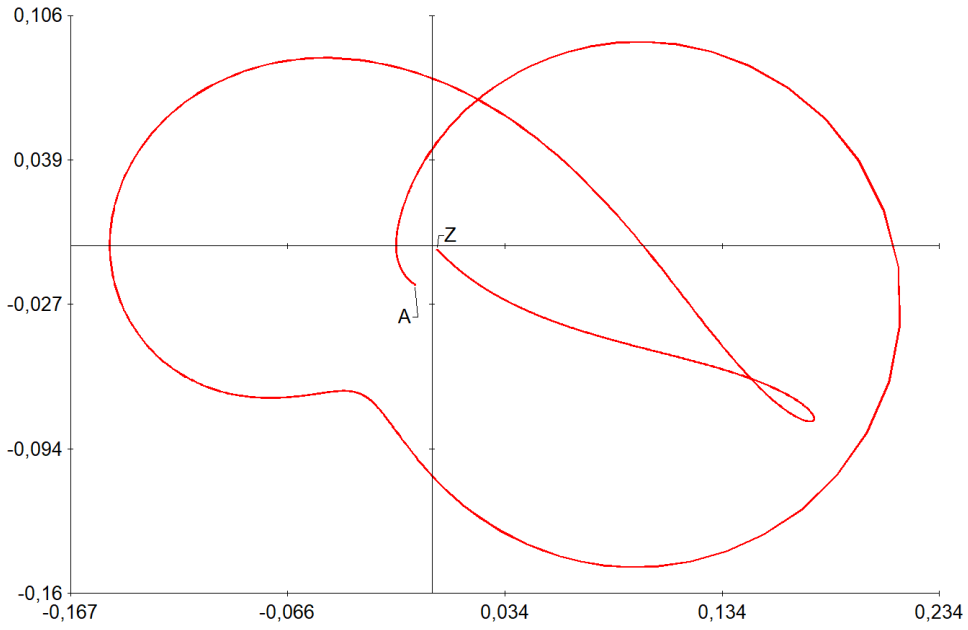

Figure 4.22: Uncompensated Nyquist Diagram for The Second PSS Design.

The point with frequency 8.36 rad/s is used for the pole placement. The Compensated Nyquist diagram (blue) is shown in Figure 4.23.

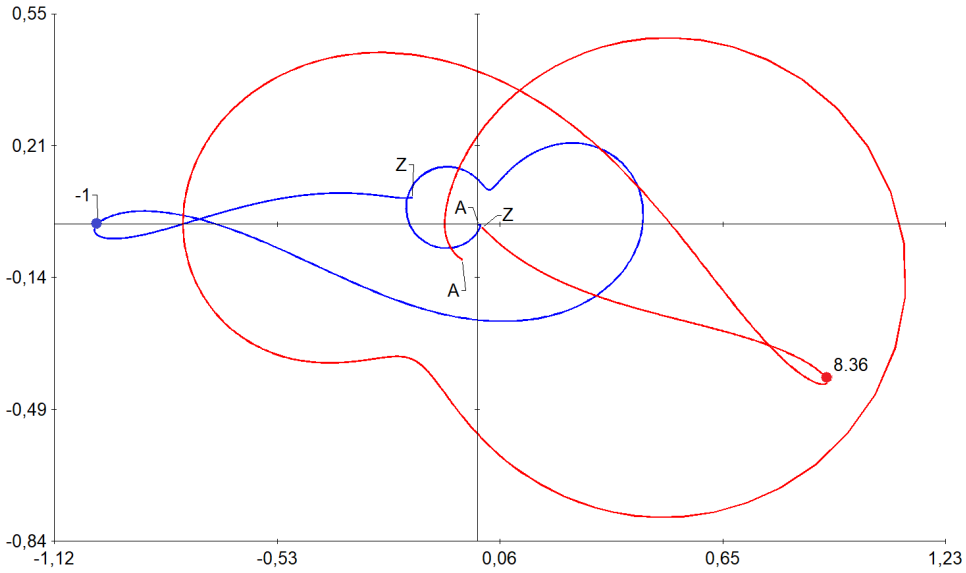

Figure 4.23: Compensated and Uncompensated Nyquist Diagram for The Second PSS Design.

The PSS parameters are presented in the second row of Table 4.38.

Table 4.38: Second Power System Stabilizer, Signals From G2 and G1, Acting at G1.

Generator	**n**	**K**	T_w	**T**	α	w_c	w_{max}
G21	3	0.17761	3	0.02	17.895	8.36	11.76

The poles with PSS G43 and G21 at G1 are presented in Table 4.39.

Table 4.39: Electromechanical System Poles, with PSS G43 and G21 at G1.

Poles	**Frequency (Hz)**	**Damping Ratio (%)**
-0.8402 + j 8.3600	1.33	10.00
-0.4850 + j 4.1158	0.66	11.70
-1.9449 + j 6.8857	1.10	27.18

4.1.4 Comparative Analysis with Small Time Delay

This section presents comparative results considering the step response with amplitude $0.01V$ at time $(t = 1s)$ in the Automatic Voltage Regulator (AVR) connected to generator G1 for the solutions proposed in 4.1.3.1.

The voltage deviation at each generator is compared in Figures 4.24, 4.25, 4.26 and 4.27, considering the first order approximation and the complete model as well.

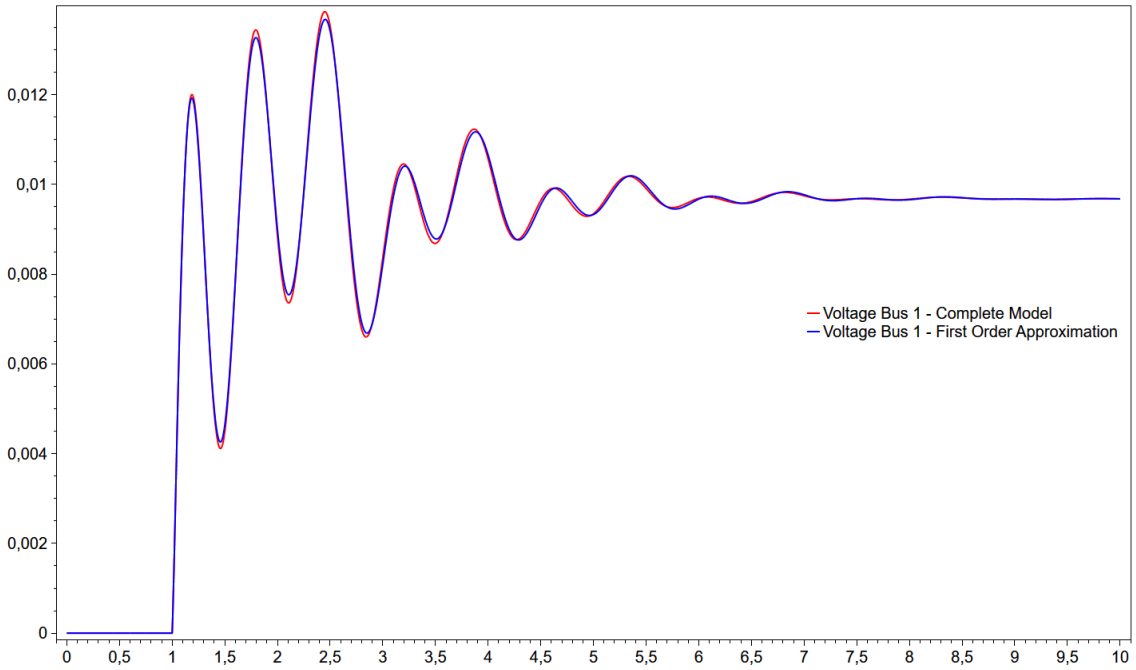

Figure 4.24: Voltage at Bus 1 - Small Time Delay.

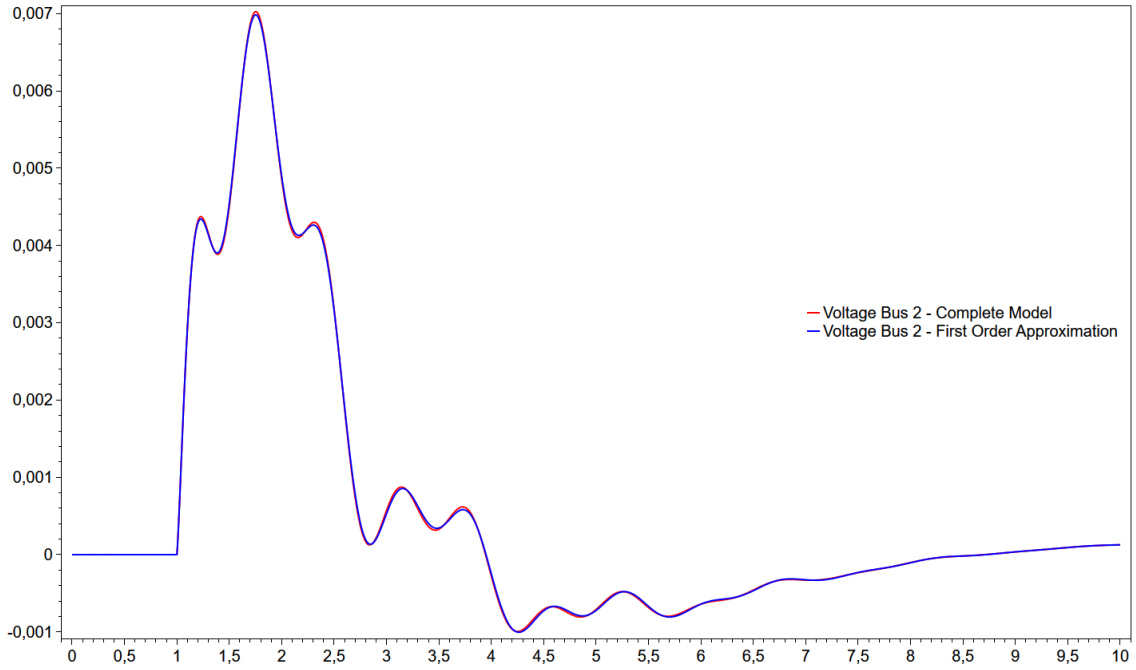

Figure 4.25: Voltage at Bus 2 - Small Time Delay.

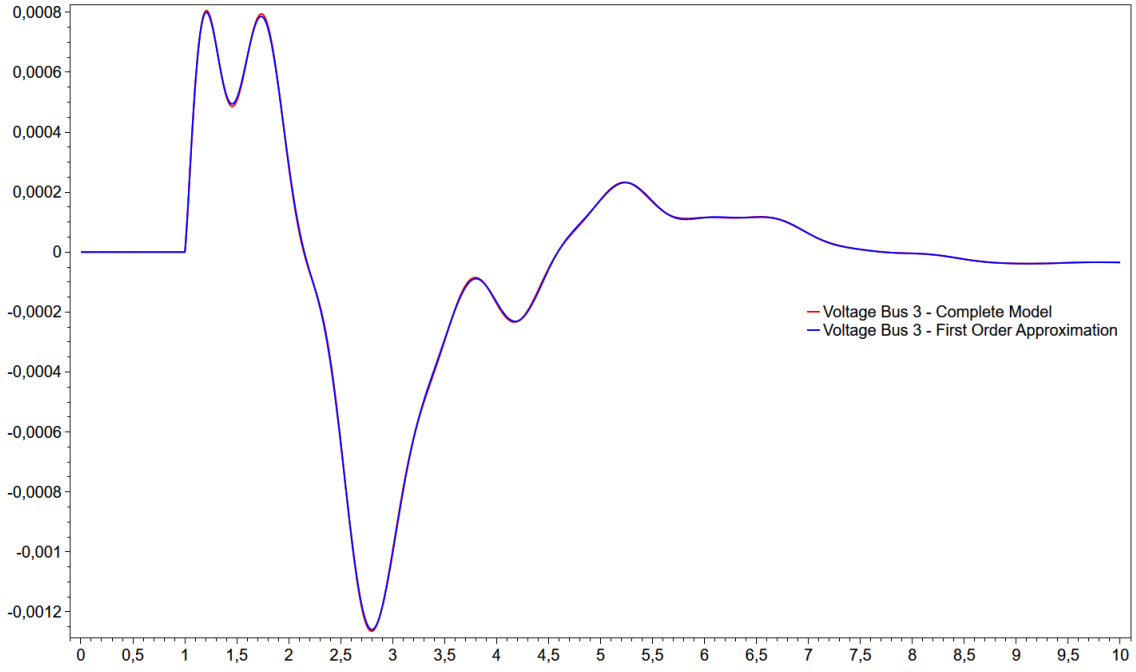

Figure 4.26: Voltage at Bus 3 - Small Time Delay.

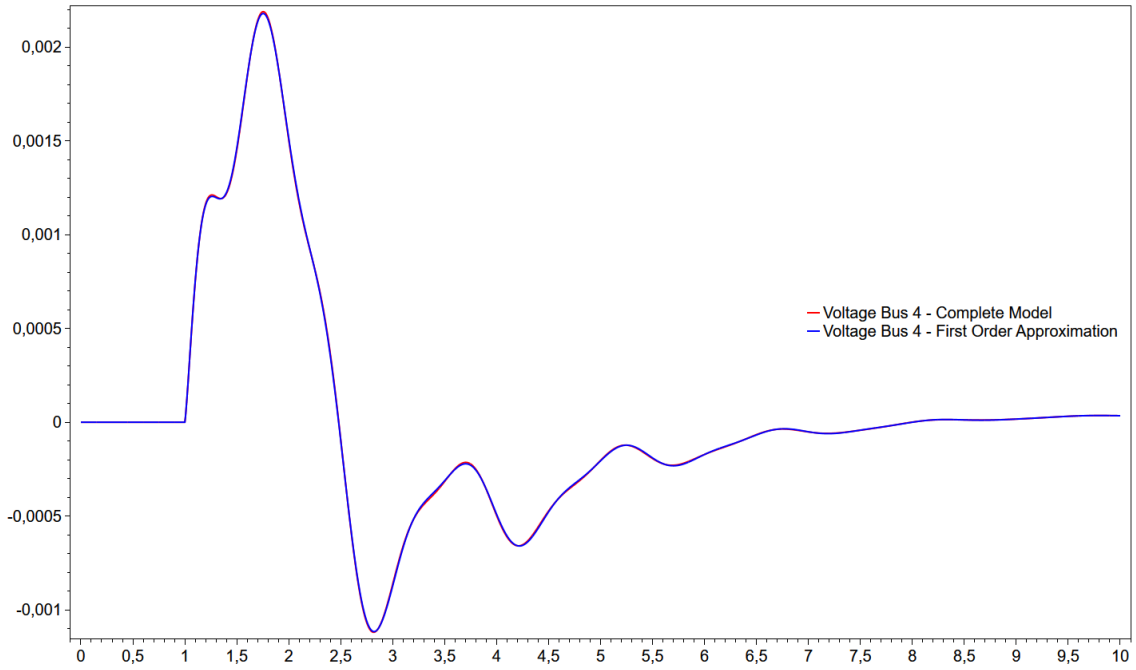

Figure 4.27: Voltage at Bus 4 - Small Time Delay.

The frequency deviation at each generator is compared in Figures 4.28, 4.29, 4.30 and 4.31, considering the first order approximation and the complete model as well.

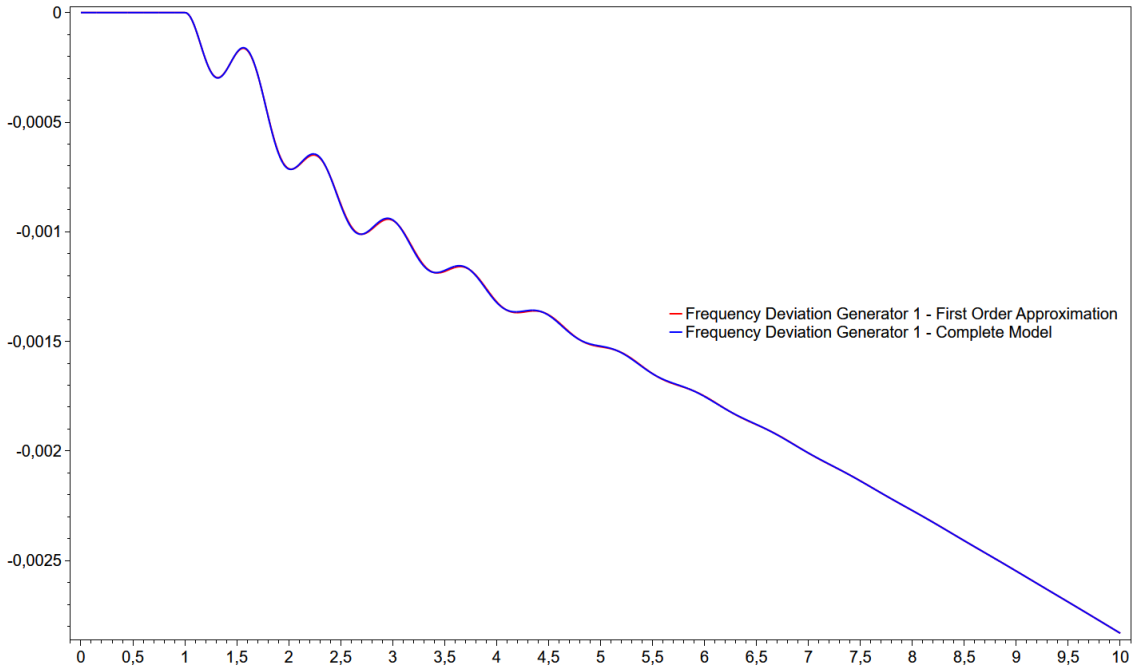

Figure 4.28: Frequency at Generator 1 - Small Time Delay.

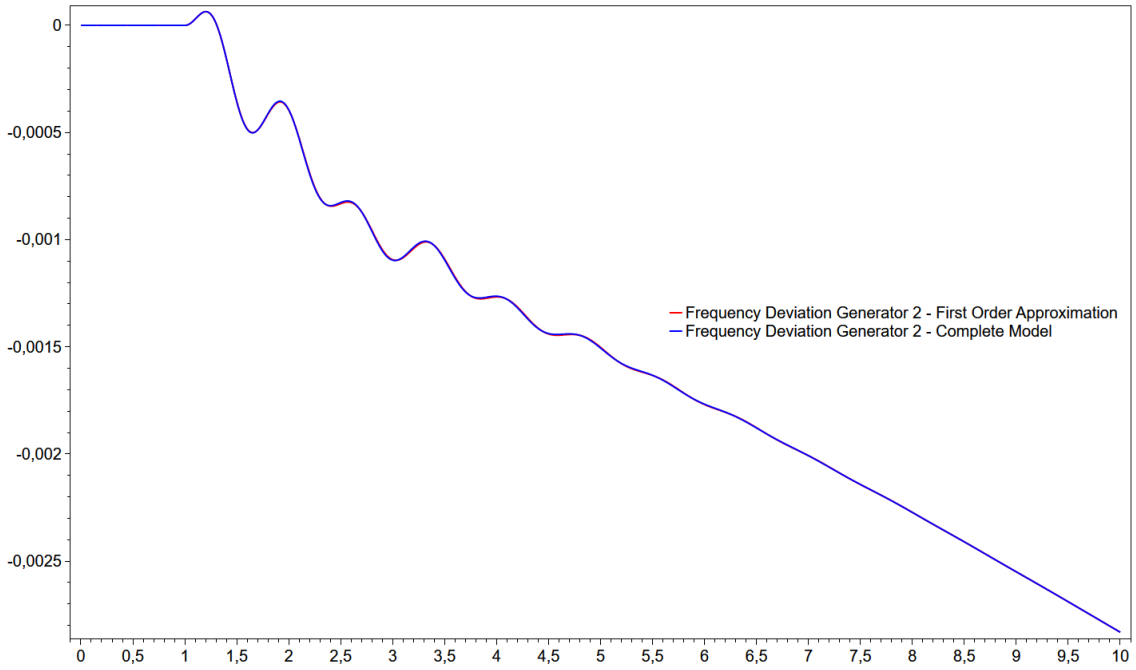

Figure 4.29: Frequency at Generator 2 - Small Time Delay.

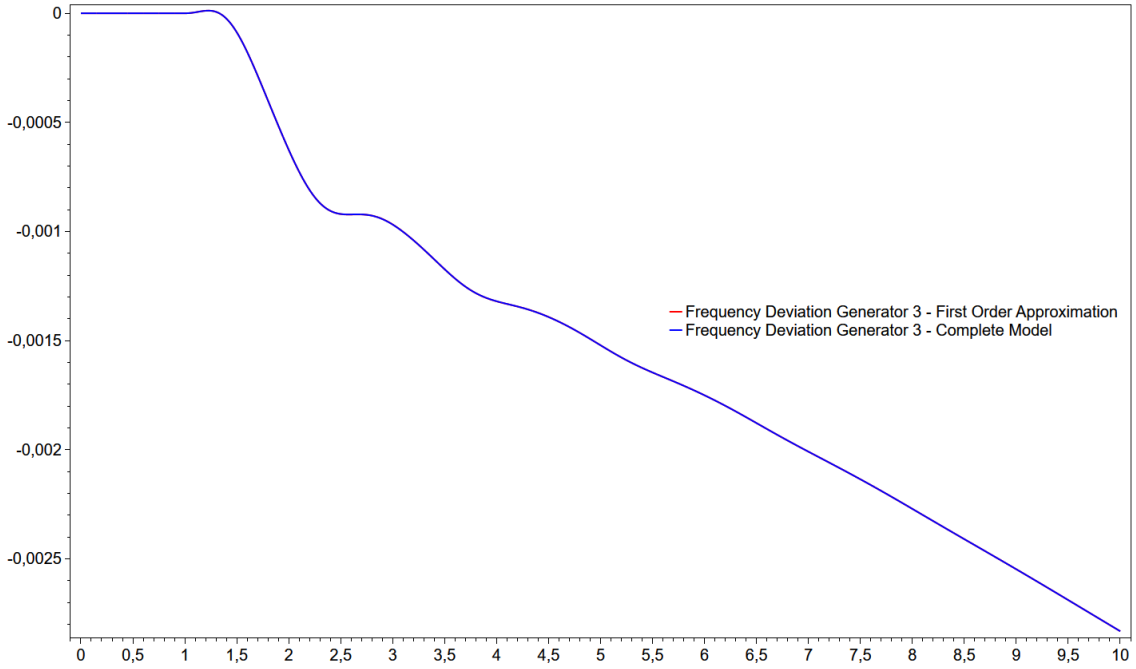

Figure 4.30: Frequency at Generator 3 - Small Time Delay.

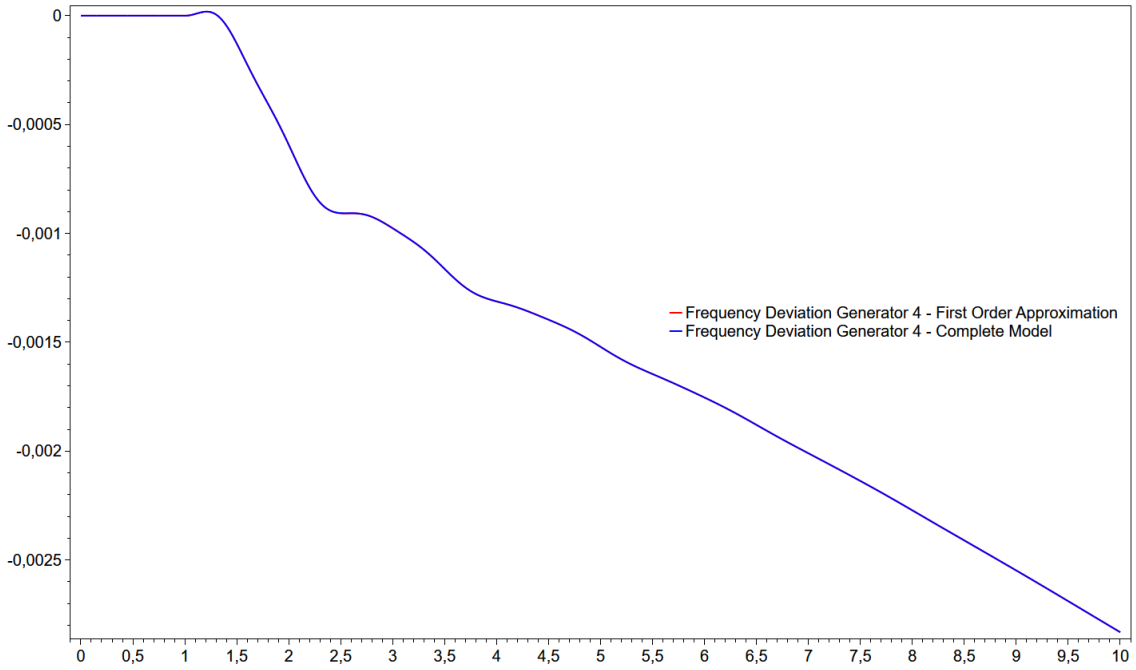

Figure 4.31: Frequency at Generator 4 - Small Time Delay.

As suggested in Section 4.1.3.2 and discussed in the literature [2–4, 26–31], a small time delay can be represented using polynomial approximations.

4.1.5 Comparative Analysis with Relevant Time Delay

This section compares the step response in the Automatic Voltage Regulator (AVR) connected to generator G1 considering the solutions proposed in Section 4.1.3.3 using the complete modelling of transport delay as well as the first order approximation.

The voltage deviation at each generator is compared in Figures 4.32, 4.33, 4.34 and 4.35, considering the complete modelling of transport delay as well as the first order approximation.

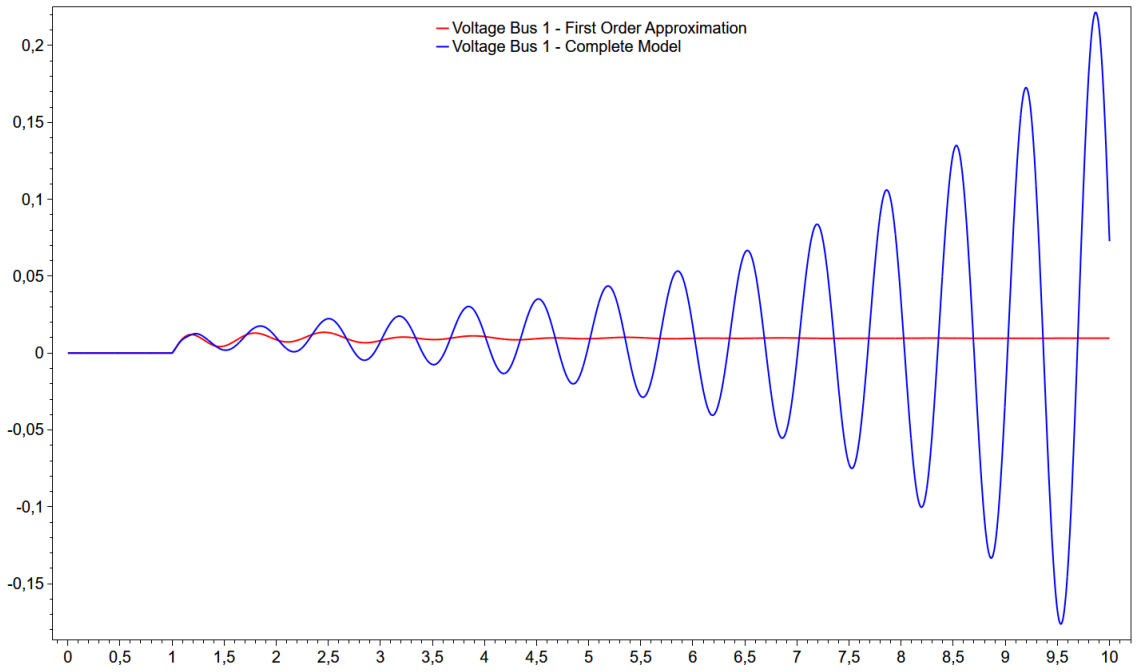

Figure 4.32: Voltage at Bus 1 - Relevant Time Delay.

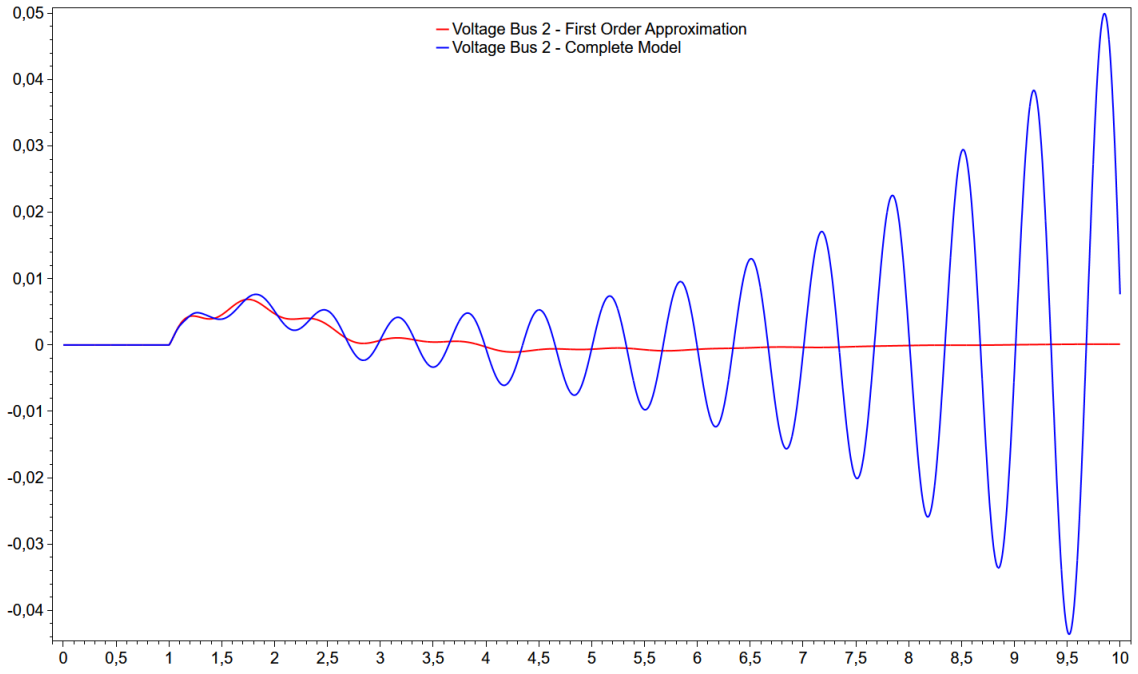

Figure 4.33: Voltage at Bus 2 - Relevant Time Delay.

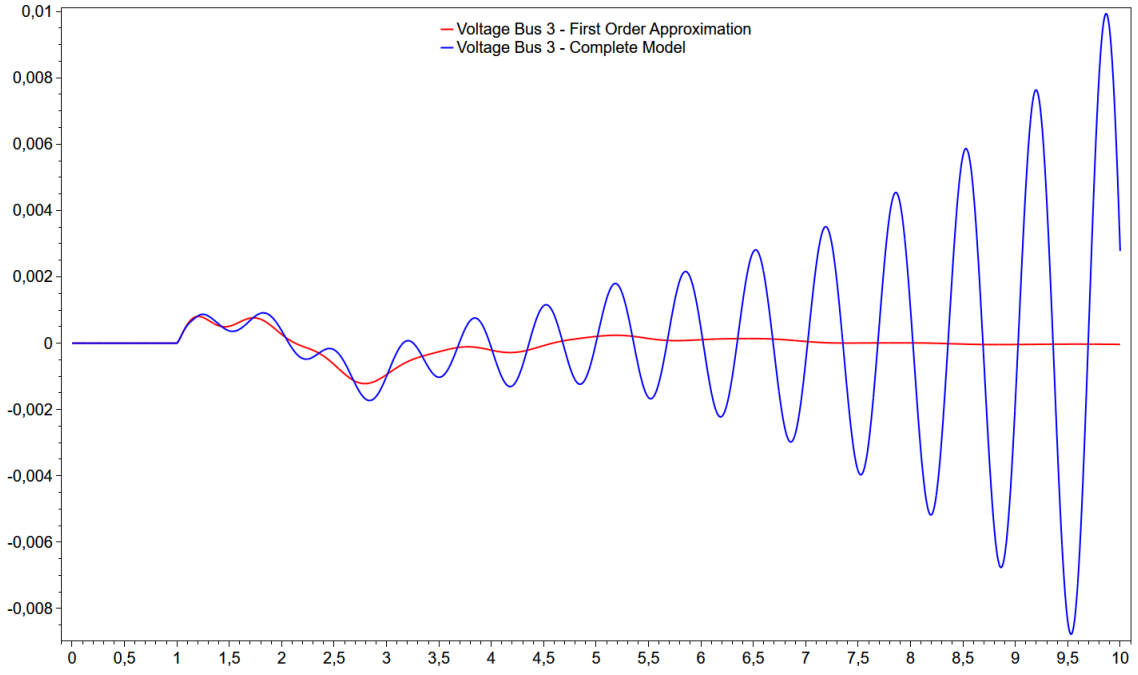

Figure 4.34: Voltage at Bus 3 - Relevant Time Delay.

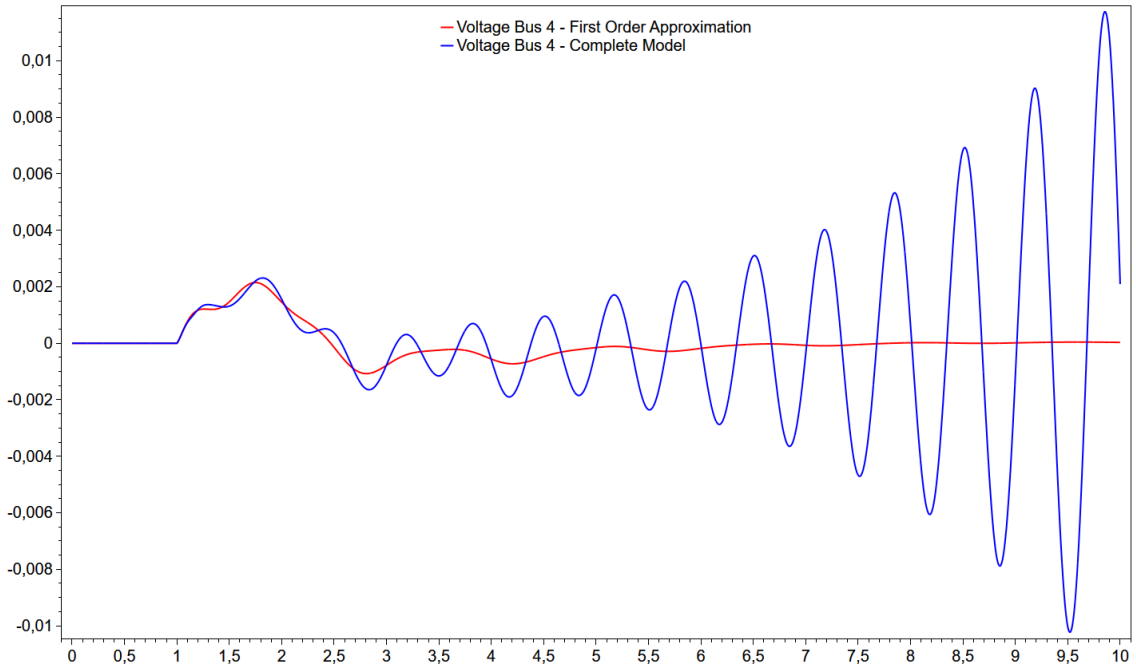

Figure 4.35: Voltage at Bus 4 - Relevant Time Delay.

The frequency deviation at each generator is compared in Figures 4.36, 4.37, 4.38 and 4.39, considering the complete modelling of transport delay as well as the first order approximation.

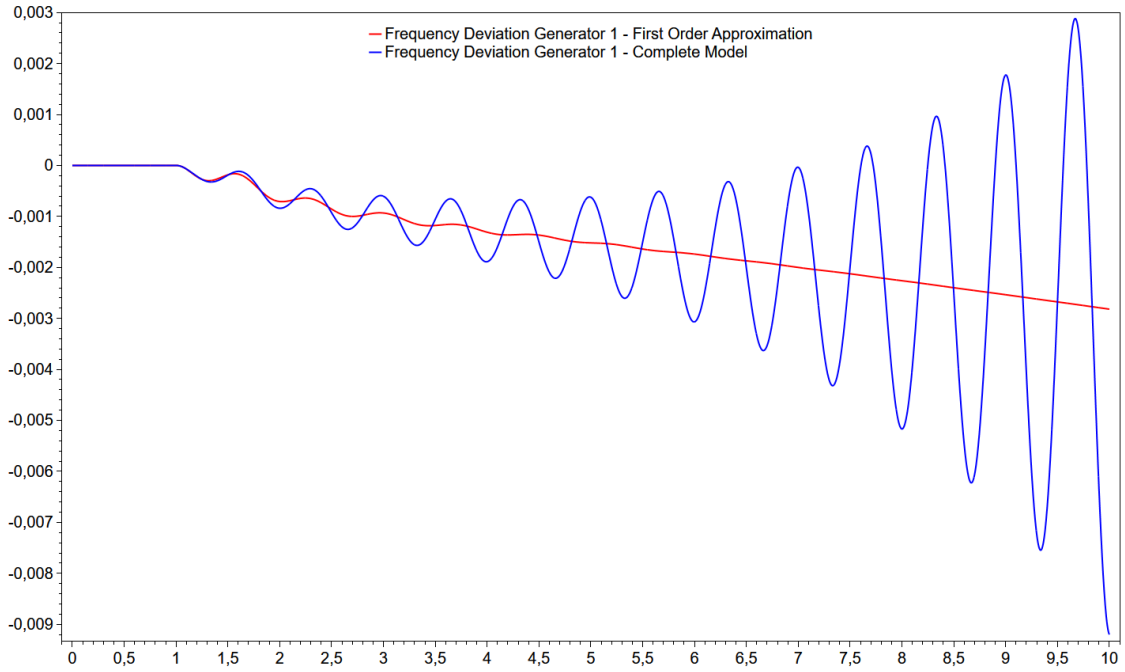

Figure 4.36: Frequency at Generator 1 - Relevant Time Delay.

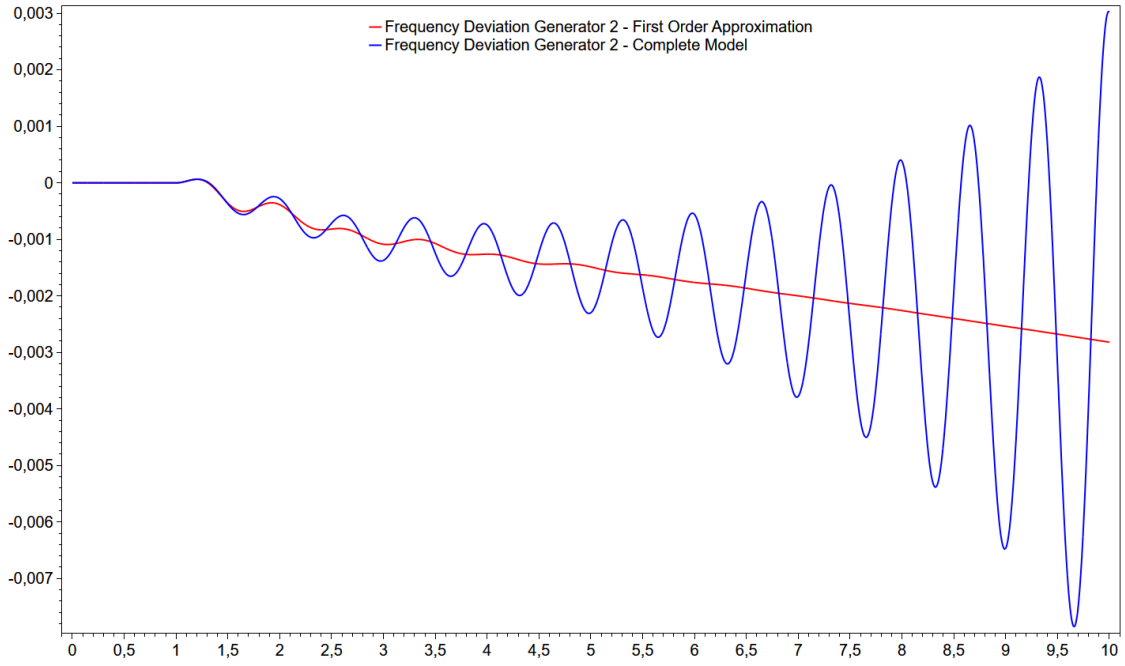

Figure 4.37: Frequency at Generator 2 - Relevant Time Delay.

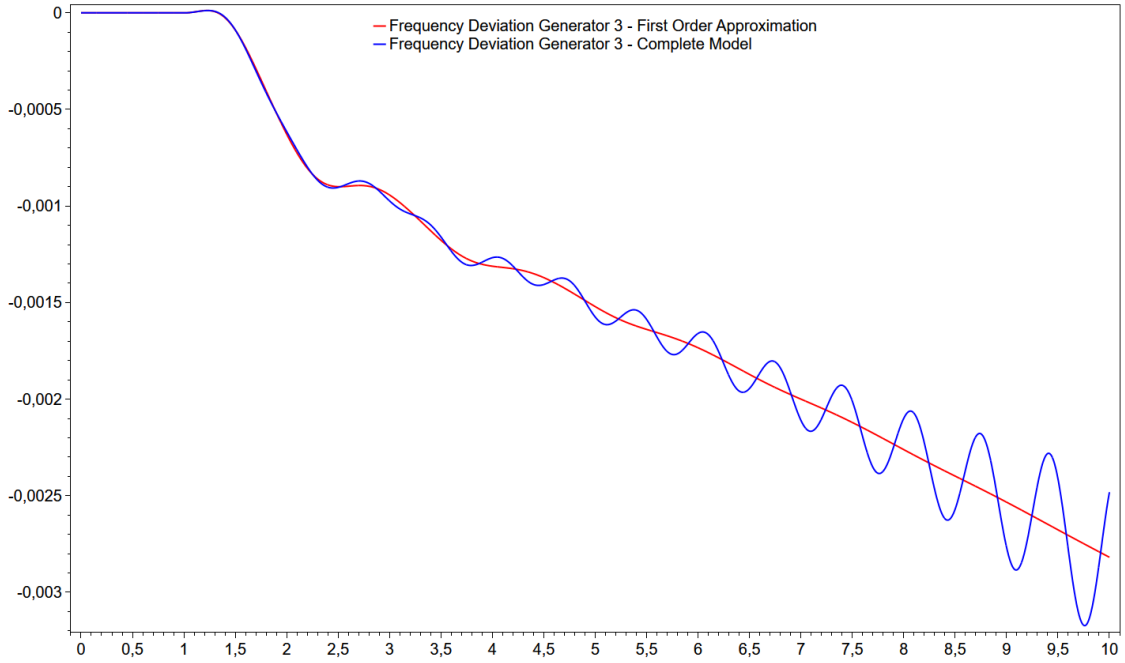

Figure 4.38: Frequency at Generator 3 - Relevant Time Delay.

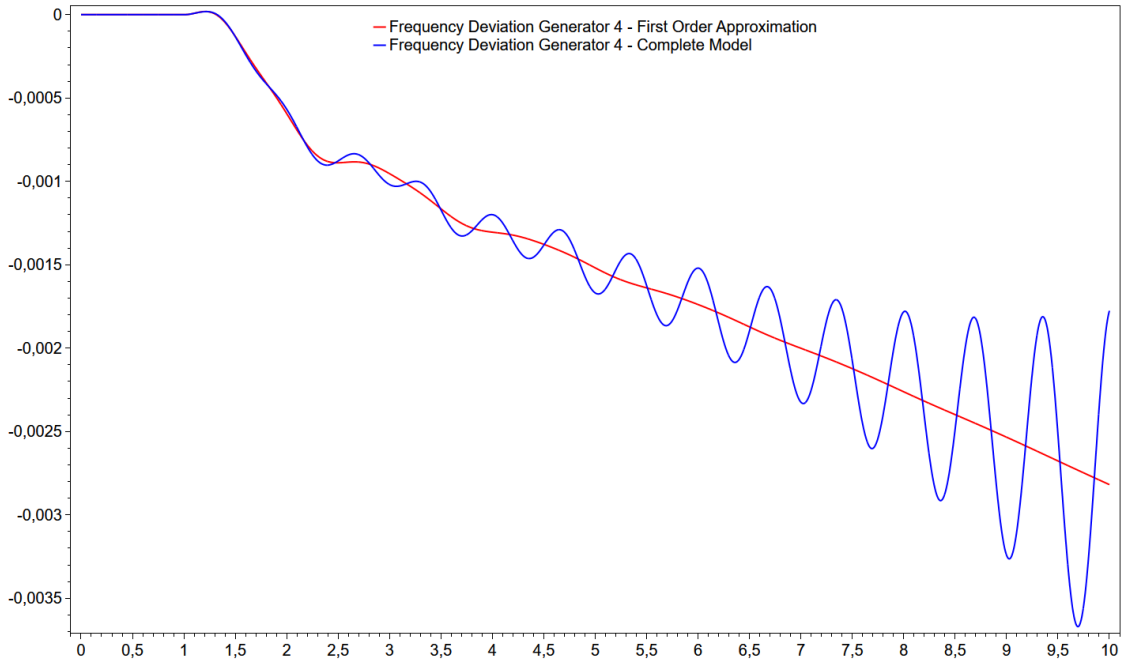

Figure 4.39: Frequency at Generator 4 - Relevant Time Delay.

The results shown that the first order approximation is not suitable for transport delay modelling when a relevant time delay exists.

4.2 Brazilian Interconnected Power System

The modal analysis tools for systems with transport delays is tested in Brazilian Interconnected Power System (BIPS), illustrated in Figure 4.40. The studies are developed using two different load-flow database cases as described in the following sections.

Figure 4.40: Brazilian Interconnected Power System (BIPS).

4.2.1 Southeast System Exporter

In this section, the proposed modal analysis tool for systems with transport delays is tested in the BIPS, considering its full database for a planning scenario of 2020 with 6620 buses, 257 power plants and 6,824 state variables. The studies are developed using a critical scenario where the Southeastern region (SE) exports

power to the North Region (N). It presents a high power flow (6400 MW, SE ⇒ N) through the HVDC line that connects substations Estreito (S) and Xingu (N). In this scenario, there is a moderate damped electromechanical mode (7%) with frequency 3.2 rad/s. In order to increase this damping factor, a remote signal from Belo Monte power plant (bus 6728), located close to the Xingu substation (17 km), is used. The remote signal is the rotor speed deviation at Belo Monte and the PSS acts at the rectifiers located at Estreito substation, through the converter modulation signals (referred to as CMS).

This scenario was used in [5], where remote signals are used in order to increase damping factor of electromechanical modes without take into account any transport delay. As presented in [5], the electromechanical mode with frequency 3.2 rad/s is allocated at (-0.6144+j3.010) in the complex plane with 20% of damping.

Including the time delay on the remote signals and varying the time constant from 0 to 0.25 seconds, it is possible to account the impact of the delay omission on the mode damping. The sequential dominant pole algorithm [11, 14] is used in order to calculate the root locus varying time constant τ.

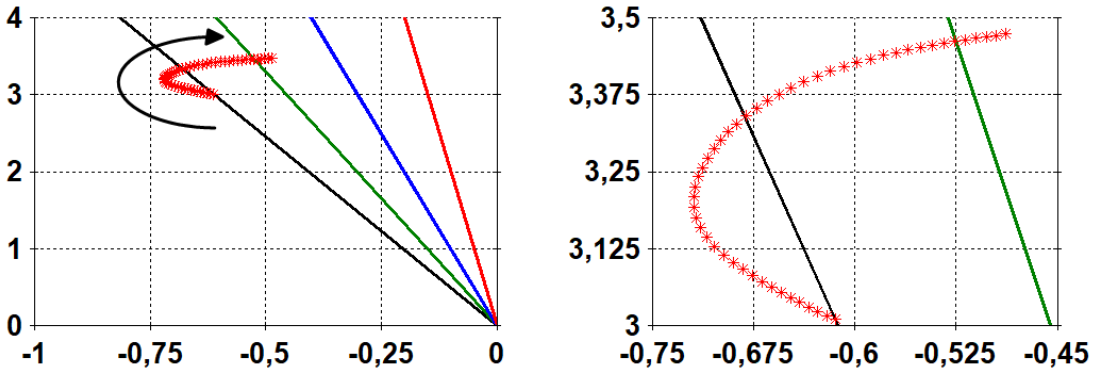

Figure 4.41: Root-Locus of time constant τ.

In Figure 4.41 it is possible to analyze the transport delay impact on the control development. The bigger the time delay, the bigger its impact on damping control.

4.2.1.1 PSS Design Including Transport Delay

The PSS will be re-designed considering the time delay associated to the remote signals. For research proposes, a big time delay (0.25 s) is used. For project proposes, the complete model of transport delay developed in this thesis is considered.

In order to increase this damping factor, a remote signal from Belo Monte power plant (bus #6728), located close to the Xingu substation (17 km), is used. The remote signal is the rotor speed deviation at Belo Monte and the PSS acts at the

rectifiers (converters #3201 and #3203) located at Estreito substation, through the converter modulation signals (referred to as CMS).

$$\frac{CMS3201(s) + CMS3203(s)}{\omega 6728(s)} \tag{4.11}$$

The DNP of 4.11 for $\xi = 20\%$ is shown in Figure 4.42.

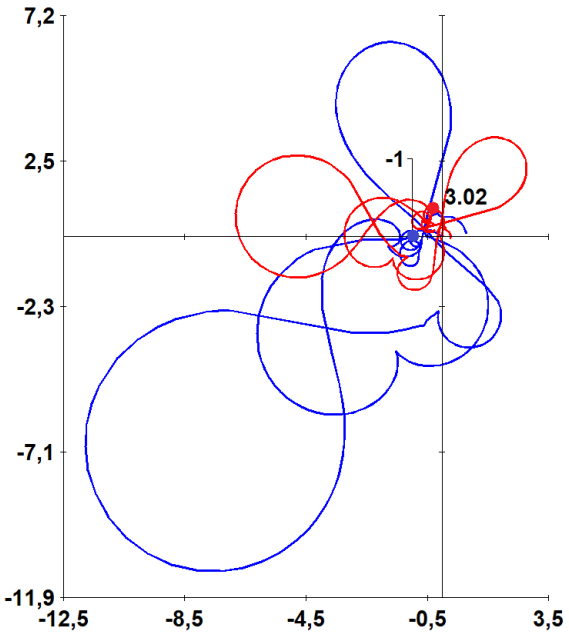

Figure 4.42: Uncompensated and Compensated Nyquist Diagram for The PSS Re-Design.

The parameters for re-designed PSS are shown in Table 4.40.

Table 4.40: Re-designed PSS, for Southeast System Exporter of Electric Power.

Generator	**n**	**K**	T_w	**T**	α	w_c	w_{max}
CS-6728	1	-15.044	3	0.11036	8.6416	3.02	3.02

Figure 4.43 shows the time response comparison for system without PSS (red), system with PSS but no time delay accounting (blue) and system with PSS accounting time delay (green).

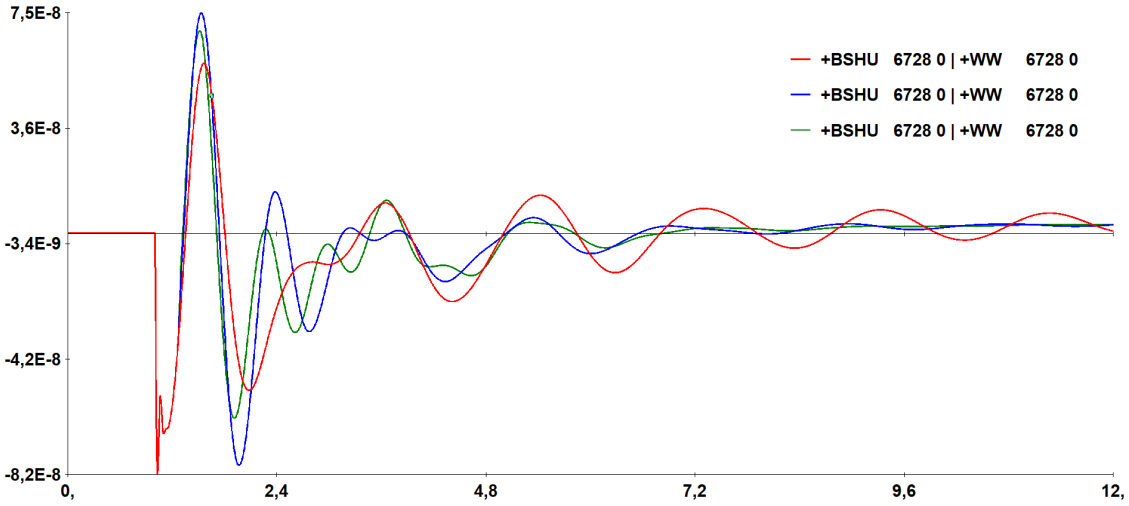

Figure 4.43: Time Response Comparison - Southeast System Exporter of Energy.

As expected, the system performance with PSS accounting time delay is superior when compared to the one that does not considers the transport delay.

4.2.2 North System Exporter

The second case has an high power flow (7200 MW) on DC line from Belo Monte hydroelectric plant North-Southeast direction. In order to increase the damping factor of poorly damped electromechanical mode (10.58%) with frequency 2.41 rad/s, converged using the Dominant Pole Algorithm [14], remote signals are used from rotor speed deviation from machine located on Belo Monte hydroelectric plant and act at the rectifier located at the HVDC that links Belo Monte hydroelectric plant to the Southeast of Brazil. The control acts at the rectifier of the substation located in Xingu-PA, located only 17 km away from the origin of input signals.

This scenario was also used in [5], where remote signals are used in order to increase damping factor of electromechanical modes without take into account any transport delay. As presented in [5], the electromechanical mode with frequency 2.41 rad/s is allocated at $(-0.4922 + j2.4111)$ in the complex plane with 20% of damping.

The transport delay modelling is included considering the developed complete model. The time delay on signals coming from Belo Monte machines is varied from 0 to 0.5 seconds. The sequential dominant pole algorithm [11, 14] is used in order to calculate the root locus varying time constant τ.

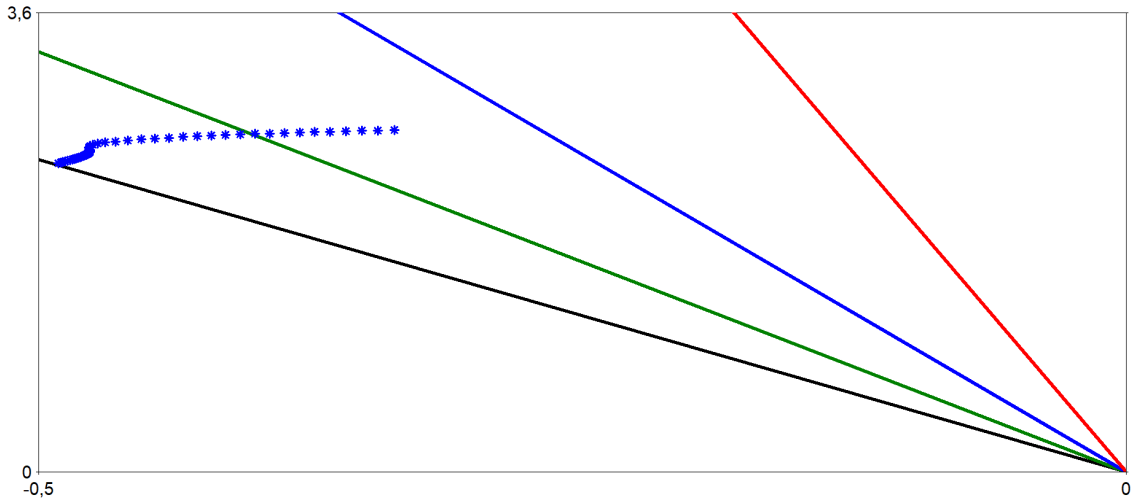

Figure 4.44: Root-Locus of time constant τ - North System Exporter of Energy.

In 4.44 it is possible to analyse the transport delay impact on control development. The bigger the time delay, The bigger its impact on damping control.

4.2.3 Computational Performance

For the computational performance evaluation, a computer with an Intel (R) Core (TM) i7-3517U CPU @ 1.90 GHz-2.40 GHz, 4,00 Gbytes of RAM and Windows 10 was used. The computational time for the BIPS case of Southeast System Exporter is 59 seconds for the root locus calculation, 23 seconds for the frequency response calculation and 1 minute and 33 seconds for the time response calculation, all of them using the proposed methods applied to the $Y(s)$-formulation. On the other hand, using a first order approximation in place of the transport delay with the conventional descriptor system modeling, the computational time is 59 seconds for root locus, 11 seconds for frequency response and 1 minute and 21 seconds for time response. Therefore, there was no significant loss of computational performance for the proposed method.

4.3 Final Considerations

In this chapter, a two-area system has been used to evaluate three aspects: first, the importance of the advances in modal analysis tools for systems with transport delay. Second, the comparison between solutions using local and remote sensing aiming at the damping of electromechanical oscillations. Third, the impact of using the first order approximation delay and the complete time delay model proposed in this work in the PSSs design.

An analysis of the Brazilian Interconnected Power System has been conducted to highlight the importance of time delay modelling in the controller design. The results have evidenced that the omission of time delay may cause lack of damping.

The results obtained in this chapter evidence benefits brought by the methods developed in this thesis for power system analysis.

Chapter 5

Conclusion

The development of modal analysis tools for systems with transport delays represents an advance in the state of art of power system stability and control area. With the recent widespread usage of communication systems in electrical networks, it is expected that stability analysis and control design methods must consider time delays. In this way, practical tools should be developed to study the complex dynamic behavior of time-delayed power systems.

The main contributions of this work are the mathematical and computational developments of modal analysis tools for systems that use remote signals in their control structure. The developments, based on s-domain methods, allow including more precise modelling of transport delays. When modelling infinite systems by non-linear functions of s, as proposed in the beginning of this thesis, the eigenvectors are not available. Therefore, the sensitivity tools of modal analysis (mode-shapes, transfer function residues, participation, observability and controllability factors) must be calculated by different numerical algorithms, based on the general complex variable theory, which is still valid for the proposed modelling form. Moreover, such methods consider the impact of the infinite system on the system dynamics, historically ignored in electromechanical stability studies. It should be noted that the proposed methodology does not cause significant loss of computational performance.

Concluding, the methods and methodologies proposed in this work have been implemented in software PacDyn and contribute greatly to small-signal analysis of delayed power systems, enabling a better planning and operation processes.

5.1 Future Works

The following future works can be proposed:

- Expansion of theoretical developed in this work for system with other non-linear system representation such as lines with distributed parameters;

- Investigation of a stochastic approach in the transport delay modelling;
- Perform additional tests in other power systems worldwide with a large quantity of remote measurements spread along the system.

Referências

[1] KUNDUR, P., PASERBA, J., AJJARAPU, V., et al. "Definition and Classification of Power System Stability", *IEEE Transactions on Power Systems*, v. 19, n. 2, pp. 1387–1401, junho, 2004.

[2] MILANO, F., ANGHEL, M. "Impact of time delays on power system stability", *IEEE Transactions on Circuits and Systems I: Regular Papers*, v. 59, n. 4, pp. 889–900, 2012.

[3] MILANO, F. "Small-signal stability analysis of large power systems with inclusion of multiple delays", *IEEE Transactions on Power Systems*, v. 31, n. 4, pp. 3257–3266, 2016.

[4] MILANO, F., DASSIOS, I. "Small-Signal Stability Analysis for Non-Index 1 Hessenberg Form Systems of Delay Differential-Algebraic Equations." *IEEE Trans. on Circuits and Systems*, v. 63, n. 9, pp. 1521–1530, 2016.

[5] DANIEL, L. O., GOMES JUNIOR, S. "Amortecimento de Modos Eletromecânicos Utilizando Estabilizadores em Elos HVDC Considerando-se Diferentes Estratégias de Controle", *XXIV Seminário Nacional de Produção e Transmissão de Energia Elétrica - SNPTEE*, outubro, 2017.

[6] MACHOWSKI, J., BIALEK, J., BUMBY, J. R., et al. *Power system dynamics and stability*. John Wiley & Sons, 1997.

[7] KUNDUR, P. *Power System Stability and Control*. 4 ed. Nova Iorque, McGraw-Hill, 1994.

[8] PARREIRAS, T. J. M. A., GOMES JUNIOR, S., TARANTO, G. N., et al. "Desenvolvimentos no PacDyn para Análise da Estabilidade a Pequenos Sinais de Múltiplos Cenários em Sistema de Potência de Grande Porte", *XII Simpósio de Especialistas em Planejamento da Operação e Expansão Elétrica - SEPOPE*, maio, 2012.

[9] OGATA, K. *Engenharia de Controle Moderno*. 4 ed. Nova Iorque, Prentice Hall, 2003.

[10] STEVENSON, W. D., GRAINGER, J. J. *Power System Analysis*. 4 ed. Nova Iorque, McGraw-Hill, 1994.

[11] GOMES JUNIOR, S. *Modelagem e Métodos Numéricos para Análise Linear de Estabilidade Eletromecânica, Ressonância Subsíncrona, Transitórios Eletromagnéticos e Desempenho Harmônico de Sistemas de Potência*. Tese de D.Sc., COPPE/UFRJ, Rio de Janeiro, RJ, Brasil, 2002.

[12] VARRICCHIO, S. L., FREITAS, F. D., MARTINS, N., et al. "Computation of dominant poles and residue matrices for multivariable transfer functions of infinite power system models", *IEEE Transactions on Power Systems*, v. 30, n. 3, pp. 1131–1142, 2015.

[13] SEMLYEN, A. "S-domain methodology for assessing the small signal stability of complex systems in nonsinusoidal steady state", *IEEE Transactions on Power Systems*, v. 14, n. 1, pp. 132–137, 1999.

[14] GOMES JR, S., MARTINS, N., PORTELA, C. "Sequential computation of transfer function dominant poles of s-domain system models", *IEEE Transactions on Power Systems*, v. 24, n. 2, pp. 776–784, 2009.

[15] GOMES, S., MARTINS, N., VARRICCHIO, S. L., et al. "Modal analysis of electromagnetic transients in ac networks having long transmission lines", *IEEE transactions on power delivery*, v. 20, n. 4, pp. 2623–2630, 2005.

[16] VARRICCHIO, S., GOMES JR, S. "Electrical network dynamic models with application to modal analysis of harmonics", *Electric Power Systems Research*, v. 154, pp. 433–443, 2018.

[17] MACHADO, J. G. D. S., GOMES, S., PARREIRAS, T. J. M. A. "Linear analysis of systems containing transport delays". In: *2018 Simposio Brasileiro de Sistemas Eletricos (SBSE)*, pp. 1–6. IEEE, 2018.

[18] CEPEL. *PacDyn - Program of Small Signal Stability Analysis and Control - Version 9.7.1*. User's manual, Rio de Janeiro, RJ, Brasil, 2015.

[19] GOMES, S., GUIMARÃES, C., MARTINS, N., et al. "Damped Nyquist Plot for a pole placement design of power system stabilizers", *Electric Power Systems Research*, v. 158, pp. 158–169, 2018.

[20] PAGOLA, F. L., PEREZ-ARRIAGA, I. J., VERGHESE, G. C. "On sensitivities, residues and participations: applications to oscillatory stability analysis and control", *IEEE Transactions on Power Systems*, v. 4, n. 1, pp. 278–285, 1989.

[21] VARRICCHIO, S. L., FREITAS, F. D., MARTINS, N., et al. "Computation of dominant poles and residue matrices for multivariable transfer functions of infinite power system models", *IEEE Transactions on Power Systems*, v. 30, n. 3, pp. 1131–1142, 2014.

[22] GUIMARAES, C. H. C., TARANTO, G. N., GOMES JUNIOR, S., et al. "Projeto de Estabilizadores de Sistemas de Potência por Posicionamento Parcial de Par de Pólos Complexos Conjugados", *XIII Congresso Brasileiro de Automática - CBA*, setembro, 2000.

[23] FRANCIS, J. G. "The QR transformation a unitary analogue to the LR transformation—Part 1", *The Computer Journal*, v. 4, n. 3, pp. 265–271, 1961.

[24] FRANCIS, J. G. "The QR transformation—part 2", *The Computer Journal*, v. 4, n. 4, pp. 332–345, 1962.

[25] CHEN, C. T. *Linear System Theory and Design*. 2 ed. Nova Iorque, CBS College Publishing, 1984.

[26] JIA, H., GUANGYU, N., LEE, S. T., et al. "Study on the impact of time delay to power system small signal stability". In: *Electrotechnical Conference, 2006. MELECON 2006. IEEE Mediterranean*, pp. 1011–1014. IEEE, 2006.

[27] WU, H., NI, H., HEYDT, G. T. "The impact of time delay on robust control design in power systems". In: *Power Engineering Society Winter Meeting, 2002. IEEE*, v. 2, pp. 1511–1516. IEEE, 2002.

[28] WU, H., TSAKALIS, K. S., HEYDT, G. T. "Evaluation of time delay effects to wide-area power system stabilizer design", *IEEE Transactions on Power Systems*, v. 19, n. 4, pp. 1935–1941, 2004.

[29] AYASUN, S., NWANKPA, C. O. "Probability of small-signal stability of power systems in the presence of communication delays". In: *Electrical and Electronics Engineering, 2009. ELECO 2009. International Conference on*, pp. I–70. IEEE, 2009.

[30] JIA, H., GUANGYU, N., LEE, S. T., et al. "Study on the impact of time delay to power system small signal stability". In: *Electrotechnical Conference, 2006. MELECON 2006. IEEE Mediterranean*, pp. 1011–1014. IEEE, 2006.

[31] NATORI, K., OBOE, R., OHNISHI, K. "Stability analysis and practical design procedure of time delayed control systems with communication disturbance observer", *IEEE Transactions on Industrial Informatics*, v. 4, n. 3, pp. 185–197, 2008.